CHARGED PARTICLE BEAM TRANSPORT FOR A CYCLOTRON FACILITY

by

Corinne M Merry (M.Sc.)

A thesis submitted in partial fulfilment of the requirement for the degree of Doctor of Philosophy at the University of Cape Town.

July, 1980

ABSTRACT

We develop a number of new techniques and systems to be used in the design of beamlines for charged particle beam transport. A few of these refer specifically to beamlines to or from a cyclotron, while others may be used in beamlines from any accelerator. In the former category, we develop a method for determining the eigen-ellipsoid in all six dimensions of phase space, when the beam under consideration is to be (a) extracted from a cyclotron, or (b) injected into a cyclotron. We also develop an alternative method to (a) above, which uses the data derived from tracking (i) central momentum particles through the extraction elements of an accelerator in 4-dimensional (x, x′, y, y′) phase space and (ii) a single particle with higher momentum. For this purpose we expand the convenient E-matrix formalism from a 2-dimensional treatment to a 6-dimensional treatment, and relate this to the more usual σ-matrix formalism.

We describe the eight possible symmetry types of beams transport systems and examine their group properties. We also examine the second-order aberrations in these systems. We use the symmetry properties to examine various configurations of two quadrupole triplets. This system may be used to achieve unit magnification, as is well known, or variable magnification in one or both of the horizontal or vertical planes, independently of the beam parameters, as we describe.

We also develop a system of quadrupoles which may be used for independent horizontal and vertical beam control. We calculate the optimum spacing and field strength of these quadrupoles.

Dipole systems which are used to control the dispersed rays are discussed. In particular we consider a system of two quadrupoles between two dipoles: this system has the least number of beamline elements necessary to control the position and direction of the dispersed ray while simultaneously permitting momentum-selection.

We discuss the principles of transfer beamline design and illustrate these

(and the techniques described above) by reference to the design of a specific transfer beamline between cyclotrons. The design of a specific external beamline is also described and used to illustrate the techniques developed.

ACKNOWLEDGEMENTS

I wish to thank my supervisor, Dr. John Cornell, for his invaluable guidance and assistance throughout, especially in the preparation of this thesis. I would also like to express my appreciation to Prof. F.D. Brooks for his support.

I would like to thank my colleagues at the National Accelerator Centre for their co-operation, and the C.S.I.R. for financial support for my studies.

I wish to express my appreciation to Mrs. S.W. de Jager for the excellent typing of this manuscript, and to Mrs. J. Longden for her assistance in preparing the diagrams.

Lastly, I thank my husband Charles for his constant encouragement and moral support.

TABLE OF CONTENTS

1. INTRODUCTION

A beam of charged particles which is obtained from an accelerator often has to be transported some distance from the accelerator to its destination, which may be either an external target or a post-accelerator which will further increase the energy of the beam.

To transfer the beam we use a beam transport system, made up of elements such as quadrupole magnets for focussing the beam and dipole magnets for changing the direction of the beam. The beam transport system also has to match the properties of the initial beam to those required at the external target, or at the post-accelerator. These requirements differ widely for various facilities, and may also vary greatly for different uses or modes of operation within one facility.

This matching of beam properties has become more important since the advent of accelerators which deliver variable-energy beams of a range of particle types for a number of purposes. Not only must the beamlines match the properties of all possible beams, but the tuning of the beamline must be such as to facilitate rapid setting up of the system.

The beam may be described by parameters in six-dimensional phase space, namely horizontal and vertical size and divergence, bunch length, momentum-spread, and correlations between these parameters. The problem, then, is matching the beam in six-dimensional phase space to a variety of possible requirements (in systems which are easy to operate).

Although this has been done before, it has always been on an ad hoc basis: specific solutions have been obtained which are applicable only to specific accelerator facilities and in many cases these provide incomplete matching. The correct correlations at the ends of the beamlines (e.g. at injection into the main accelerator) have often not been determined or taken account of, and as a result the systems may not be capable of achieving perfect matching. The beam parameters are seldom properly separated for ease of operation: by careful placing of the beamline elements one beam parameter may be controlled without disturbing another.

What we have done is to analyse the matching requirements and to propose a general, ordered system of matching, taking into account the characteristics

of the real devices which must be used. We have also designed techniques and systems for matching various parameters, which may be applied to beam= line design in general.

Thus, when a new beamline is to be designed, these systems may be used with the relevant initial and final beam parameters and combined to form a complete matching system. We have also developed methods for deter= mining these parameters in certain cases.

The general method of beamline design which we have developed is illustrated by means of an application to a specific cyclotron facility. This appli= cation includes a transfer beamline between cyclotrons and the design of external beamlines from a cyclotron to various types of targets.

The mathematical formalism used to describe beam transport characteristics will be introduced in chapter 2. In chapter 3 we discuss the properties of a beam extracted from a cyclotron, and the properties required for a beam injected into a cyclotron for optimal acceleration. It is essential to know these properties when designing any specific beamline.

In chapter 4 we give a brief description of the beam transport elements and their relevant characteristics. These will be applied to various systems. We discuss the properties of symmetrical systems in general in chapter 5. In chapter 6 we describe quadrupole systems whose special properties are independent of the beam parameters, while in chapter 7 we discuss quadrupole systems which are dependent on the beam parameters. Beamline systems containing dipoles are described in chapter 8.

Transfer between cyclotrons is discussed in chapter 9. We illustrate the methods involved by applying them to the design of a transfer beam= line at a specific cyclotron facility. In this beamline we make use of systems described in chapters 7 and 8, and of beam properties derived in chapter 3.

The transport of an external beam to various types of targets is the sub= ject of chapter 10. This is again illustrated by means of the design of specific external beamlines, which make use of systems described in chap= ters 6, 7 and 8.

Conclusions are presented in chapter 11.

It may be noticed that in the preceeding paragraphs we have referred to beams from accelerators in general and beams from cyclotrons in particular. While chapter 3 refers exclusively to cyclotron beams and parts of chapters 9 and 10 refer to a specific cyclotron facility, the theory developed in the other chapters may be applied to any accelerator beam, provided that it is borne in mind that beams extracted from various accelerators have differing characteristics: e.g. cyclotron beams are generally more divergent and have a higher energy spread than those extracted from a Van de Graaff accelerator; they are also pulsed beams rather than d.c. beams, with the particles accelerated in "bunches".

An additional factor which has to be taken into consideration in designing a beam transport system is that of cost. The total number of beamline elements should be restricted, and the apertures of quadrupoles and dipoles should be limited to bring down the costs of individual elements. This implies that we should attempt to limit the size of the beam along the beamline. We have attempted, therefore, to strike a balance between:

(a) minimizing the number of beamline elements
(b) minimizing the apertures of these elements, and
(c) providing easy tuning of the beamline.

2. MATHEMATICAL FORMALISM

2.1 Introduction

The co-ordinates of an arbitrary charged particle in phase-space may be represented by a vector, X. The components of this vector are measured with respect to a specified reference trajectory, which is taken to be the trajectory of the central particle of the ensemble of particles under consideration. The 6-dimensional vector X is made up as follows:

$$X = \begin{bmatrix} x_1 \\ x_2 \\ x_3 \\ x_4 \\ x_5 \\ x_6 \end{bmatrix} = \begin{bmatrix} x \\ x' \\ y \\ y' \\ \ell \\ \delta \end{bmatrix} \qquad (2.1)$$

where:

- x is the radial displacement of the particle (by convention positive x is to the left when positive dipole fields deflect the particle to the right)
- x' is the angle the particle trajectory makes in the radial plane
- y is the vertical displacement of the particle (by convention positive y is upwards)
- y' is the angle the particle trajectory makes in the vertical plane
- ℓ is the displacement of the particle from the central particle measured along the central trajectory
- δ is the fractional momentum deviation of the particle $\frac{\Delta p}{p}$

The trajectory of the particle is often referred to as a ray, and X then specifies ray co-ordinates.

We may express the co-ordinates of a ray at a point z_1 as a Taylor's expansion in terms of the co-ordinates of the ray at an earlier point z_0. If we assume a linear relationship (i.e. first order terms only) then we may write (PEN61, BRO64):

$$X(z_1) = R\, X(z_0) \qquad (2.2)$$

where R is a 6 x 6 matrix, called the first order transfer matrix. The elements of R are found by solving the equations of motion of a particle in a magnetic field to first order. If we also include the second-order terms of the solution then we can find a second-order transfer matrix T where

$$x_i(z_1) = \sum_{j=1}^{6} R_{ij}\, x_j(z_0) + \sum_{j=1}^{6}\sum_{k=1}^{6} T_{ijk}\, x_j(z_0)\, x_k(z_0) \qquad \ldots (2.3)$$

The transfer matrix therefore describes the effect of a beam transport element on a particle. The effect of a system of elements is then described by the total transfer matrix $R_{(T)}$ found from the product of the individual matrices $R_{(i)}$ as follows

$$R_{(T)} = R_{(n)}\, R_{(n-1)} \cdots R_{(3)}\, R_{(2)}\, R_{(1)} \qquad (2.4)$$

If we now assume that we are dealing with static magnetic fields having midplane symmetry, then R has several identically zero elements and takes the form (BRO71):

$$R = \begin{bmatrix} R_{11} & R_{12} & 0 & 0 & 0 & R_{16} \\ R_{21} & R_{22} & 0 & 0 & 0 & R_{26} \\ 0 & 0 & R_{33} & R_{34} & 0 & 0 \\ 0 & 0 & R_{43} & R_{44} & 0 & 0 \\ R_{51} & R_{52} & 0 & 0 & 1 & R_{56} \\ 0 & 0 & 0 & 0 & 0 & 1 \end{bmatrix} \qquad (2.5)$$

From the zero elements R_{13}, R_{14}, R_{23}, R_{24}, R_{31}, R_{32}, R_{41}, R_{42}, R_{36} and R_{46} (arising from the symmetry of the field) we see that the horizontal and vertical planes are decoupled, and may be treated independently. The zero elements R_{15}, R_{25}, R_{35}, R_{45} and R_{65} result from the fact that none of the variables depend on ℓ. The time-independence of the field ensures that the momentum of the particle remains constant and independent of the other parameters - hence the zero elements R_{61}, R_{62}, R_{63}, R_{64} and R_{65}. A further result of the field being static is that (BRO72, PEN61, EMM63)

$$\det[R] = 1 \tag{2.6}$$

Looking now at the decoupled subsystem of x, x', ℓ and δ we find that the pairs of co-ordinates x and x' and ℓ and δ, are canonical. Then the necessary and sufficient condition for the transformation matrix R to be canonical is that it should be symplectic (DRA76, DRA79, SCH79) i.e.

$$R\,J\,R^{T} = J \tag{2.7}$$

where

$$J = \begin{bmatrix} 0 & 1 & 0 & 0 \\ -1 & 0 & 0 & 0 \\ 0 & 0 & 0 & 1 \\ 0 & 0 & -1 & 0 \end{bmatrix} \tag{2.8}$$

From equations (2.5) through (2.8) we can derive the following symplectic equations:

$$R_{51} = R_{16}\,R_{21} - R_{26}\,R_{11} \tag{2.9}$$

$$R_{52} = R_{16}\,R_{22} - R_{26}\,R_{12} \tag{2.10}$$

These may also be derived using the equations of Brown (BRO72) which employ Green's functions instead of the matrix treatment.

In practice we are interested in the behaviour of the beam of particles rather than in the behaviour of an individual particle. We assume that the beam is pulsed and that we may consider a single pulse, or "bunch" of particles. (For d.c. beams bunches follow each other without a gap in-between.)

There are two methods of extending equation (2.2) to encompass the behaviour of the bunch, termed the σ-matrix formalism and the E-matrix formalism respectively. These will be dealt with individually below. In each case it is assumed that every particle in the bunch can be represented by a point in 6-dimensional phase space. The phase space volume taken up by the points is assumed to be an ellipsoid.

2.2 σ-matrix Formalism

The equation of an n-dimensional ellipsoid may be written in matrix form as follows (BRO72):

$$X(0)^T \sigma(0)^{-1} X(0) = 1 \qquad (2.11)$$

where $X(0)^T$ is the transpose of the n-dimensional co-ordinate vector $X(0)$, and $\sigma(0)$ is an n x n real, positive definite, symmetric matrix. Applying the identity

$$R R^{-1} = I$$

to equation (2.11), we get

$$\left[X(0)^T R^T\right] \left[R \sigma(0)^{-1} R^T\right]^{-1} \left[R X(0)\right] = 1 \qquad (2.12)$$

Applying equation (2.2) to (2.12), we find that the equation of the new ellipsoid (after transformation) becomes:

$$X(1)^T \sigma(1)^{-1} X(1) = 1 \qquad (2.13)$$

where

$$\sigma(1) = R \sigma(0) R^T \qquad (2.14)$$

Together with equation (2.6), equation (2.14) predicts equal determinants for $\sigma(1)$ and $\sigma(0)$. This implies equal phase space volumes for the two ellipsoids, and phase space is thus conserved under the transformation R. This is an expression of Liouville's theorem (BAN66).

It can be shown (LOB70, BRO71) that the square roots of the diagonal terms of the σ-matrix represent the maximum beam extent in each co-ordinate:

$$\sqrt{\sigma_{ii}} = x_i \text{ (maximum)} \qquad (2.15)$$

The off-diagonal terms determine the orientation of the ellipsoid in phase space. These terms are often easier to interpret after conversion to the (also symmetric) correlations r_{ij}, where

$$r_{ij} = r_{ji} \equiv \frac{\sigma_{ij}}{\sqrt{\sigma_{ii}\,\sigma_{jj}}} \qquad (2.15)$$

The interpretation of these terms may be seen from the two-dimensional projection of the ellipsoid onto the $x - x'$ plane shown in figure 2.1.

When this ellipse is upright (the axes of the ellipse coinciding with the co-ordinate axes) then the correlation r_{12} is zero. This condition is termed a beam "waist", and in general may be applied for any r_{ij} which is zero.

The area of the 2-dimensional ellipse is given by:

$$\begin{aligned} A &= \pi\,(\det\sigma)^{\frac{1}{2}} \\ &= \pi\,(\sigma_{11}\,\sigma_{22} - \sigma_{12}^{\,2})^{\frac{1}{2}} \\ &= \pi\,[\sigma_{11}\,\sigma_{22}\,(1 - r_{12}^{\,2})]^{\frac{1}{2}} \qquad (2.16) \\ &= \pi\,x_{max}\,x'_{int} \\ &= \pi\,x_{int}\,x'_{max} \end{aligned}$$

The expression for the volume of the ellipsoid in the three dimensions x, x' and δ contains the three correlations r_{12}, r_{16} and r_{26}. It may be written as follows:

$$V = \frac{4}{3}\,\pi\left[\sigma_{11}\,\sigma_{22}\,\sigma_{66}\,\{1 - (r_{12}^{\,2} + r_{16}^{\,2} + r_{26}^{\,2}) + 2r_{12}\,r_{16}\,r_{26}\}\right]^{\frac{1}{2}} \qquad \ldots (2.17)$$

Thus for a fixed phase volume the correlations may not be chosen completely arbitrarily, as they are restricted to values satisfying equation (2.17). We show the allowed values of the correlations in figure 2.2, where the surface of the 3-dimensional figure represents zero phase space volume. Positive volumes are represented by surfaces within this: any point on the relevant surface represents an allowed combination of the three correlations.

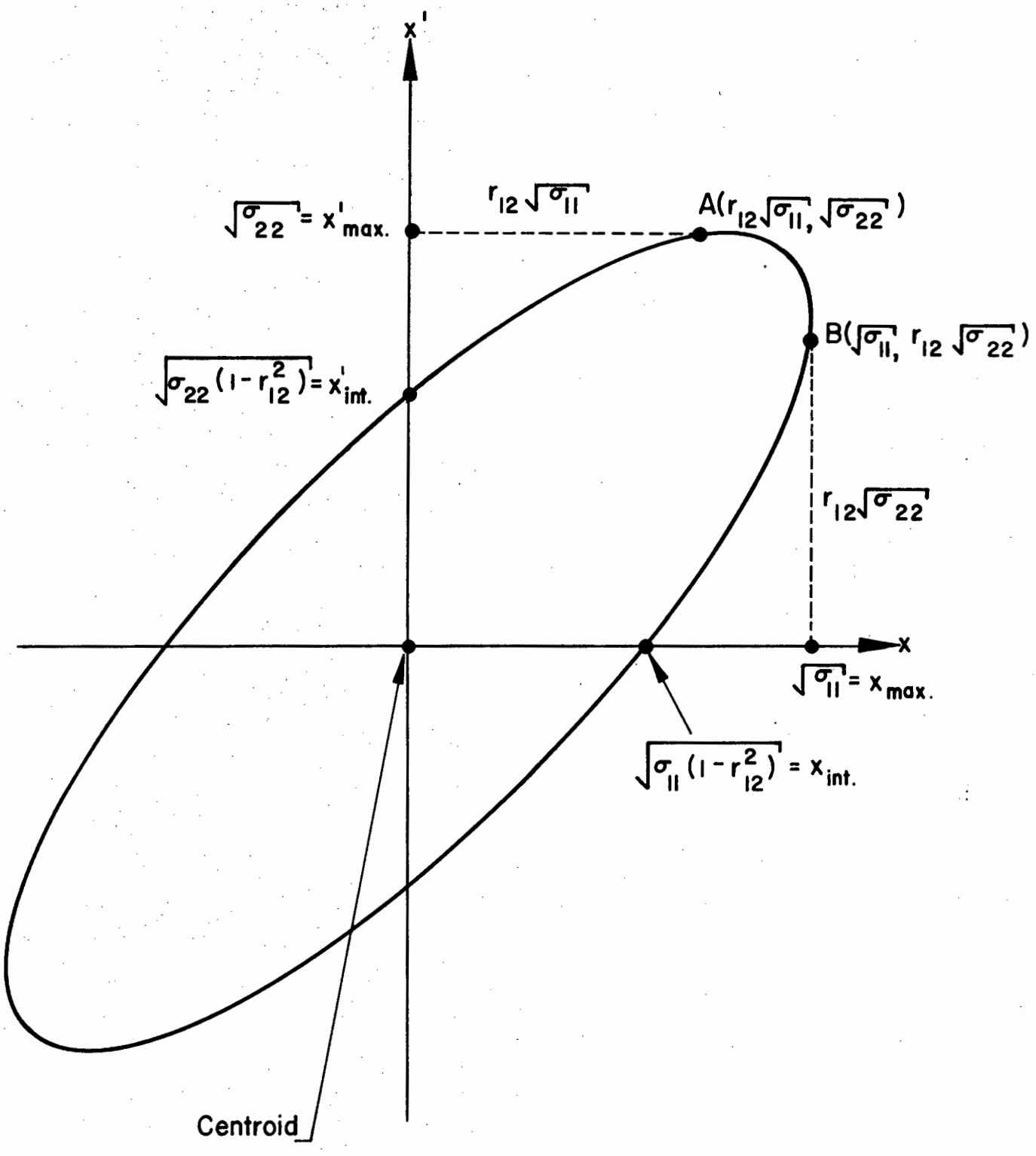

Figure 2.1: Projection of a phase-space ellipsoid onto the x - x´ plane. The two extreme points A and B are shown, together with their co-ordinates. The values of the intercepts x_{int} and x'_{int} are shown.

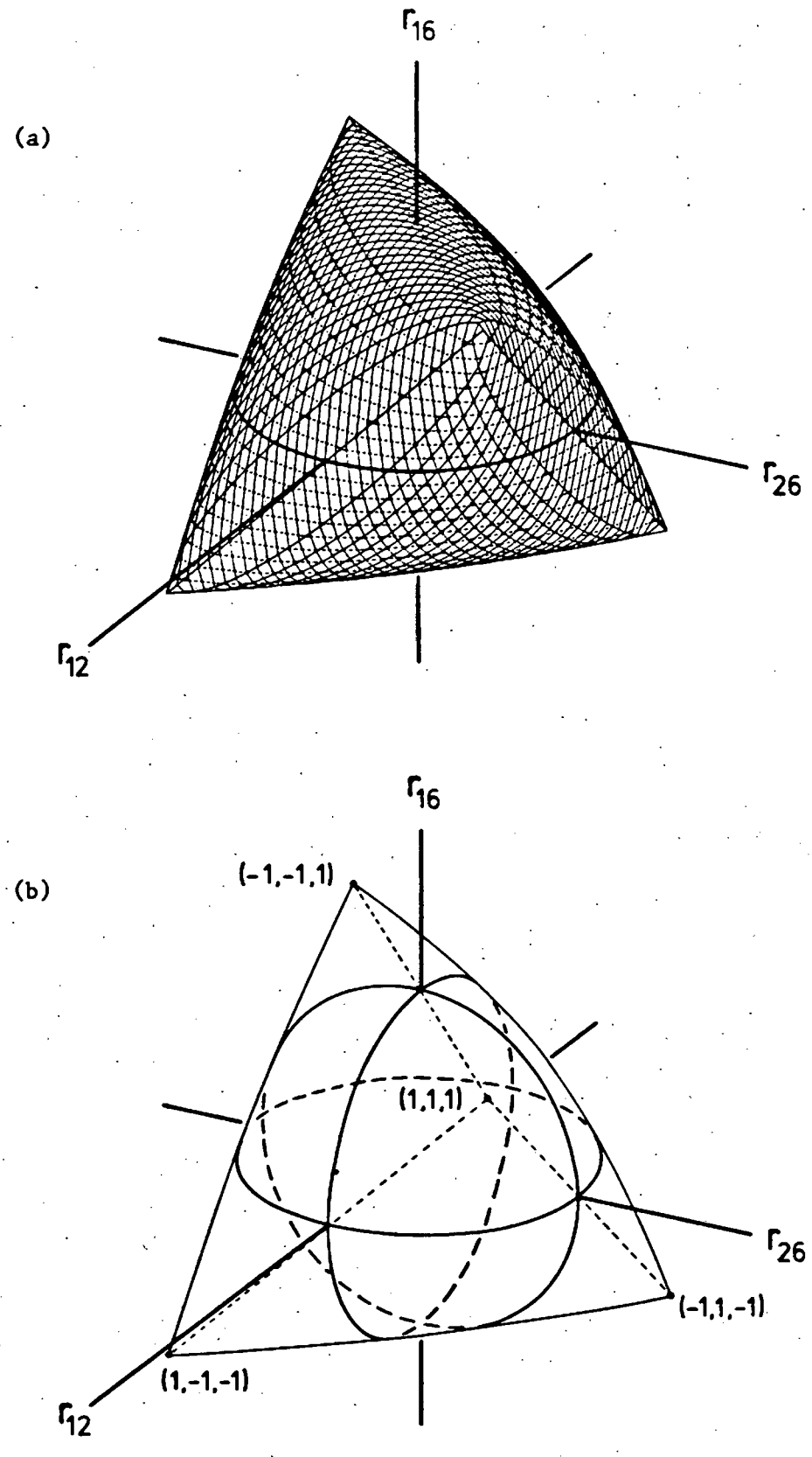

Figure 2.2: The surface representing zero volume in 3-D phase space as a function of correlations r_{12}, r_{26} and r_{16}:

(a) lines of equal r_{12}, r_{26} and r_{16} are shown;

(b) the extreme points on the surface are labelled with their co-ordinates. The three circles inscribing the surface each represent one of the correlations as zero.

In the 4-dimensional phase space of x, x′, ℓ and δ we have derived further restrictions on the correlations, using the symplectic conditions expressed in equations (2.9) and (2.10). The derivation is shown in Appendix A, the results being as follows:

$$\sigma_{15} = \frac{\sigma_{12}\,\sigma_{16} - \sigma_{11}\,\sigma_{26} + \sigma_{16}\,\sigma_{56}}{\sigma_{66}} \qquad (2.18)$$

$$\sigma_{25} = \frac{\sigma_{22}\,\sigma_{16} - \sigma_{12}\,\sigma_{26} + \sigma_{26}\,\sigma_{56}}{\sigma_{66}} \qquad (2.19)$$

which may be rewritten as:

$$r_{15} = \left(\frac{\sigma_{11}\,\sigma_{22}}{\sigma_{55}\,\sigma_{66}}\right)^{\frac{1}{2}} (r_{12}\,r_{16} - r_{26}) + r_{16}\,r_{56} \qquad (2.20)$$

$$r_{25} = \left(\frac{\sigma_{11}\,\sigma_{22}}{\sigma_{55}\,\sigma_{66}}\right)^{\frac{1}{2}} (r_{16} - r_{12}\,r_{26}) + r_{26}\,r_{56} \qquad (2.21)$$

The σ-matrix method is used extensively in computer programs for beamline design, the best known program being TRANSPORT (BRO77, COL70, PAU75). We have used this program for many of our computations. The beam matrix is printed in the following format:

$$\begin{array}{lllll}
\sqrt{\sigma_{11}} & & & & \\
\sqrt{\sigma_{22}} & r_{12} & & & \\
\sqrt{\sigma_{33}} & 0 & 0 & & \\
\sqrt{\sigma_{44}} & 0 & 0 & r_{34} & \\
\sqrt{\sigma_{55}} & r_{15} & r_{25} & 0 & 0 \\
\sqrt{\sigma_{66}} & r_{16} & r_{26} & 0 & 0 \quad r_{56}
\end{array}$$

with the interpretation of the non-zero elements being:

$\sqrt{\sigma_{11}}$ maximum projection onto x-axis

$\sqrt{\sigma_{22}}$ maximum projection onto x′-axis

$\sqrt{\sigma_{33}}$ maximum projection onto y-axis

$\sqrt{\sigma_{44}}$ maximum projection onto y′-axis

$\sqrt{\sigma_{55}}$ maximum projection onto ℓ-axis

$\sqrt{\sigma_{66}}$ maximum projection onto δ-axis

r_{12} correlation, between x and x′, of the projection onto the x - x′ plane. $r_{12}\sqrt{\sigma_{11}}$ is the x-co-ordinate of the particle with maximum x′

r_{34} correlation, between y and y′, of the projection onto the y - y′ plane. $r_{34}\sqrt{\sigma_{33}}$ is the y-co-ordinate of the particle with maximum y′

r_{15} correlation, between x and ℓ, of the projection onto the x - ℓ plane. $r_{15}\sqrt{\sigma_{55}}$ is the ℓ-co-ordinate of the particle with maximum x

r_{25} correlation, between x′ and ℓ, of the projection onto the x′- ℓ plane. $r_{25}\sqrt{\sigma_{55}}$ is the ℓ-co-ordinate of the particle with maximum x′

r_{16} correlation, between x and δ, of the projection onto the x - δ plane. $r_{16}\sqrt{\sigma_{11}}$ is the x-co-ordinate of the particle with maximum δ

r_{26} correlation, between x′ and δ, of the projection onto the x′- δ plane. $r_{26}\sqrt{\sigma_{22}}$ is the x′- co-ordinate of the particle with max δ

r_{56} correlation, between ℓ and δ, of the projection onto the ℓ - δ plane. $r_{56}\sqrt{\sigma_{55}}$ is the ℓ-co-ordinate of the particle with maximum δ

The advantages of the σ-matrix include:

(i) the symmetry of the matrix, which implies that the minimum number of variables is used in computation

(ii) interpretation of diagonal elements of the matrix as the square of the maximum projections onto a given axis. This is useful when apertures of beamline elements are compared to beam size.

(iii) convenient incorporation of second-order effects on the beam (CAR72a), (see section 4.6) and

(iv) use in predicting eigen-ellipses (see chapter 3).

Disadvantages of the method are listed below:

(i) extra matrix multiplication incorporated in equation (2.14) and

(ii) difficulty in interpretation of the matrix elements.

The latter arises from the fact that the σ matrix-elements always refer to the projection of the entire ellipsoid onto a given plane, and not to the parameters of the ellipse actually in that plane (i.e. slice of the ellipsoid). The projection and the slice are depicted in figure 2.3 (for a 3-dimensional ellipsoid).

The disadvantages of the σ-matrix method are avoided in the E-matrix formalism, described in the next section.

2.3 E-matrix Formalism

The alternative description of the phase space ellipsoid, represented by E in the propagation equation:

$$E(1) = R\,E(0) \qquad (2.22)$$

has been described previously for three dimensions, and the transformation from E to σ carried out for a two-dimensional ellipse (LAR71). We have described the ellipsoid in all six dimensions in the E-formalism, and have calculated the transformation from σ to E and vice versa for this 6-D ellipsoid. We give the mathematical details of the transformation in Appendix B and the derivation of the symplectic equations for E in Appendix A(b). We use the results here to determine the physical interpretation of the matrix elements E_{ij}.

From Appendix B we get: (for the 4-D subspace in x, x′, ℓ, δ)

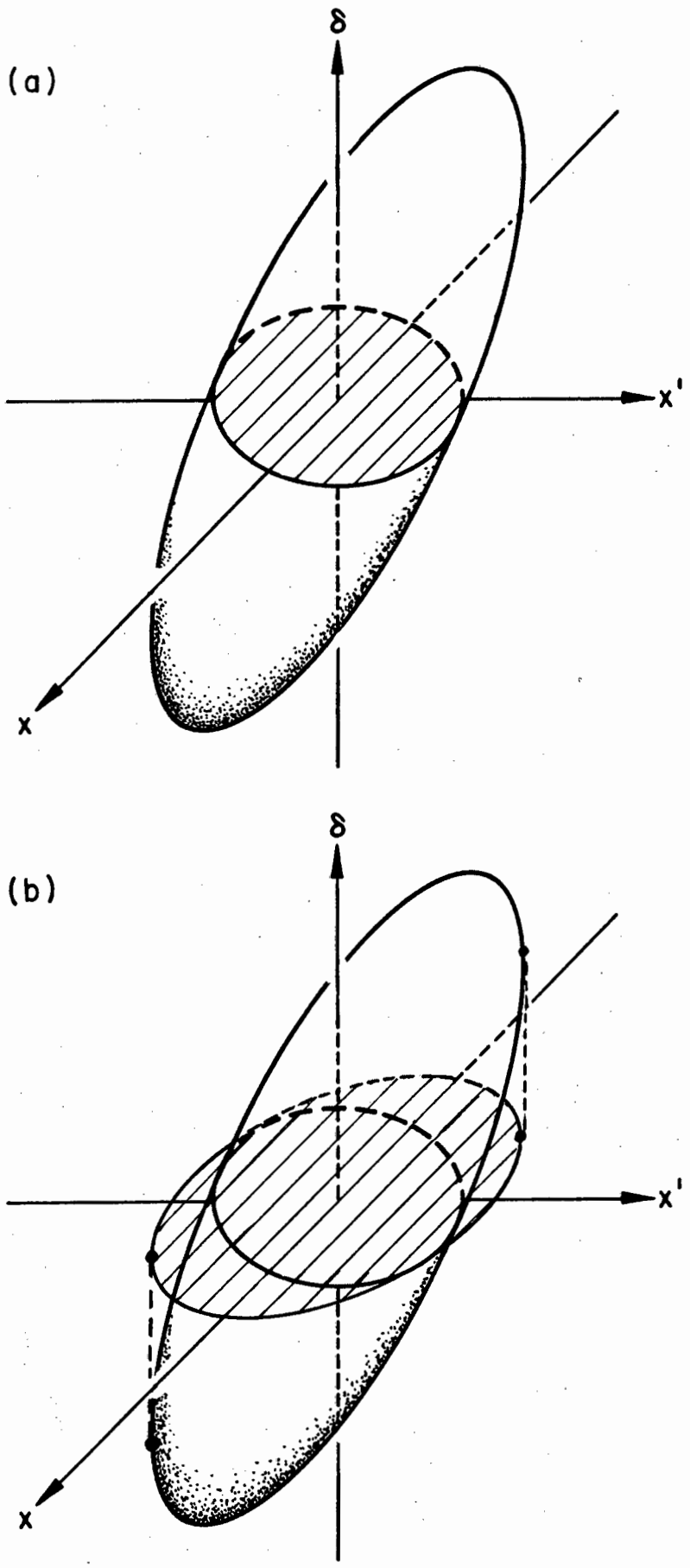

Figure 2.3: A three-dimensional ellipsoid showing

(a) the x - x´ slice through the ellipsoid at $\delta = 0$, and

(b) the projection of the ellipsoid onto the x - x´ plane, where $\delta = 0$

$$\sigma_{11} = E_{11}^2 + E_{12}^2 + E_{16}^2 \quad \text{(a)}$$

$$\sigma_{12} = E_{12}\,E_{22} + E_{16}\,E_{26} \quad \text{(b)}$$

$$\sigma_{15} = E_{11}\,E_{51} + E_{12}\,E_{52} + E_{16}\,E_{56} \quad \text{(c)}$$

$$\sigma_{16} = E_{16}\,E_{66} \quad \text{(d)}$$

$$\sigma_{22} = E_{22}^2 + E_{26}^2 \quad \text{(e)}$$

$$\sigma_{25} = E_{22}\,E_{52} + E_{26}\,E_{56} \quad \text{(f)} \qquad (2.23)$$

$$\sigma_{26} = E_{26}\,E_{66} \quad \text{(g)}$$

$$\sigma_{55} = E_{51}^2 + E_{52}^2 + E_{55}^2 + E_{56}^2 \quad \text{(h)}$$

$$\sigma_{56} = E_{56}\,E_{66} \quad \text{(i)}$$

$$\sigma_{66} = E_{66}^2 \quad \text{(j)}$$

The expression for E_{16} is then (from equation (2.23d)

$$E_{16} = r_{16}\sqrt{\sigma_{11}}$$

This is the x-co-ordinate of the particle with maximum momentum, referred to as the dispersion, d.

Similarly, from equation (2.23g) we have

$$E_{26} = r_{26}\sqrt{\sigma_{22}}$$

which is the x´-co-ordinate of the same particle, referred to as angular dispersion, d´, while from (2.23i) we find

$$E_{56} = r_{56}\sqrt{\sigma_{55}}$$

which is the position in the bunch of the same particle. We call this co-ordinate longitudinal dispersion, m.

From (2.23e) we find

$$E_{22} = \sqrt{\sigma_{22}\,(1 - r_{26}^2)}$$

This implies that E_{22} is the intercept on the x′-axis of the projection of the ellipsoid onto the x′- δ plane (i.e. where x = ℓ = 0). This is then the maximum value of x′ in the x - x′ plane.

Similarly we may interpret

E_{12} = s = the x-co-ordinate of the particle with maximum x′ in the x - x′ slice

E_{11} = the value of x at which the ellipsoid cuts the x-axis (i.e. for which x′ = ℓ = δ = 0)

E_{55} = the value of ℓ at which the ellipsoid cuts the ℓ-axis (x = x′= δ = 0)

E_{51} = t = the ℓ-co-ordinate of the particle with maximum x, where x′ = δ = 0

E_{52} = u = the ℓ-co-ordinate of the particle with maximum x′ where x = δ = 0

Figure 2.4 shows the interpretation of the elements E_{ij}.

The E-matrix elements E_{ij} (i ≠ j) are thus a measure of the skewing of the slice of the ellipsoid in the (i - j) plane, whereas the σ-matrix elements σ_{ij} or r_{ij} (i ≠ j) are a measure of the skewing of the projection of the ellipsoid onto the (i - j) plane. The former method is much easier to use when information about the beam is obtained from particle tracking calculations (e.g. through the final orbits of a cyclotron). This information could typically consist of the following:

(i) horizontal emittance $\pi\varepsilon_x$

(ii) x_{max} in the x - x′ plane

(iii) x'_{max} in the x - x′ plane

(iv) d (dispersion)

(v) d′ (angular dispersion)

(vi) m (longitudinal dispersion)

(vii) ℓ_0 the minimum possible bunch length

(viii) δ the fractional momentum spread

(ix) vertical emittance $\pi\varepsilon_y$

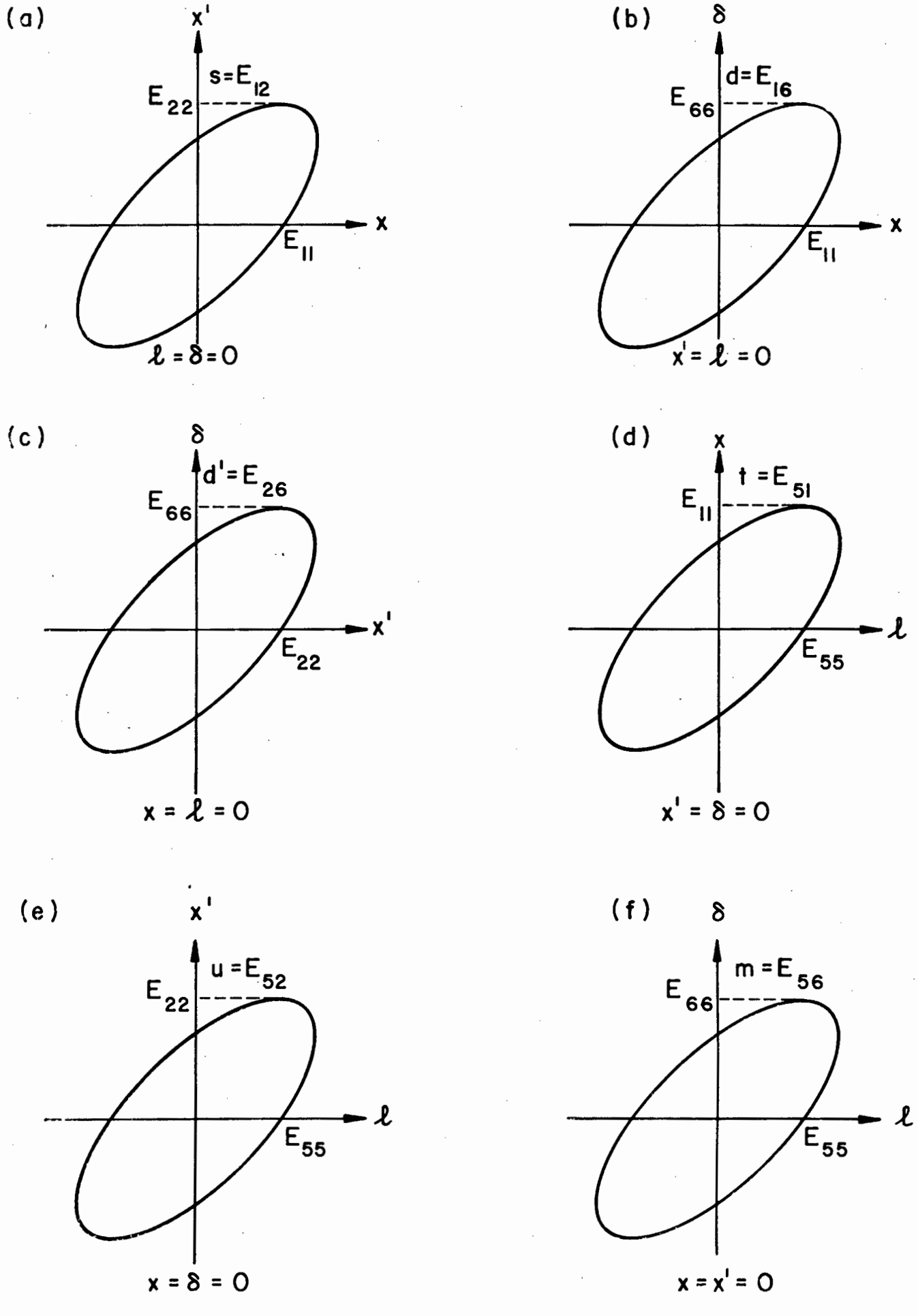

Figure 2.4: Interpretation of the E-matrix elements.

(x) y_{max} in the y - y´ plane

(xi) y'_{max} in the y - y´ plane

We have shown in Appendix C that it is a simple matter to construct the E-matrix from this data, but constructing the σ-matrix is more complicated.

A disadvantage of the E-formalism is its inability to predict eigen-ellipses, discussed in chapter 3. This is due to the arbitrary phase factor which need not repeat itself after one cyclotron orbit. Hence the equation

$$E_e = R\, E_e$$

always implies that R is a unit matrix and thus yields no information about E_e. (The arbitrary phase factor is defined in reference (LAR71).)

2.4 Other Methods of Beamline Calculation

The simplest method of determining beamline characteristics is that using graphical representations (KNO63, RAN66, RES69) but this method is limited in its accuracy and is more time-consuming than using computer calculations.

Other possible methods include the following:

(i) use of a second-order differential equation to solve for the beam envelope parameters (KNO75). This method has been used mainly to supplement a basic computer program where a more sophisticated program would not fit into the computer memory;

(ii) a method of "transfer maps" which includes treatment of non-linear elements (DRA79). This is useful specifically where non-linear elements are to be included in the beamline and where accuracy to higher orders is essential;

(iii) solution of trajectory equations by a method of successive approximations (FUJ77, FUJ78). This is clumsy when used to first order only, and is more useful only when higher order (at least 3rd order) terms have to be included;

(iv) use of a general transformation function to describe beamline

elements (EMM63), which is advantageous when very broad beams are encountered;

(v) the lumped element approach, incorporated in computer program TURTLE (CAR71, CAR72b, CAR73, BRO74). This method involves tracing several thousand particles through a system of elements, with each element represented by its transfer matrix. An advantage of this method is that the phase space area of the beam is not assumed to be elliptical (except at the entrance to the beamline), and the distorting effects of multipoles and aberrations can be examined; and

(vi) raytracing techniques in which particles are tracked through magnetic fields by means of numerical integration of the equations of motion. This technique has been incorporated into the computer program RAYTRACE (SPE67, ENG70). This method is often used in designing magnetic spectrographs as coefficients up to fifth order can be determined (ENG79), but it uses a lot of computer time.

In spite of the numerous methods available to the beam transport designer, the one most often employed is the transfer matrix method, using the σ-beam matrix.

3. EIGEN-ELLIPSES

3.1 Introduction

For beam transport calculations we need to know what the shape of the beam ellipsoid will be at the start of the beamline. If the beam is being injected into a post-accelerator, we also need to know what beam ellipsoid is required there, so that we can match the transferred beam to this ellipsoid. We will show here how to calculate the ellipsoid for either the starting- or end-point of the beamline if the accelerator is a cyclotron.

In a cyclotron the beam will travel round in a closed orbit if there is no accelerating voltage. This orbit is termed an equilibrium orbit, and its radius is dependent on the energy of the particle. (For a separated-sector cyclotron, the "average radius" is dependent on particle energy.)

The beam at any given point on this equilibrium orbit may then be represented by an ellipsoid, termed the eigen-ellipsoid (GOR68). This is defined as that beam-ellipsoid which will be exactly reproduced after one orbit, or in the case of N-sector symmetry, after each (360/N) degrees.

In practice the beam does not travel along an equilibrium orbit, but along a centered, accelerated orbit (i.e. a non-closed,spiral path). To determine the ideal beam ellipsoid along this orbit we would have to track representative particles along the entire path. However, when the number of revolutions through the cyclotron is large, the eigen-ellipsoid will be a good approximation to this ideal beam, as the change of radius (or average radius) per revolution is then small.

If we know the transfer matrix, R, of the equilibrium orbit (or of one sector), we can find the expression for the eigen-ellipsoid, σ_E, from the equation:

$$\sigma_E = R\,\sigma_E\,R^T \qquad (3.1)$$

To find R we approximate each (small) segment of the magnetic field along the orbit by a dipole with a non-zero field gradient. We track the cen=

tral particle of the beam through these successive dipole elements and accumulate the effect of the dipoles into the total transfer matrix of the orbit. We have written a computer program STRAY to do this. The small dipole elements must be short enough, so that halving their length does not significantly change the resultant matrix.

3.2 Solution of the Eigen-Ellipsoid Equation

We choose to calculate the eigen-ellipsoid at either a magnetic hill or valley so that we can make the following assumptions:

(i) the beam is at a waist in the horizontal plane ($x - x'$ for $\delta = 0$) and the vertical plane ($y - y'$); and

(ii) the off-momentum rays are travelling parallel to the central orbit i.e. $d' = 0$.

The following elements of the ellipsoid are thus zero:

$$\sigma_{12} = \sigma_{34} = \sigma_{26} = 0 \qquad (3.2)$$

If we now also assume mirror symmetry about the centre of the orbit then we find

$$R_{11} = R_{22} \qquad (a)$$

$$R_{33} = R_{44} \qquad (b)$$

$$R_{16} = -R_{52} \qquad (c) \qquad (3.3)$$

and $$R_{26} = -R_{51} \qquad (d)$$

This is shown in chapter 5.

Combining equations (3.1), (3.2) and (3.3) allows us to write (for the subspace in x, x', ℓ and δ):

$$\begin{bmatrix} \sigma_{11} & 0 & \sigma_{15} & \sigma_{16} \\ 0 & \sigma_{22} & \sigma_{25} & 0 \\ \sigma_{15} & \sigma_{25} & \sigma_{55} & \sigma_{56} \\ \sigma_{16} & 0 & \sigma_{56} & \sigma_{66} \end{bmatrix} = \begin{bmatrix} R_{11} & R_{12} & 0 & R_{16} \\ R_{21} & R_{11} & 0 & R_{26} \\ -R_{26} & -R_{16} & 1 & R_{56} \\ 0 & 0 & 0 & 1 \end{bmatrix} \begin{bmatrix} \sigma_{11} & 0 & \sigma_{15} & \sigma_{16} \\ 0 & \sigma_{22} & \sigma_{25} & 0 \\ \sigma_{15} & \sigma_{25} & \sigma_{55} & \sigma_{56} \\ \sigma_{16} & 0 & \sigma_{56} & \sigma_{66} \end{bmatrix} \begin{bmatrix} R_{11} & R_{21} & -R_{26} & 0 \\ R_{12} & R_{11} & -R_{16} & 0 \\ 0 & 0 & 1 & 0 \\ R_{16} & R_{26} & R_{56} & 1 \end{bmatrix}$$

... (3.4)

This leads to the expression:

$$\sigma_{56} = \sigma_{56} - R_{26}\,\sigma_{16} + R_{56}\,\sigma_{66} \qquad (3.5)$$

which implies that σ_{56} is undefined. If the eigen-ellipsoid is at a valley a possible choice is

$$\sigma_{56} = 0 \qquad (3.6)$$

i.e. no correlation between the particle momentum and bunch length.

If we now use the symplectic equations (2.18) and (2.19) together with equations (3.2) and (3.6), we also find

$$\sigma_{15} = 0 \qquad (3.7)$$

and

$$\sigma_{25} = \frac{\sigma_{22}\,\sigma_{16}}{\sigma_{66}} \qquad (3.8)$$

Equation (3.5) also implies that

$$\sigma_{16} = \frac{R_{56}}{R_{26}}\,\sigma_{66} \qquad (3.9)$$

This defines the correlation between position (x) and momentum.

Another expression for σ_{16} may be found from calculating the value for σ_{26} on the left-hand side of equation (3.4) and then setting it equal to zero:

$$\sigma_{26} = 0 = R_{21}\,\sigma_{16} + R_{26}\,\sigma_{66}$$

which implies

$$\sigma_{16} = - \frac{R_{26}}{R_{21}} \sigma_{66} \qquad (3.10)$$

A third expression for σ_{16} comes from equation (3.4) in the form

$$\sigma_{16} = R_{11}\, \sigma_{16} + R_{16}\, \sigma_{66}$$

which leads to

$$\sigma_{16} = \frac{R_{16}}{1 - R_{11}}\, \sigma_{66} \qquad (3.11)$$

Combining equations (3.10) and (3.11), we find

$$\frac{R_{16}}{1 - R_{11}} = - \frac{R_{26}}{R_{21}} \qquad (3.12)$$

This expression may also be derived using the symplectic equation (2.9) and the symmetry condition (3.3c). However if we combine equations (3.9) and (3.11) we find

$$\frac{R_{16}}{1 - R_{11}} = \frac{R_{56}}{R_{26}} \qquad (3.13)$$

Now R_{11} relates the final beam width to the initial width, while R_{16} describes the broadening of the beam caused by the dispersion of the system. On the right hand side of (3.13) we have R_{56}, which describes the lengthening of the beam as a result of the momentum spread, while R_{26} describes the angular broadening of the beam which results. For the eigen-ellipsoid to be unchanged after the transformation R, this puts a restriction on the magnetic field. In fact the field must be isochronous i.e. shaped so that all particles take the same time to traverse one orbit (or sector) for all momenta.

From equation (3.4) we find the expression for σ_{11}:

$$\sigma_{11} = R_{11}^{\,2}\, \sigma_{11} + R_{12}^{\,2}\, \sigma_{22} + R_{16}^{\,2}\, \sigma_{66} + 2R_{11}\, R_{16}\, \sigma_{16}$$

Together with equation (3.11) this gives us

$$\sigma_{11} = \left(\frac{R_{12}^2}{1 - R_{11}^2}\right)\sigma_{22} + \left(\frac{R_{16}}{1 - R_{11}}\right)^2 \sigma_{66} \qquad (3.14)$$

which we rewrite as

$$\sigma_{11} = a^2 + d^2$$

The two terms contributing to σ_{11} arise from

a: the extent of the ellipse in the x - x′ plane, i.e. the horizontal extent of the beam of particles with central momentum, and

d: the dispersion i.e. the horizontal extent of particles with higher (and lower) momentum. This term is always positive, which confirms that particles with higher momenta have larger radii than the central momentum particles, as we would expect.

Figures 3.1a and 3.1b show the physical interpretation of a and d.

We can now solve for a if we know the horizontal emittance $\pi\varepsilon_x$. We know that $\sqrt{\sigma_{22}}$ is the maximum extent along the x′-axis in the x - x′ plane ($\delta = 0$) because $\sigma_{26} = 0$. So, because $\sigma_{12} = 0$ as well, we can state

$$a \cdot \sqrt{\sigma_{22}} = \varepsilon_x$$

Substituting for a, and solving for σ_{22}, we get

$$\sigma_{22} = \frac{(1 - R_{11}^2)^{\frac{1}{2}}}{R_{12}} \varepsilon_x \qquad (3.15)$$

which we use in equation (3.14) to find

$$\sigma_{11} = \left[\frac{R_{12}}{(1 - R_{11}^2)^{\frac{1}{2}}}\right]\varepsilon_x + \left[\frac{R_{16}}{1 - R_{11}}\right]^2 \sigma_{66} \qquad (3.16)$$

We can now solve for σ_{25} using equations (3.10) and (3.15) in (3.8):

$$\sigma_{25} = \left[\frac{R_{16}}{R_{12}\,(1 - R_{11}^2)^{\frac{1}{2}}}\right]\varepsilon_x \qquad (3.17)$$

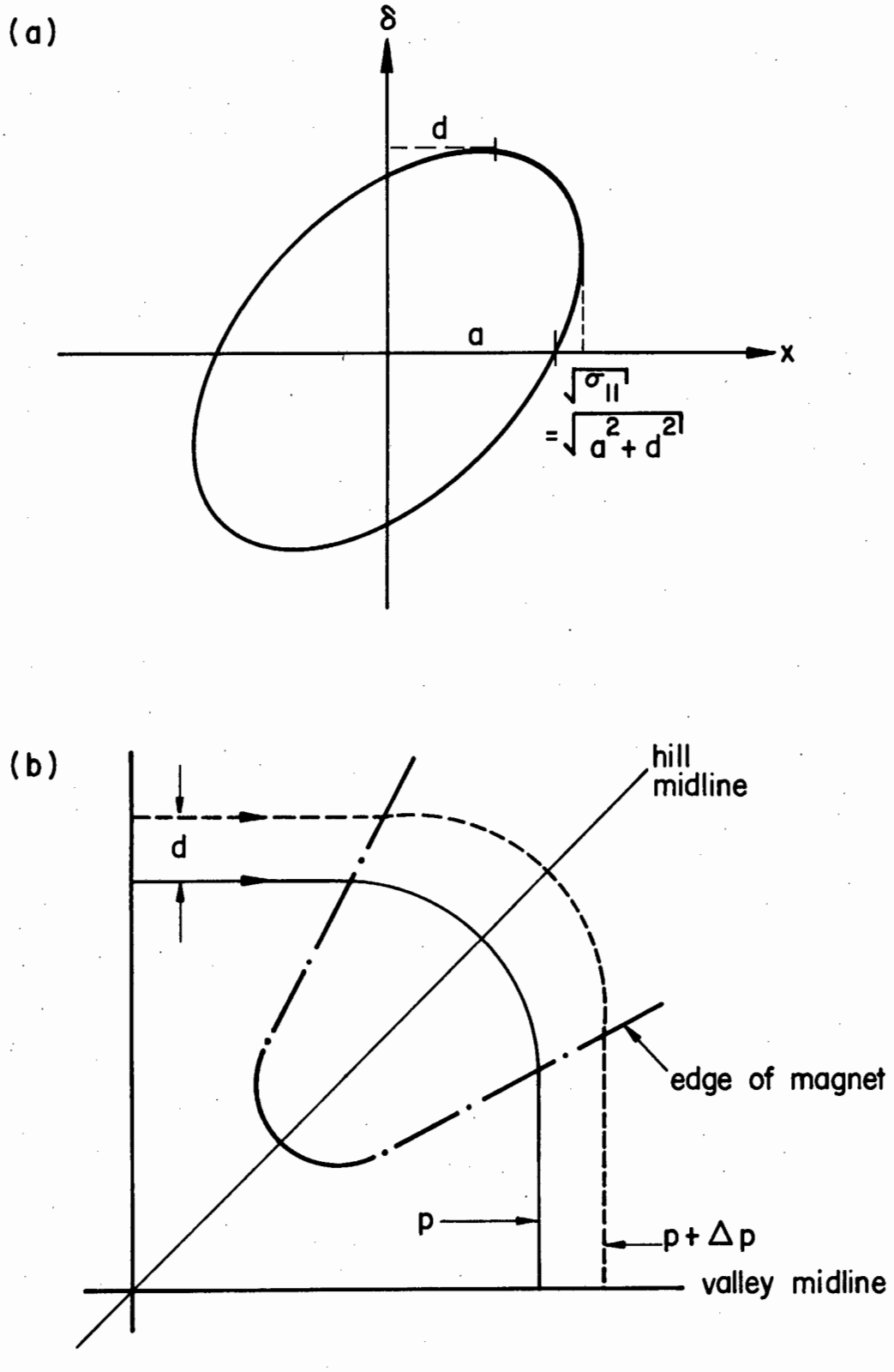

Figure 3.1: (a) The projection of the eigen-ellipsoid onto the x - δ plane.

(b) An equilibrium orbit shown in one quadrant of a 4-sector cyclotron.

Looking back at equation (3.8) we can see that positive σ_{16} implies positive σ_{25}. We can understand that σ_{25} must be positive by referring to figure 3.2. Consider particles with positive radial divergence at the valley. These must start forward of the bunch centre, as they will take a longer path through the sector magnet and will end up at the next valley with a negative divergence and a lag. Thus the positive correlation is conserved.

If σ_{25} is not correct, then the bunch length will oscillate on successive orbits. σ_{25} incorrect also implies σ_{16} wrong and the bunch width will oscillate as well. These effects are shown in figure 3.3.

Approximate values for the correlations r_{16} and r_{25} and $r_{26} = 0$ have recently been derived empirically for a sector cyclotron (CHA79a, CHA79b).

The vertical components of the eigen-ellipsoid are easily calculated: They are analogous to the horizontal components when we put $\sqrt{\sigma_{66}} = \delta = 0$ Thus from equation (3.16) we can find

$$\sigma_{33} = \left[\frac{R_{34}}{(1 - R_{33}^2)^{\frac{1}{2}}} \right] \varepsilon_y \qquad (3.18)$$

and from equation (3.15)

$$\sigma_{44} = \frac{(1 - R_{33}^2)^{\frac{1}{2}}}{R_{34}} \varepsilon_y \qquad (3.19)$$

We cannot find σ_{55} or σ_{66} from equation (3.4). These components of the eigen-ellipsoid are determined by the beam entering the cyclotron, and by the characteristics of the cyclotron other than the magnetic field, such as the size of the accelerating gaps, the voltage distribution along these gaps, etc. Initially assumptions have thus to be made about the bunch length and the momentum spread of the beam.

When making use of the eigen-ellipsoid to calculate the shape of the beam, we must remember to take into account the effect of the stray field through which it passes, either during extraction from the cyclotron, or during in-

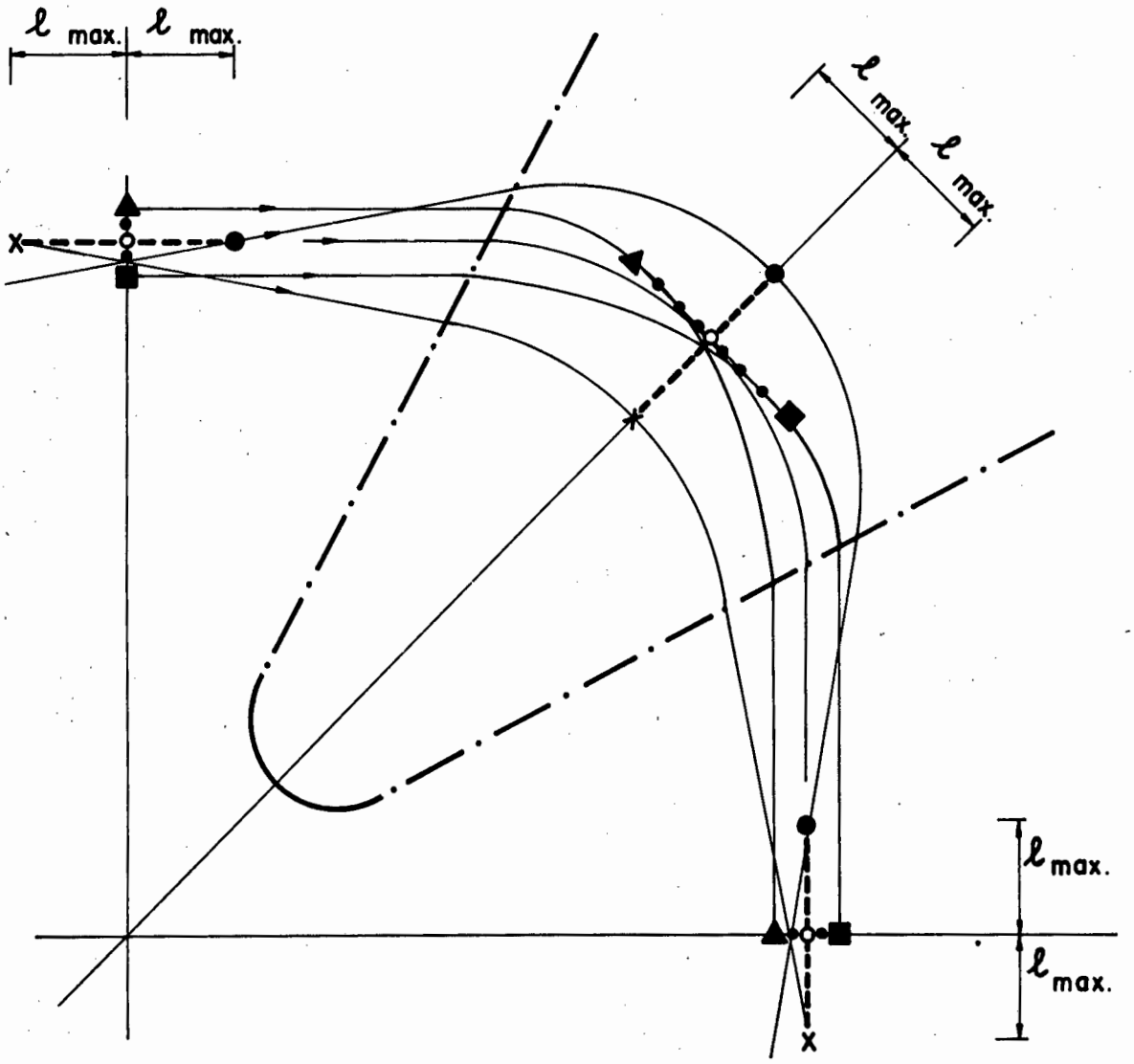

Figure 3.2: Five particles of a single bunch shown at various instants in time: at t = 0 the central particle crosses the valley; at t = $\tau/8$ the central particle crosses the hill; and at t = $\tau/4$ the central particle crosses the next valley. (τ is the period of revolution of particles along an equilibrium orbit.) The particles all have momentum p.

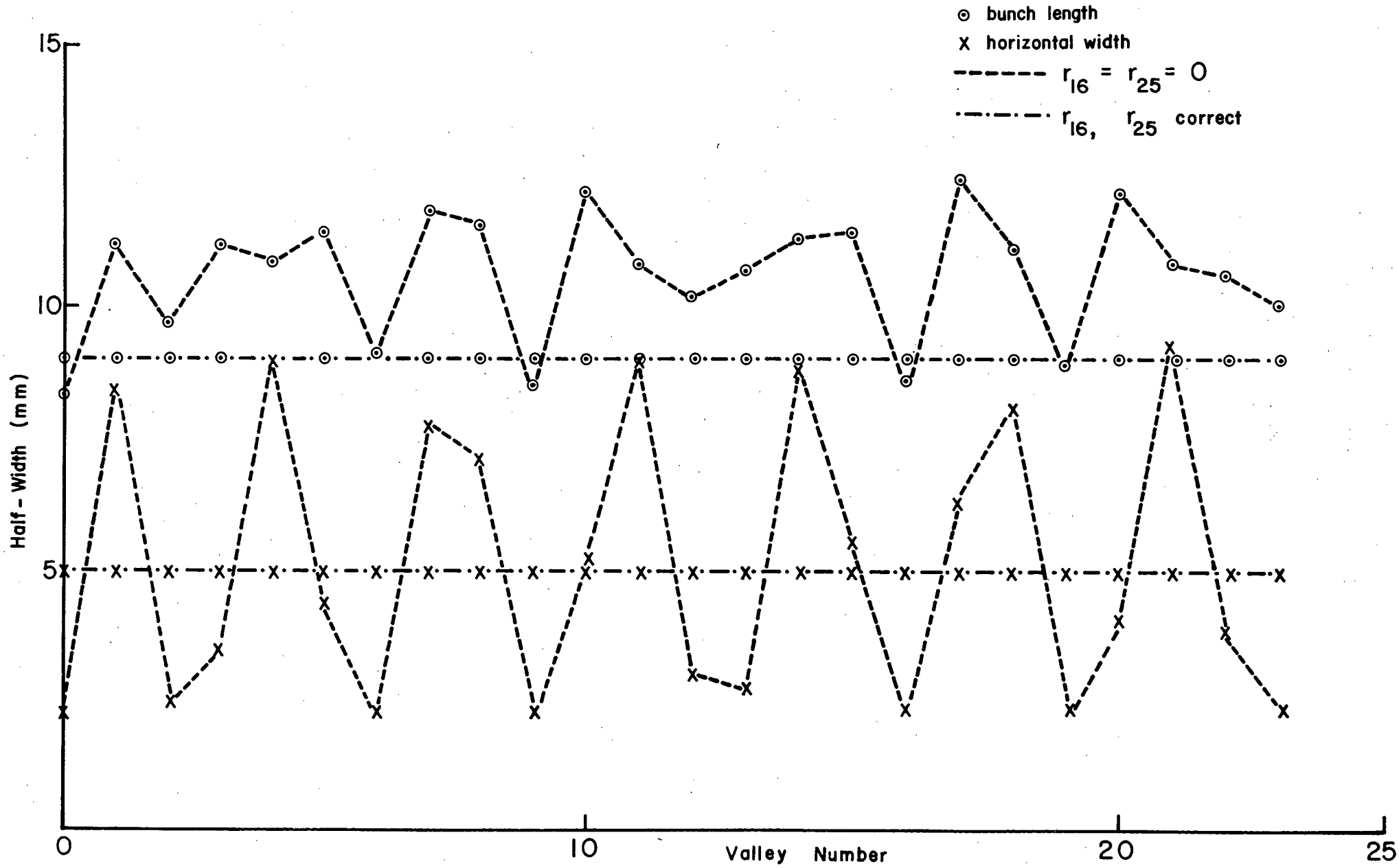

Figure 3.3: Oscillations in x and ℓ when $r_{16} = r_{25} = 0$, as compared to the constant values of x and ℓ when r_{16} and r_{25} have correct values.

jection into a cyclotron. We use the program STRAY mentioned above to find the direction of the beam and the transfer matrix of the stray field region.

4. BEAM TRANSPORT ELEMENTS

4.1 Introduction

A beam of particles traversing a field-free region will gradually spread out, increasing in the horizontal and vertical extent. This is due to the finite divergence of the beam. To counteract this transverse spreading we use magnetic quadrupoles, which act as lenses to focus the beam.

A pulsed beam traversing a field free region will also have its pulses spread longitudinally. This spreading arises from the momentum-spread of the beam, in that particles with higher momenta drift to the front of the pulse and their distance from the central particle gradually increases. We use bunchers to slow the front (faster) particles, and to speed up the rear (slower) particles. The buncher thus acts as a lens in longitudinal space.

Magnetic dipoles are used to bend the beam in the desired direction. Dipoles also have focussing properties but, for a fixed change in beam direction, these are not adjustable. Dipoles are not thus considered as variable focussing elements, but as beam-bending devices with focussing properties chosen and fixed before manufacture. Variable edge-angles (which introduce vertical focussing) are possible with some dipoles but this requires physical changes to the geometry which are best avoided.

We discuss below the characteristics and transfer matrices of drift lengths, quadrupoles, bunchers and dipoles. We also give a brief description of the aberrations associated with them.

4.2 Drift Lengths

Drift lengths are field-free regions of beamline. The divergence of a particle is thus not altered, and only its positional co-ordinates x and y change due to its divergence, in the following manner:

$$x(1) = x(0) + L\,x'(0) \qquad (4.1)$$

$$x'(1) = x'(0)$$

$$y(1) = y(0) + L\,y'(0) \qquad (4.2)$$

$$y'(1) = y(0)$$

where L is the distance through which the particle has drifted.

The co-ordinate ℓ specifying the distance from the centre of the bunch changes in a similar manner. If we consider the momentum spread δ as the longitudinal divergence, then the equation

$$\ell(1) = \ell(0) + \frac{L}{\gamma^2}\,\delta \qquad (4.3)$$

expressing the change in ℓ takes the same form as (4.1), (4.2).

The coefficient

$$1/\gamma^2 = 1 - v^2/c^2$$

is the relativistic correction.

The transfer matrix for a drift length L is thus

$$R = \begin{bmatrix} 1 & L & 0 & 0 & 0 & 0 \\ 0 & 1 & 0 & 0 & 0 & 0 \\ 0 & 0 & 1 & L & 0 & 0 \\ 0 & 0 & 0 & 1 & 0 & 0 \\ 0 & 0 & 0 & 0 & 1 & L/\gamma^2 \\ 0 & 0 & 0 & 0 & 0 & 1 \end{bmatrix} \qquad (4.4)$$

The effect of a drift length on an upright ellipse may be seen from figure 4.1.

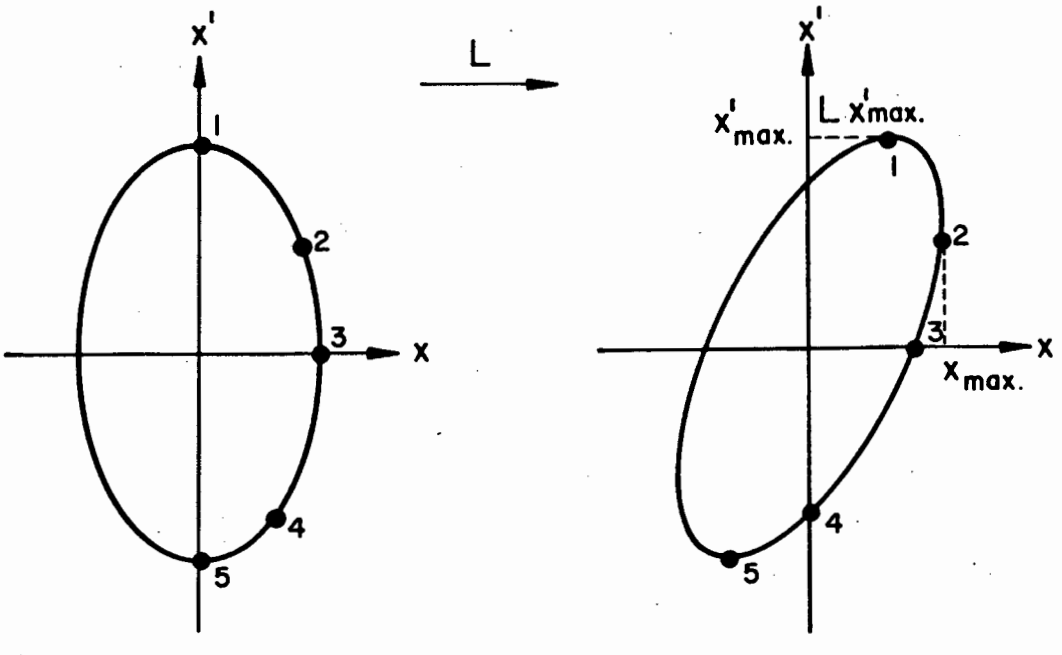

Figure 4.1: The effect of drift length L on an initially upright ellipse, showing individual particles 1 through 5 moving only laterally in x - x´ phase space.

4.3 Quadrupole Magnets

The ideal quadrupole magnet has hyperbolic poles. The shape of the resulting magnetic field is shown in figure 4.2.

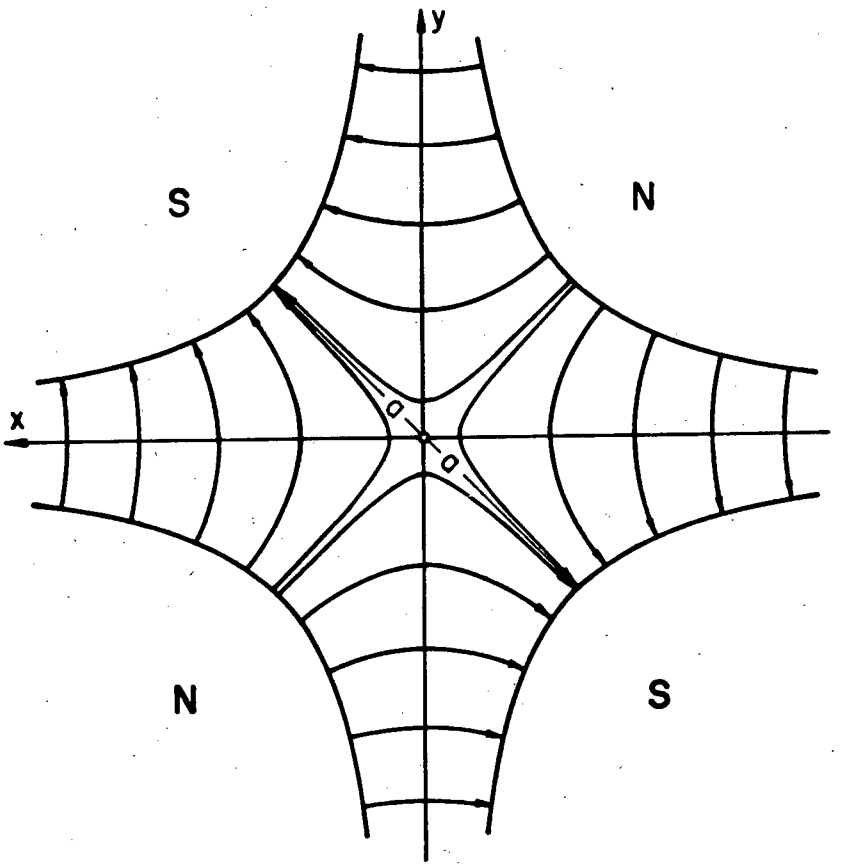

Figure 4.2: Field lines in a quadrupole magnet. A quadrupole with this configuration of polarities is termed positive for a beam travelling into the paper.

The equations of motion for a particle in a positive quadrupole field are

$$\frac{d^2x}{dz^2} + k^2 x = 0 \qquad (4.5)$$

$$\frac{d^2y}{dz^2} - k^2 y = 0 \qquad (4.6)$$

where $k^2 = \frac{B_o}{a} \frac{1}{(B\rho)}$

and B_0 is the magnetic field at the pole tip

a is the aperture radius

and $B\rho$ is the magnetic ridigity of the particle (equal to the ratio of particle momentum to particle charge $\frac{p}{q}$)

Equations (4.5) and (4.6) have solutions

$$\begin{aligned} x &= (\cos kL)\, x_0 + \left(\frac{\sin kL}{k}\right) x_0' \\ x' &= (-k \sin kL)\, x_0 + (\cos kL)\, x_0' \\ y &= (\cosh kL)\, y_0 + \left(\frac{\sinh kL}{k}\right) y_0' \\ y' &= (k \sinh kL)\, y_0 + (\cosh kL)\, y_0' \end{aligned} \qquad (4.7)$$

where L is the length of the quadrupole. These solutions imply focussing in the horizontal plane and defocussing in the vertical plane. If the quadrupole polarities were reversed so as to form a negative quadrupole, then the focussing properties in x and y would be reversed too.

From equations (4.7) we can write the transfer matrix for a (positive) quadrupole as follows (CHA60):

$$R = \begin{bmatrix} \cos kL & \frac{1}{k}\sin kL & 0 & 0 & 0 & 0 \\ -k \sin kL & \cos kL & 0 & 0 & 0 & 0 \\ 0 & 0 & \cosh kL & \frac{1}{k}\sinh kL & 0 & 0 \\ 0 & 0 & k \sinh kL & \cosh kL & 0 & 0 \\ 0 & 0 & 0 & 0 & 1 & L/\gamma^2 \\ 0 & 0 & 0 & 0 & 0 & 1 \end{bmatrix} \qquad (4.8)$$

If (for convenience) we look now at only the horizontal subspace we see that the transfer matrix for a quadrupole may be equated to the transfer matrices for two drift lengths d_x on either side of a thin lens, with focal length f_x, as follows (KNO63)

$$\begin{bmatrix} \cos kL & \frac{1}{k}\sin kL \\ -k \sin kL & \cos kL \end{bmatrix} = \begin{bmatrix} 1 & d_x \\ 0 & 1 \end{bmatrix} \begin{bmatrix} 1 & 0 \\ -1/f_x & 1 \end{bmatrix} \begin{bmatrix} 1 & d_x \\ 0 & 1 \end{bmatrix} \qquad (4.9)$$

where $d_x = \frac{1}{k} \tan \frac{kL}{2}$ and $f_x = \frac{1}{k \sin kL}$ (4.10)

The effect of a thin lens on a particle is to change its divergence while leaving its displacement unaltered, i.e.

$$\begin{aligned} x(1) &= x(0) \\ x'(1) &= -x(0)/f_x + x'(0) \end{aligned} \tag{4.11}$$

If the lens is focussing in the horizontal direction, it will defocus in the vertical, and the equivalent equations to (4.11) will be:

$$\begin{aligned} y(1) &= y(0) \\ y'(1) &= y(0)/f_y + y'(0) \end{aligned} \tag{4.12}$$

where $f_y = \dfrac{1}{k \sinh kL}$ and $d_y = \dfrac{1}{k} \tanh \dfrac{kL}{2}$ (4.13)

For small values of k we make the following approximations (STE65)

$$f_o = f_x = f_y = 1/(k^2 L) \tag{4.14}$$

and $d_x = d_y = L/2$

i.e. the quadrupole may be approximated by a thin lens at its centre.

The action of a thin lens on a phase ellipse is shown in figure 4.3.

The representation of a quadrupole as a thin lens using the approximation (4.14) is extremely useful in the analytic treatment of systems containing many quadrupoles (REG67, BAN66, STEF65, BRO71). We will use it in chapter 5, while in chapter 6 we use a better approximation to equations (4.10) and (4.13)(REG67), namely

$$\begin{aligned} f_x &= f_o + L/6 \\ f_y &= f_o - L/6 \end{aligned} \tag{4.15}$$

for a positive quadrupole.

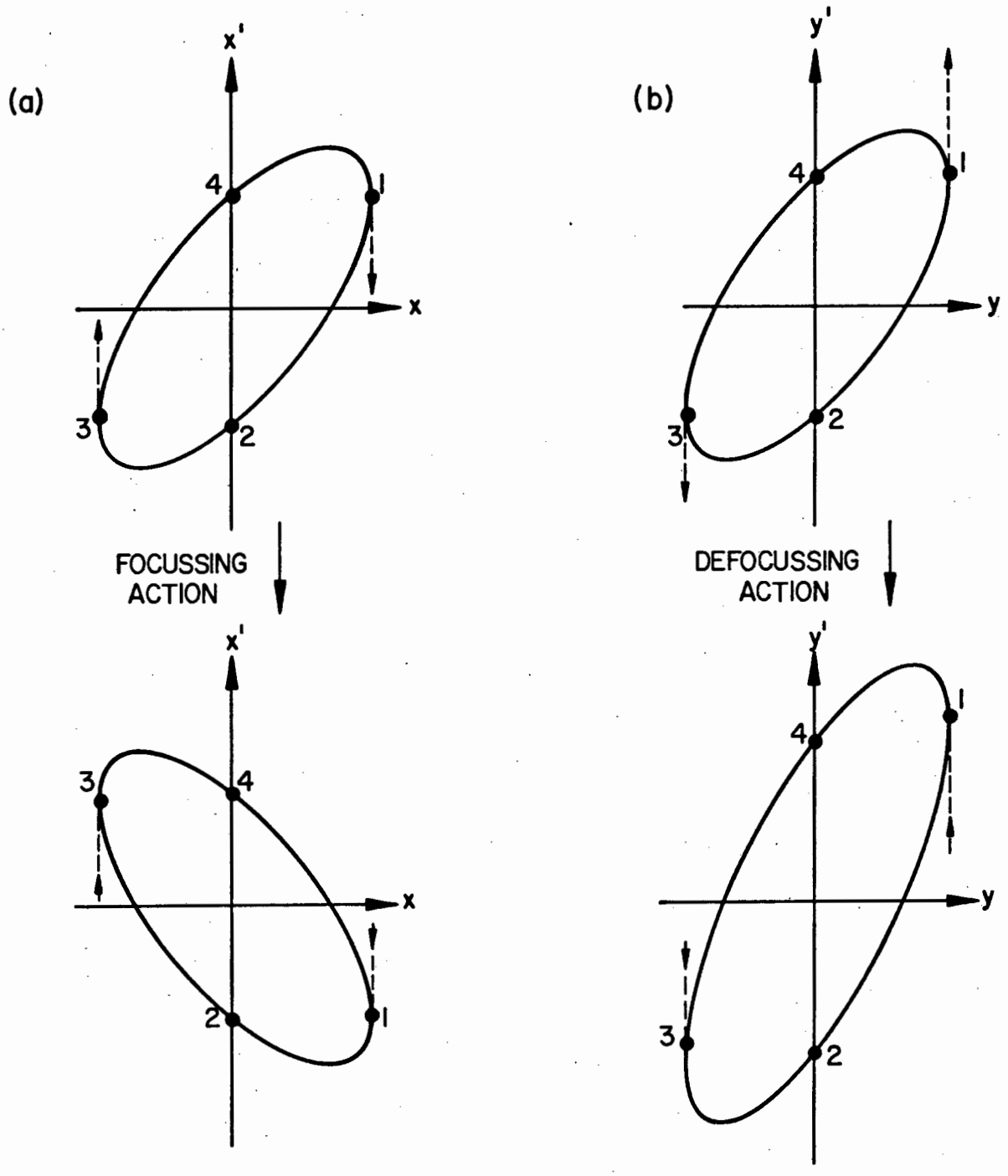

Figure 4.3: Simultaneous effect of a thin lens on an x - x´ ellipse-focus= sing action - and on the corresponding y - y´ ellipse-defocus= sing action.

4.4 Bunchers

Bunchers are used to shorten the pulse length of a beam. Klystron bunchers (BAN66, HIN75b) are the type most commonly used with cyclotron beams. They consist of a drift tube, connected to a radio-frequency voltage, separated from earthed tubes on either side by short gaps. This is shown in figure 4.4.

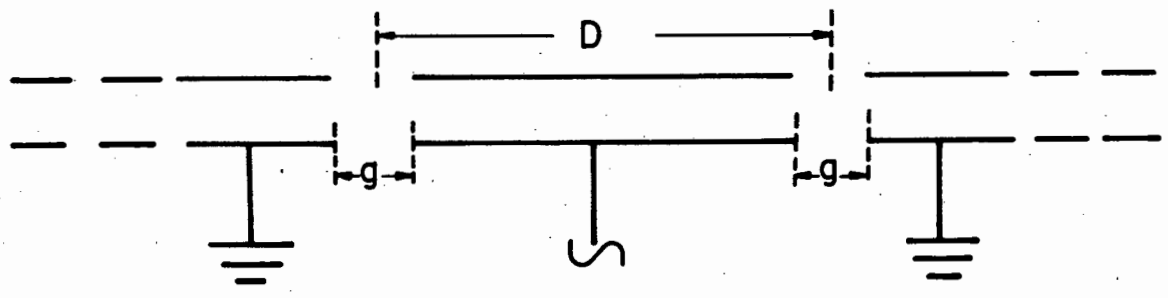

Figure 4.4: Buncher configuration. We assume that the gap width g is small compared to D, the length of the drift tube.

The particle at the centre of the bunch should cross the gaps when the voltage on the drift tube is zero to avoid a nett change in the beam energy. The particles at the front of the bunch must be decelerated, and those at the back accelerated, to achieve a pulse shortening further down the beamline. This implies that in the time taken for the particles with velocity v to cross from one gap to the next (D/v), the phase of the voltage should have changed by π, (or $[2n + 1]\pi$). If the frequency of the voltage is $f = \frac{\omega}{2\pi}$,

then the length of the drift tube D may be found from the expression

$$\frac{D}{v} = \frac{\pi}{\omega} \qquad (4.16)$$

At any gap the bunch length ℓ is not altered (assuming the gap length g is small compared to D), but the momentum spread changes, as expressed by:

$$\delta(\ell) = \delta(0) - \frac{V(\ell)}{V_o}$$

where $V(\ell) = V_{max} \sin(\omega \ell / v)$.

V_{max} being the amplitude of the sinusoidally varying voltage, and

$$V_o = \frac{p^2}{2\,mq}$$

the electric rigidity of the particles. If we assume that we use only the linear portion of the sine wave for bunching, then we can write

$$V(\ell) \simeq V_{max}\, \omega \ell / v$$

For the longitudinal co-ordinates ℓ and δ we have thus

$$\begin{aligned} \ell(\ell) &= \ell(0) \\ \delta(\ell) &= -\left(\frac{V_{max}\,\omega}{V_o\, v}\right) \ell + \delta(0) \end{aligned} \qquad (4.17)$$

If we compare equations (4.17) to (4.11) we see that the focal length of the total buncher, f_b, is then half the focal length of each gap, i.e.

$$f_b = \tfrac{1}{2} \left(\frac{V_o\, v}{V_{max}\, \omega}\right) \qquad (4.18)$$

[In practice this is only approximately true. The correct expression for f_b is:

$$f_b = \frac{(f_s/2)^2}{f_s/2 - D}$$

where $f_s = \dfrac{V_o\, v}{V_{max}\, \omega}$

The approximation is valid for $f_s >> D$, which is generally true.]

The transfer matrix in longitudinal phase space is

$$\begin{bmatrix} R_{55} & R_{56} \\ R_{65} & R_{66} \end{bmatrix} = \begin{bmatrix} 1 & 0 \\ -1/f_b & 1 \end{bmatrix} \qquad (4.19)$$

Because we are not dealing with static fields here, Liouville's theorem is not valid, and thus phase space is not conserved. The momentum spread of the beam may be altered by the buncher. However if the buncher is placed midway in the beamline then δ will remain approximately the same. This positioning of the buncher also results in minimum buncher strength.

A side-effect of longitudinal bunching is a radial defocussing due to the variation of buncher potential in time. Hinderer (HIN75b) has derived the relationship between this defocussing action and the longitudinal focussing as follows:

$$f_r = -2 f_b$$

where f_r is the focal length in either the horizontal or vertical planes. As the focal lengths of Klystron bunchers tend to be fairly long, the effect of the radial defocussing is not large. The effect may be further reduced by arranging for horizontal and vertical waists at the centre of the buncher.

4.5 Dipole Magnets

The equation describing the trajectory of a particle of mass m, charge q and velocity v through a dipole with field strength B_o is

$$\frac{mv^2}{\rho} = q B_o v$$

where ρ is the radius of the trajectory.

If the length of the trajectory through the dipole is L, then the particle is deflected through an angle α, where

$$\alpha = L/\rho$$

Since ρ is proportional to mv, the deflection through a given magnet becomes less as the momentum increases, and particles with different momenta are bent through different angles. A beam with no correlation between horizontal position and momentum (upright ellipse in $x - \delta$, $r_{16} = 0$) and

no correlation between horizontal divergence and momentum (upright ellipse in $x'-\delta$, $r_{26} = 0$) is termed achromatic. An achromatic beam passing through a dipole ($<360^{o}$) will become dispersed, and can only be made achromatic again by passing the beam through another dipole with the correct initial dispersion (r_{16}) and angular dispersion (r_{26}).

We consider firstly a dipole with straight entry and exit faces at right angles to the central trajectory, shown in figure 4.5. We define the field index n as follows (PEN61).

$$n \equiv -\frac{\rho}{B}\frac{\partial B}{\partial \rho}$$

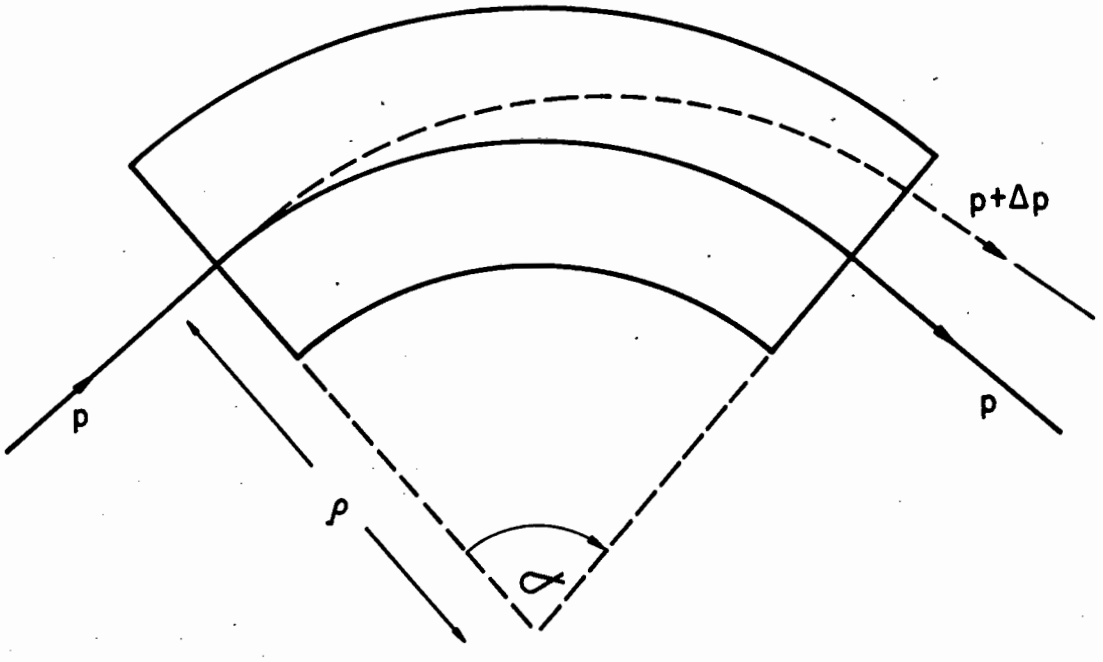

Figure 4.5: A dipole with entry and exit faces at right angles to the central trajectory, momentum p. The path of the dispersed ray momentum(p+Δp) is also shown.

The transfer matrix of the dipole has been derived (PEN61, BRO72) to be

$$
R = \begin{bmatrix}
\cos k_x L & \frac{1}{k_x}\sin k_x L & 0 & 0 & 0 & \frac{1}{\rho k_x^2}(1-\cos k_x L) \\
-k_x \sin k_x L & \cos k_x L & 0 & 0 & 0 & \frac{1}{\rho k_x}\sin k_x L \\
0 & 0 & \cos k_y L & \frac{1}{k_y}\sin k_y L & 0 & 0 \\
0 & 0 & -k_y \sin k_y L & \cos k_y L & 0 & 0 \\
-\frac{1}{\rho k_x}\sin k_x L & -\frac{1}{\rho k_x^2}(1-\cos k_x L) & 0 & 0 & 1 & -\frac{1}{\rho^2 k_x^3}(k_x L - \sin k_x L) + L/\gamma^2 \\
0 & 0 & 0 & 0 & 0 & 1
\end{bmatrix}
\quad \ldots (4.20)
$$

where $k_x^2 \equiv (1 - n)/\rho^2$ $\qquad$ $k_y^2 \equiv n/\rho^2$ $\qquad$ (4.21)

We get various focussing effects depending on the value of n:

$n<0$	focussing horizontally, defocussing vertically
$n=0$	focussing horizontally, no effect in the vertical plane
$0<n<1$	focussing both horizontally and vertically
$n=1$	focussing vertically, no effect horizontally
$n>1$	focussing vertically, defocussing horizontally

We now look at a dipole with arbitrary entrance and exit angles, β_1 and β_2 respectively, as shown in figure 4.6.

From purely geometrical considerations we can see that a particle will be focussed horizontally by a negative edge angle, and defocussed by a positive edge angle. To explain the effect on the vertical extent we have to take into account the fringing field at the edge of the dipole, as shown in figure 4.7. The radial component B_x of the horizontal field B_H causes a focussing force in the vertical direction (proportional to $\underline{B}_x \times \underline{v}$) for positive values of β, and a defocussing force for negative values of β.

The effect of the edge angle may thus be compared to that of the thin-lens effect of a quadrupole, and the transfer matrix of edge-angle β is written as follows:

$$R = \begin{bmatrix} 1 & 0 & 0 & 0 & 0 & 0 \\ \frac{\tan\beta}{\rho} & 1 & 0 & 0 & 0 & 0 \\ 0 & 0 & 1 & 0 & 0 & 0 \\ 0 & 0 & \frac{-\tan(\beta-\psi)}{\rho} & 1 & 0 & 0 \\ 0 & 0 & 0 & 0 & 1 & 0 \\ 0 & 0 & 0 & 0 & 0 & 1 \end{bmatrix} \qquad (4.22)$$

where ψ is a parameter depending on the shape of the fringing field (ENG64, BRO72).

Positive edge-angles provide a useful means of achieving vertical focussing in a uniform-field dipole. The edge-angles should not, however, be

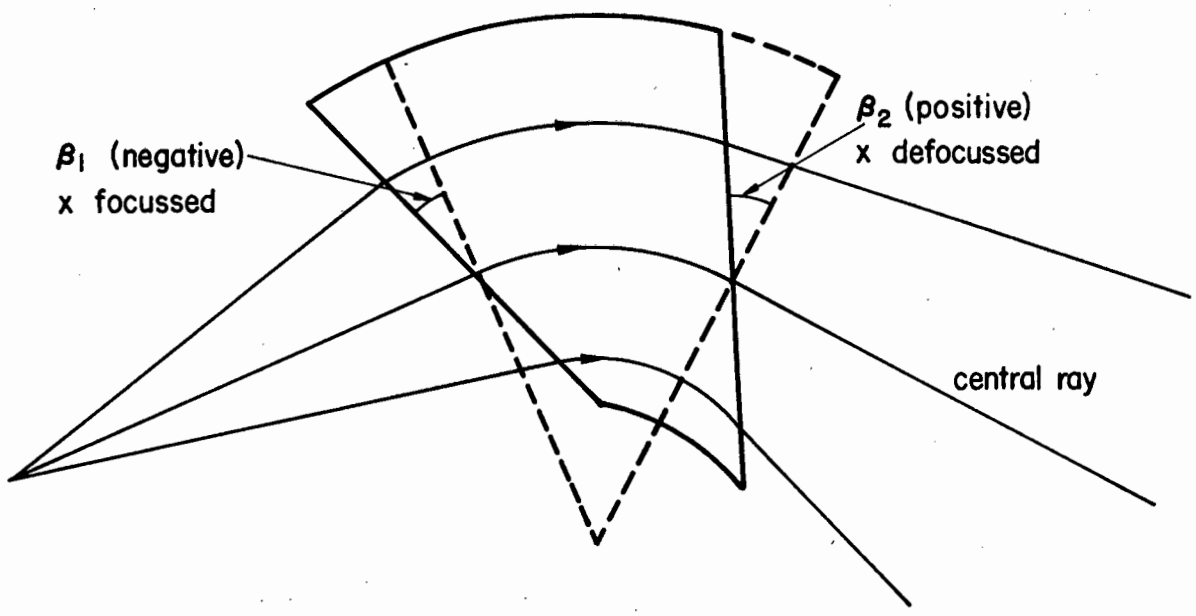

Figure 4.6: Dipole with edge angles β_1 and β_2.

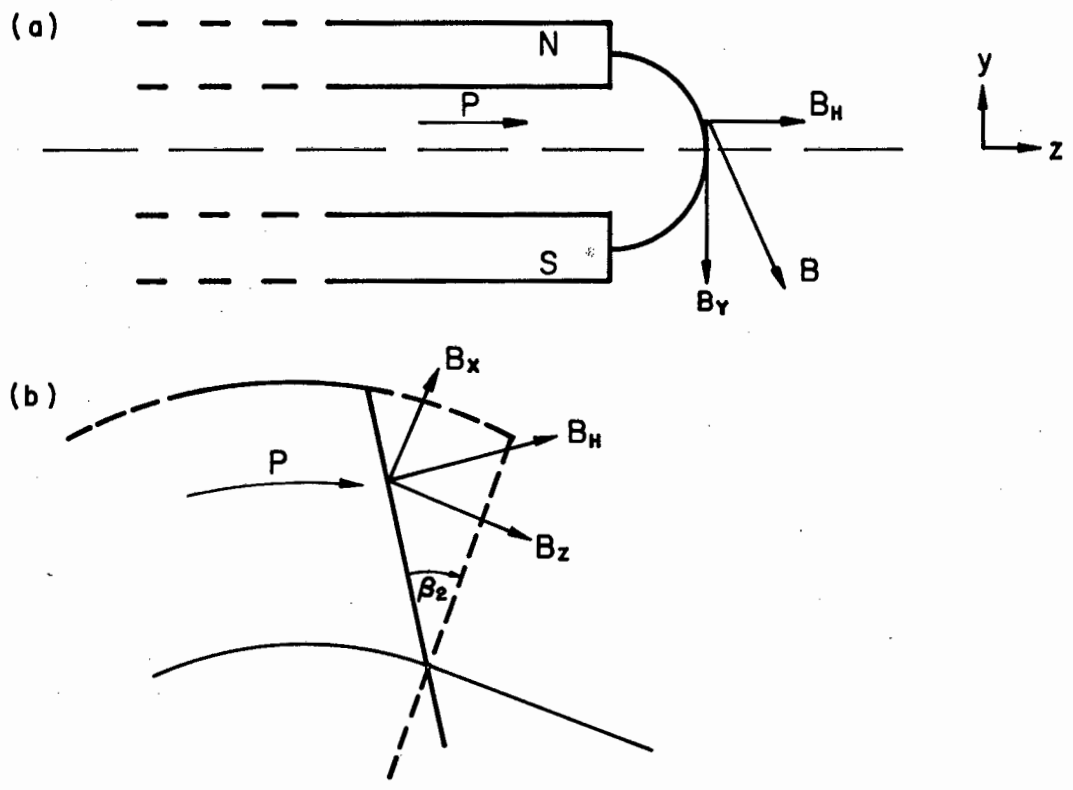

Figure 4.7: Components of the fringing field:

(a) side view showing horizontal (B_H) and vertical (B_y) components at a point y>0

(b) plan view at y>0 showing radial (B_x) and longitudinal (B_z) components of the horizontal field (B_H).

too large, otherwise second-order terms may cause undesirable effects (BAN66).

Edge angles may be chosen to bring both the horizontal and vertical point-rays to a focus at the same image point. The dipole is then said to be "double-focussing" (CRO51, ENG67). A pair of identical edge-angles is often used, thus forming a symmetrical dipole. The double focussing edge-angles $\beta_1 = \beta_2$ may then be calculated from the equation

$$\tan \beta_1 = \tan \beta_2 = \tfrac{1}{2} \tan \alpha/2$$

and the image and object distances, D, from

$$D = \frac{2\rho}{\tan \alpha/2}$$

where α is the bending angle and ρ the bending radius.

A vast amount of literature on dipoles exists, especially (LIV69) and references therein. No further discussion of dipoles is thus warranted here, as equations (4.20) through (4.22) are sufficient for our use in subsequent chapters.

4.6 Aberrations

The aberrations present in a beamline represent a departure from the ideal first-order design. The second-order terms are represented by the matrix elements T_{ijk}, which were defined in equation (2.3):

$$x_i(1) = \sum_{j=1}^{6} R_{ij} x_j(0) + \sum_{j=1}^{6} \sum_{k=1}^{6} T_{ijk} x_j(0) x_k(0) \qquad (2.3)$$

The elements T_{ijk} may be classified as geometric when i, j and k are equal to 1, 2, 3 or 4, because the effects they produce are independent of variations in momentum. When j or k is equal to 6 they are called chromatic (BRO79) because the resultant effects depend directly on particle momentum (and thus particle energy). The derivation of the second-order matrix elements T_{ijk}, where i=1, ..., 4, may be found in (BRO72). (T_{5jk} are seldom examined because the changes to the bunch length due to second-order effects are immaterial for most beamline applications.

In practice bunchers are usually tuned about the theoretical (first-order) settings to achieve the desired effect, making second-order bunch-length calculations superfluous).

The second-order terms cause a shift in the beam centroid:

$$\bar{x}_i(1) = \sum_{j=1}^{6} \sum_{k=1}^{6} T_{ijk}\, \sigma_{jk}(0) \qquad (4.23)$$

and a distortion of the ellipsoid in phase space:

$$\sigma_{ij}(1) = \sum_{k,\ell} R_{ik}\, R_{j\ell}\, \sigma_{k\ell}(0) + 2 \sum_{\ell,m}\left[\sum_{k} T_{ik\ell}\, \sigma_{km}(0)\right]\left[\sum_{n} T_{jmn}\, \sigma_{\ell n}(0)\right] \qquad \ldots (4.24)$$

Liouville's theorem is still valid and the distorted ellipsoid does not increase its phase space volume during distortion. However, if we <u>enclose</u> the distorted ellipsoid in a new ellipsoid, then it will give the appearance of a phase space increase.

The only second-order terms arising from an <u>ideal</u> quadrupole are chromatic. These arise from the fact that the quadrupole strength k is inversely proportional to the square root of particle momentum. Thus particles with momentum p + Δp are bent less than those with momentum p, and a subsequent image will be blurred rather than sharp. An example is given for a single quadrupole operating in point-to-point mode with object distance P, focal length f ($=1/k^2L$). The rays with momentum p + Δp are focussed a distance Δz beyond the focus of rays with momentum p, where (REG63)

$$\Delta z = \frac{P^2 f}{(P - f)^2} \cdot \frac{\Delta p}{p}$$

At the position where the central momentum rays focus, the image is thus broadened by Δx, where

$$\Delta x = \left[\frac{P^2}{P - f}\right] x_o \cdot \frac{\Delta p}{p}$$

The term in square brackets is thus the quantity T_{126}.

It can be shown (STE65, DYM65b, COU71) that achromatic focussing is im-

possible in a system consisting of magnetic quadrupoles only. The aberrations may be reduced, however, by using symmetrical systems (see chapter 5).

In dipoles we get geometric as well as chromatic aberrations. An example is the geometric term T_{122}, which arises when rays enter a flat-edged dipole at an angle, as in figure 4.8a. The ray with $+x_o'$ is then bent through a larger angle than the central ray, and is focussed to cross the axis before the plane of the ideal image. This effect may be corrected by using circular edges, as shown in figure 4.8b (LIV69, BRO65). Further geometric effects arise in the fringing field region (ENG64, BRO70, HEN74).

When second-order effects are large, they may have to be corrected. This may be done by shimming the pole-pieces of the dipoles (LIV69, ENG67) and/or the addition of multipoles to the beamline (BAN66). In either case the first-order optics of the beamline is not affected.

Although the computer program TRANSPORT (BRO77) calculates the second-order terms, the program TURTLE (BRO74) is more useful in this application, because it allows us to examine the distortion of the ellipsoid.

In practice the second-order contributions to the beam are small if the beam extent in the elements is small, and correcting elements are generally only necessary for high resolution beamlines such as those for magnetic spectrometers (HIN75b).

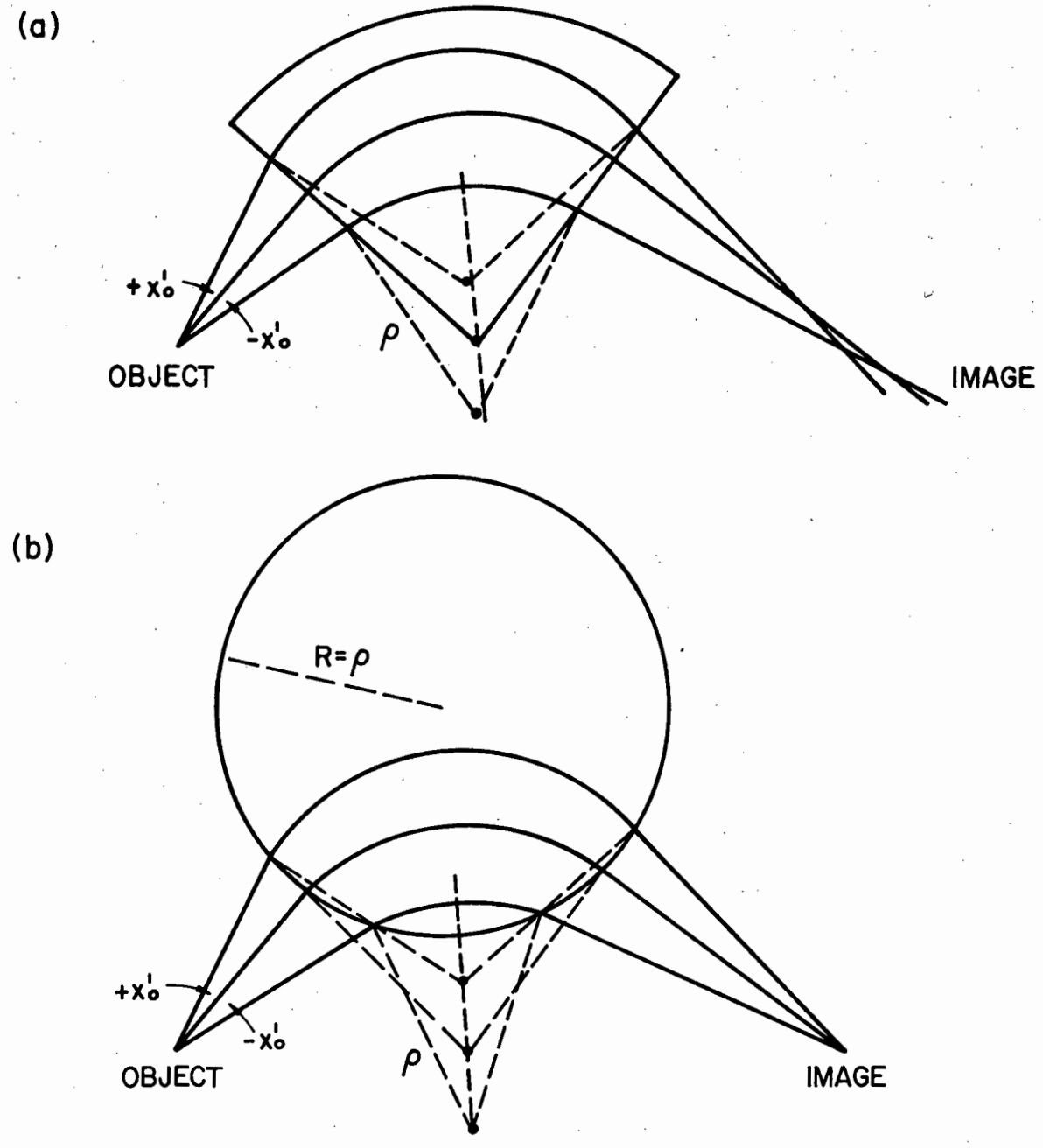

Figure 4.8 : (a) Imperfect image resulting from flat-faced dipole.
(b) Circular pole faces correct this effect.

5. PROPERTIES OF SYMMETRICAL SYSTEMS

5.1 Introduction

It is often convenient to group beamline elements into symmetrical systems because of the useful properties which these exhibit.

Six different kinds of beamline symmetry can be defined. All six have not, however, been treated together systematically before. These symmetries are defined schematically in figure 5.1, with examples of beamlines arranged according to symmetry in figure 5.2. Historically, mirror and anti-translational (i.e. rotation of translated system through 180^{o}) symmetries were examined first (PEN61, BLI64). Then anti-mirror symmetry (i.e. rotation through 180^{o} after reflection) was studied (HER66). Subsequently an analysis was made (HAL76) of cross-translational and cross-mirror symmetries (i.e. rotation through 90^{o} after translation, and after reflection, respectively). At about the same time a treatment appeared (KAR76) of the group of symmetries consisting of translational, cross-translational, mirror and cross-mirror, when only quadrupoles are present in the beamline (i.e. no dipoles). (Note: if rotation through $+90^{o}$ and -90^{o} are regarded as distinct cases, then eight symmetries exist: see section 5.8.)

We have used the symplectic equations (2.9) and (2.10) to simplify the expressions in the matrix elements of the symmetrical systems. This aids us in drawing conclusions about the properties of these systems.

In the sections below we show how the R-matrix of a symmetric system may be obtained if we know the matrix M of one half-system. We discuss the properties of the R-matrix derived for each case. We also examine the T-matrix (second-order effects) for some special cases.

5.2 Translational Symmetry

In this case the second half-system is identical to the first half-system, and

$$M_t = M$$

where M is the transfer matrix of the first half (see figure 5.1a and 5.2a). If R_t describes the composite system, then

$$R_t = MM$$

and

$$R_t = \begin{bmatrix} M_{11}(M_{11}+M_{22})-1 & M_{12}(M_{11}+M_{22}) & 0 & 0 & 0 & M_{16}(M_{11}+M_{22})+(M_{16}-M_{52}) \\ M_{21}(M_{11}+M_{22}) & M_{22}(M_{11}+M_{22})-1 & 0 & 0 & 0 & M_{26}(M_{11}+M_{22})+(M_{26}+M_{51}) \\ 0 & 0 & M_{33}(M_{33}+M_{44})-1 & M_{34}(M_{33}+M_{44}) & 0 & 0 \\ 0 & 0 & M_{43}(M_{33}+M_{44}) & M_{44}(M_{33}+M_{44})-1 & 0 & 0 \\ M_{51}(M_{11}+M_{22}) & M_{52}(M_{11}+M_{22}) & 0 & 0 & 1 & 2M_{56}+ \\ +(M_{26}+M_{51}) & -(M_{16}-M_{52}) & & & & M_{51}M_{16}+M_{52}M_{26} \\ 0 & 0 & 0 & 0 & 0 & 1 \end{bmatrix}$$

... (5.1)

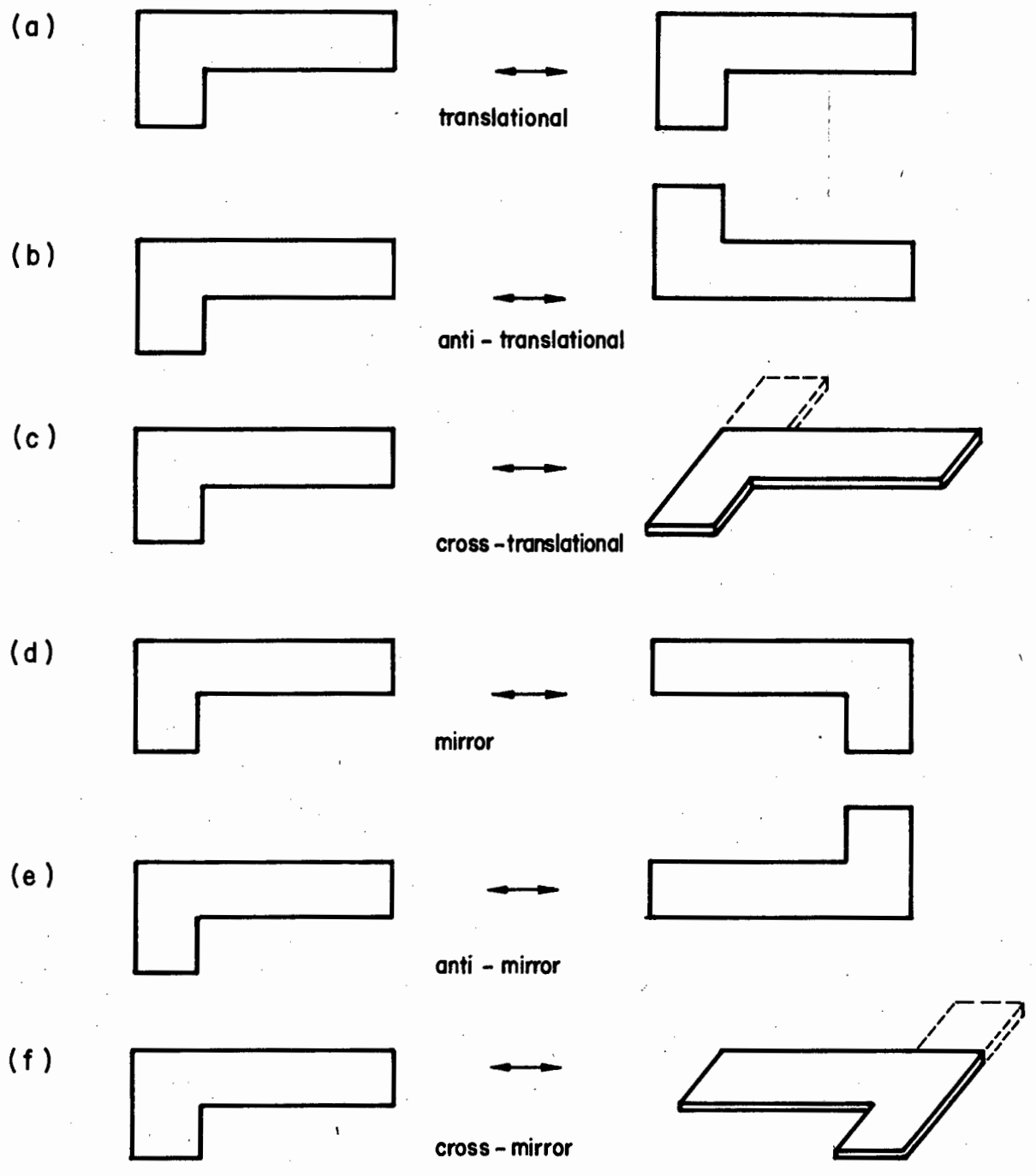

Figure 5.1: Schematic representation of the beamline symmetries discussed. Note that for quadrupoles there is no distinction between left and right (unlike dipoles), and symmetries (a) and (b) are indistinguishable, as are (d) and (e). Althought symmetries (c) and (f) each have two possibilities for dipoles, they involve bends in different planes (i.e. of little practical application) and these are thus usually restricted to quadrupole systems.

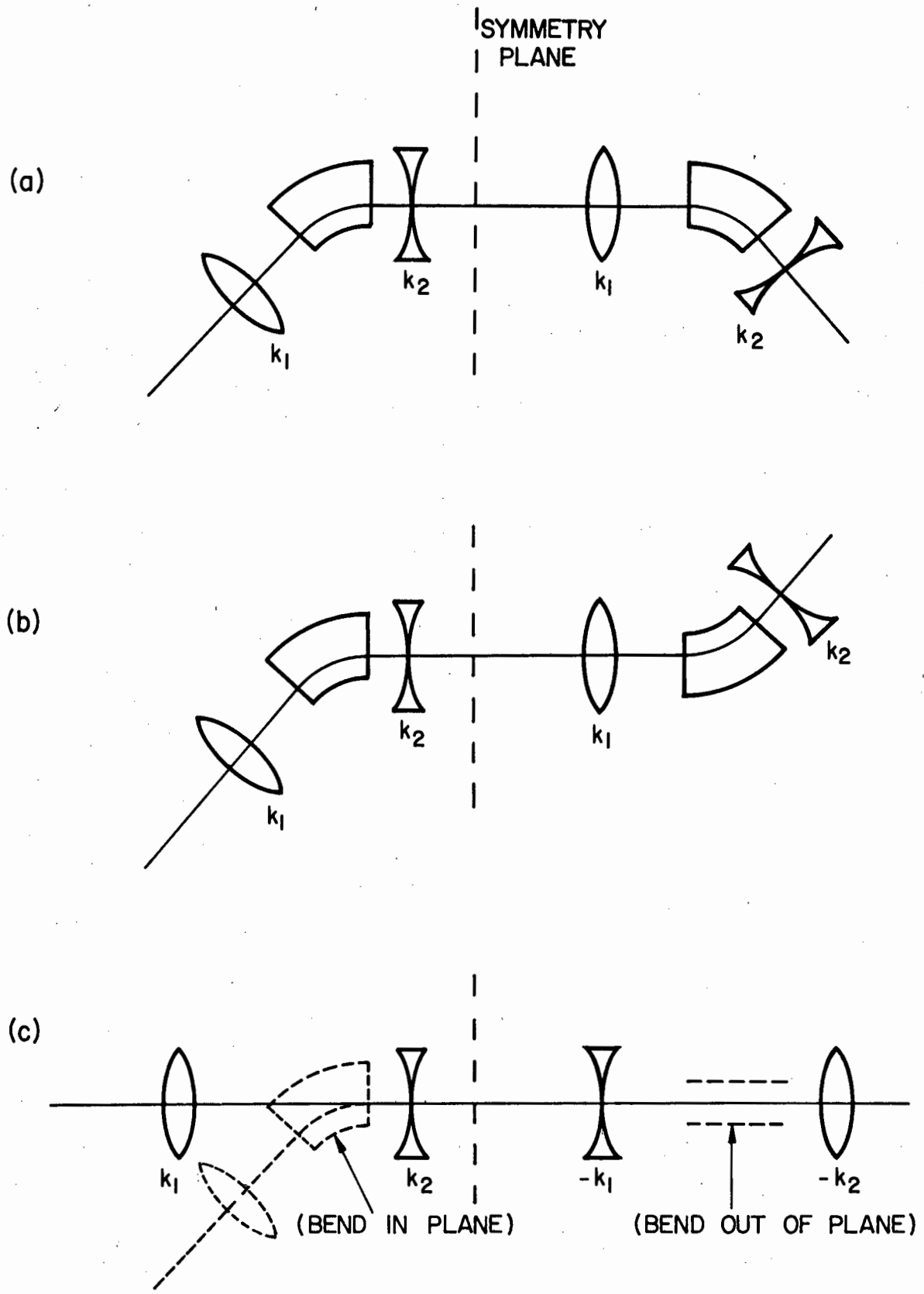

Figure 5.2: Examples of translational-type symmetries

(a) translational symmetry

(b) anti-translational symmetry

(c) cross-translational symmetry (dipoles seldom used)

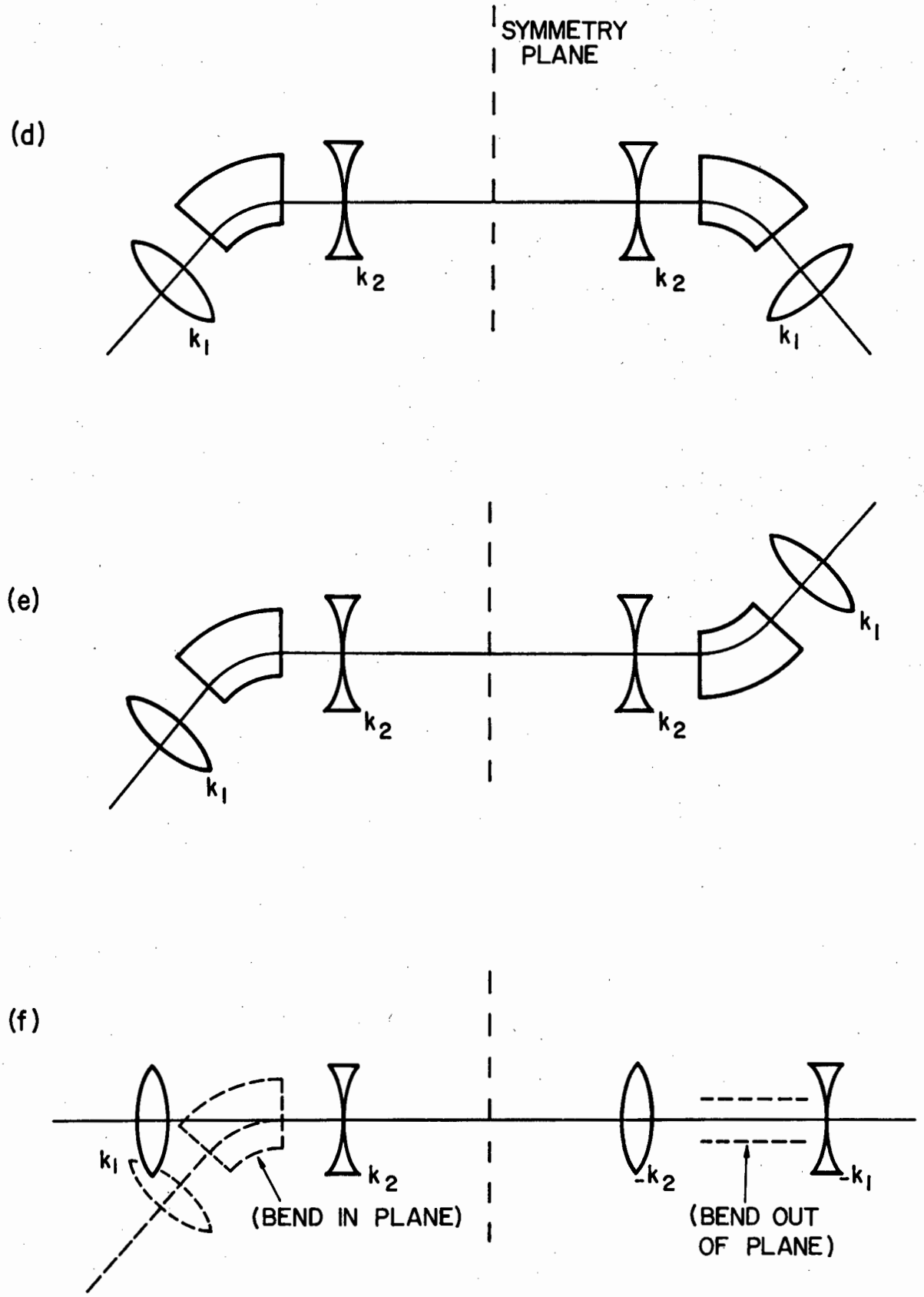

Figure 5.2 continued: Examples of mirror-type symmetries

(d) mirror symmetry

(e) anti-mirror symmetry

(f) cross-mirror symmetry

In the special case where

$$M_{11} + M_{22} = 0$$
$$M_{33} + M_{44} = 0 \qquad (5.2)$$

we get

$$R_t = \begin{bmatrix} -1 & 0 & 0 & 0 & 0 & M_{16} - M_{52} \\ 0 & -1 & 0 & 0 & 0 & M_{26} + M_{51} \\ 0 & 0 & -1 & 0 & 0 & 0 \\ 0 & 0 & 0 & -1 & 0 & 0 \\ M_{26} + M_{51} & -(M_{16} - M_{52}) & 0 & 0 & 1 & 2M_{56} + M_{51}M_{16} + M_{52}M_{26} \\ 0 & 0 & 0 & 0 & 0 & 1 \end{bmatrix}$$

... (5.3)

This system is doubly telescopic (i.e. the x, x´, y, y´subspace is exactly reproduced - with inversion in this case - at the image point: see chapter 6). In addition, this system will have zero dispersion when either $M_{16} = M_{52} = 0$, or when $M_{16} = M_{52}$. Similarly it will have zero angular dispersion when either $M_{26} = M_{51} = 0$, or when $M_{26} = -M_{51}$.

5.3 Anti-translational Symmetry

Here the second half-system is obtained by traversing the elements of the first half-system in the same order after first having rotated it by 180^{o} (HER66). This is shown in figures 5.1b and 5.2b. If there are no dipoles present then this symmetry type is identical to translational symmetry.

M_{at} differs only from M in the signs of the elements M_{16}, M_{26}, M_{51} and M_{52}. Thus

$$R_{at} = M_{at}\, M$$

becomes

$$R_{at} = \begin{bmatrix} M_{11}(M_{11} + M_{22})-1 & M_{12}(M_{11} + M_{22}) & 0 & 0 & 0 & M_{16}(M_{11}+M_{22}) - (M_{16}+M_{52}) \\ M_{21}(M_{11} + M_{22}) & M_{22}(M_{11} + M_{22})-1 & 0 & 0 & 0 & M_{26}(M_{11}+M_{22}) - (M_{26}-M_{51}) \\ 0 & 0 & M_{33}(M_{33} + M_{44})-1 & M_{34}(M_{33} + M_{44}) & 0 & 0 \\ 0 & 0 & M_{43}(M_{33}+M_{44}) & M_{44}(M_{33} + M_{44})-1 & 0 & 0 \\ -M_{51}(M_{11} + M_{22}) & -M_{52}(M_{11} + M_{22}) & 0 & 0 & 1 & 2\,M_{56} \\ +(M_{26} - M_{51}) & +(M_{16} + M_{52}) & & & & -(M_{51}\,M_{16} + M_{52}\,M_{26}) \\ 0 & 0 & 0 & 0 & 0 & 1 \end{bmatrix}$$

... (5.4)

In the special case of equation (5.2), we again get a double-telescopic sub-matrix, while the non-zero off-diagonal terms now become

$$\begin{aligned} R_{16} &= -(M_{16} + M_{52}) = -R_{52} \\ R_{26} &= -(M_{26} - M_{51}) = -R_{51} \\ R_{56} &= 2\,M_{56} - (M_{51}\,M_{16} + M_{52}\,M_{26}) \end{aligned} \qquad (5.5)$$

We can see that the dispersion, R_{16}, will now be zero for either $M_{16} = M_{52} = 0$, or for $M_{16} = -M_{52}$. Similarly the angular dispersion, R_{26}, will be zero for either $M_{26} = M_{51} = 0$, or for $M_{26} = M_{51}$.

5.4 Cross-translational Symmetry

For this symmetry the second half-system is obtained by traversing the first half-system in the same order after first having rotated it through 90^{o}. This system is shown in figures 5.1c and 5.2c. This system is not likely to be used with dipoles (HAL76), so we restrict our treatment of it to quadrupoles only (KAR76). The rotation by 90^{o} is then equivalent to a reversal of polarity in all the quadrupoles. We present transfer matrices in the four dimensions x, x´, y, y´ only, as these do not depend on ℓ or δ in this case.

For M_{ct} we find

$$M_{ct} = \begin{bmatrix} M_{33} & M_{34} & 0 & 0 \\ M_{43} & M_{44} & 0 & 0 \\ 0 & 0 & M_{11} & M_{12} \\ 0 & 0 & M_{21} & M_{22} \end{bmatrix} \qquad (5.6)$$

and

$$R_{ct} = \begin{bmatrix} M_{11}M_{33} + M_{21}M_{34} & M_{12}M_{33} + M_{22}M_{34} & 0 & 0 \\ M_{11}M_{43} + M_{21}M_{44} & M_{12}M_{43} + M_{22}M_{44} & & \\ 0 & 0 & M_{11}M_{33} + M_{12}M_{43} & M_{11}M_{34} + M_{12}M_{44} \\ 0 & 0 & M_{21}M_{33} + M_{22}M_{43} & M_{21}M_{34} + M_{22}M_{44} \end{bmatrix} \quad \ldots (5.7)$$

There are two special cases (KAR76) which each yield the identity matrix

$$R_{ct} = \begin{bmatrix} \pm 1 & 0 & 0 & 0 \\ 0 & \pm 1 & 0 & 0 \\ 0 & 0 & \pm 1 & 0 \\ 0 & 0 & 0 & \pm 1 \end{bmatrix} \quad (5.8)$$

These are (a) $M_{22} = \pm M_{33}$, $M_{11} = \pm M_{44}$, $M_{12} = \mp M_{34}$ $(\neq 0)$ (5.9)

and (b) $M_{22} = \pm M_{33}$, $M_{21} = \mp M_{43}$, $M_{12} = M_{34} = 0$ (5.10)

These conditions may be interpreted as follows:

(i) for the upper sign, x traversing the first half-system forwards behaves identically to y traversing the first half-system backwards;

traversing the whole system then results in the initial beam being reproduced at the end of the system (without inversion)

(ii) for the lower sign, we find that x traversing the first half-system forwards has the inverse relation to y traversing it backwards; the nett result is that the beam arrives at the end of the system inverted.

It is necessary to distinguish between (5.9) and (5.10) because if $M_{12} = M_{34} = 0$, then we must specify the relationships between M_{21} and M_{43} and between either M_{11} and M_{44} or between M_{22} and M_{33}. But if $M_{12} = \pm M_{34} \neq 0$, then it is not necessary to specify relationships between M_{21} and M_{43}

but only between M_{11} and M_{44}, and between M_{22} and M_{33}.

5.5 Mirror Symmetry

The second half-system is in this case obtained by traversing the first half-system in the reverse order (see figures 5.1d and 5.2d). Here

$$R_m = M_m M$$

where

$$M_m = \begin{bmatrix} M_{22} & M_{12} & 0 & 0 & 0 & -M_{52} \\ M_{21} & M_{11} & 0 & 0 & 0 & -M_{51} \\ 0 & 0 & M_{44} & M_{34} & 0 & 1 \\ 0 & 0 & M_{43} & M_{33} & 0 & 0 \\ -M_{26} & -M_{16} & 0 & 0 & 1 & M_{56} \\ 0 & 0 & 0 & 0 & 0 & 1 \end{bmatrix} \qquad (5.11)$$

and

$$R_m = \begin{bmatrix} 2M_{11}M_{22}-1 & 2M_{12}M_{22} & 0 & 0 & 0 & 2M_{12}M_{26} \\ 2M_{21}M_{11} & 2M_{11}M_{22}-1 & 0 & 0 & 0 & 2M_{11}M_{26} \\ 0 & 0 & 2M_{33}M_{44}-1 & 2M_{34}M_{44} & 0 & 0 \\ 0 & 0 & 2M_{43}M_{33} & 2M_{33}M_{44}-1 & 0 & 0 \\ -2M_{11}M_{26} & -2M_{12}M_{26} & 0 & 0 & 1 & 2(M_{56}-M_{16}M_{26}) \\ 0 & 0 & 0 & 0 & 0 & 1 \end{bmatrix}$$

... (5.12)

For the special case where the angular dispersion vanishes at the symmetry plane, i.e.

$$M_{26} = 0 \tag{5.13}$$

we get $R_{16} = R_{26} = R_{51} = R_{52} = 0$

implying that the system is then achromatic.

Another useful mode is achieved when we have parallel-to-point and point-to-parallel transfer in the half-system:

$$M_{11} = M_{22} = M_{33} = M_{44} = 0 \tag{5.14}$$

The complete system is then doubly telescopic with vanishing angular dispersion, i.e.

$$R_m = \begin{bmatrix} -1 & 0 & 0 & 0 & 0 & 2\,M_{12}M_{26} \\ 0 & -1 & 0 & 0 & 0 & 0 \\ 0 & 0 & -1 & 0 & 0 & 0 \\ 0 & 0 & 0 & -1 & 0 & 0 \\ 0 & -2\,M_{12}M_{26} & 0 & 0 & 1 & 2\,(M_{56}-M_{16}M_{26}) \\ 0 & 0 & 0 & 0 & 0 & 1 \end{bmatrix} \tag{5.15}$$

A similarly useful result arises when the half-system operates in point-to-point and parallel-to-parallel mode i.e.

$$M_{12} = M_{21} = M_{34} = M_{43} = 0 \tag{5.16}$$

In this case we find that the complete transfer is doubly telescopic with vanishing dispersion:

$$R_m = \begin{bmatrix} 1 & 0 & 0 & 0 & 0 & 0 \\ 0 & 1 & 0 & 0 & 0 & 2\,M_{11}M_{26} \\ 0 & 0 & 1 & 0 & 0 & 0 \\ 0 & 0 & 0 & 1 & 0 & 0 \\ -2\,M_{11}M_{26} & 0 & 0 & 0 & 1 & 2\,(M_{56}-M_{16}M_{26}) \\ 0 & 0 & 0 & 0 & 0 & 1 \end{bmatrix} \qquad (5.17)$$

5.6 Anti-Mirror Symmetry

For this symmetry, the second half-system is obtained by traversing the first half-system backwards after first having rotated it by 180^{o} (see figures 5.1e and 5.2e). If there are no dipoles present then this is equivalent to mirror symmetry. Thus

$$R_{am} = M_{am}\,M$$

where M_{am} is equivalent to M_m except in the sign of the terms M_{m16}, M_{m26}, M_{m51} and M_{m52}. Thus for R_{am} we get

$$R_{am} = \begin{bmatrix} 2\,M_{11}M_{22}-1 & 2\,M_{12}M_{22} & 0 & 0 & 0 & 2\,M_{22}M_{16} \\ 2\,M_{21}M_{11} & 2\,M_{11}M_{22}-1 & 0 & 0 & 0 & 2\,M_{21}M_{16} \\ 0 & 0 & 2\,M_{33}M_{44}-1 & 2\,M_{34}M_{44} & 0 & 0 \\ 0 & 0 & 2\,M_{43}M_{33} & 2\,M_{33}M_{44}-1 & 0 & 0 \\ 2\,M_{21}M_{16} & 2\,M_{22}M_{16} & 0 & 0 & 1 & 2(M_{56}+M_{16}M_{26}) \\ 0 & 0 & 0 & 0 & 0 & 1 \end{bmatrix}$$

... (5.18)

For the special case of zero dispersion in the half-system, i.e.

$$M_{16} = 0 \tag{5.19}$$

we find that R is achromatic, i.e.

$$R_{16} = R_{26} = R_{51} = R_{52} = 0$$

If we arrange for point-to-parallel and parallel-to-point transfer through the half-system in both planes, i.e.

$$M_{11} = M_{22} = M_{33} = M_{44} = 0 \tag{5.20}$$

then the overall transfer becomes doubly-telescopic, and dispersionless:

$$R_{am} = \begin{bmatrix} -1 & 0 & 0 & 0 & 0 & 0 \\ 0 & -1 & 0 & 0 & 0 & 2\,M_{21}M_{16} \\ 0 & 0 & -1 & 0 & 0 & 0 \\ 0 & 0 & 0 & -1 & 0 & 0 \\ 2\,M_{21}M_{16} & 0 & 0 & 0 & 1 & 2\,(M_{56}+M_{16}M_{26}) \\ 0 & 0 & 0 & 0 & 0 & 1 \end{bmatrix} \tag{5.21}$$

A doubly telescopic system with vanishing angular dispersion results when the half-system operates in point-to-point and parallel-to-parallel mode, i.e.

$$M_{12} = M_{21} = M_{34} = M_{43} \tag{5.22}$$

implies that

$$R_{am} = \begin{bmatrix} 1 & 0 & 0 & 0 & 0 & 2\,M_{22}M_{16} \\ 0 & 1 & 0 & 0 & 0 & 0 \\ 0 & 0 & 1 & 0 & 0 & 0 \\ 0 & 0 & 0 & 1 & 0 & 0 \\ 0 & 2\,M_{22}M_{16} & 0 & 0 & 1 & 2\,(M_{56}+M_{16}M_{26}) \\ 0 & 0 & 0 & 0 & 0 & 1 \end{bmatrix}$$

5.7 Cross-Mirror Symmetry

Here the second half-system may be found from the first half-system by traversing it backwards after a rotation by 90^{o} (see figures 5.1f and 5.2f). As in the case of cross-translational symmetry we assume that cross-mirror symmetry will only be applied to quadrupoles and the 90^{o} rotation is thus equivalent to a polarity change in all quadrupoles.

For M_{cm} we find

$$M_{cm} = \begin{bmatrix} M_{44} & M_{34} & 0 & 0 \\ M_{43} & M_{33} & 0 & 0 \\ 0 & 0 & M_{22} & M_{12} \\ 0 & 0 & M_{21} & M_{11} \end{bmatrix} \qquad (5.23)$$

and the total transfer matrix is

$$R_{cm} = \begin{bmatrix} M_{11}M_{44} + M_{21}M_{34} & M_{22}M_{34} + M_{12}M_{44} & 0 & 0 \\ M_{11}M_{43} + M_{21}M_{33} & M_{22}M_{33} + M_{12}M_{43} & 0 & 0 \\ 0 & 0 & M_{22}M_{33} + M_{12}M_{43} & M_{22}M_{34} + M_{12}M_{44} \\ 0 & 0 & M_{21}M_{33} + M_{11}M_{43} & M_{11}M_{44} + M_{21}M_{34} \end{bmatrix}$$

... (5.24)

R_{cm} takes the form of the identity matrix, equation (5.8), under the conditions

$$\begin{aligned} M_{22} &= \pm M_{44} \\ M_{12} &= \mp M_{34} \\ M_{21} &= \mp M_{43} \end{aligned} \qquad (5.25)$$

These conditions imply that the behaviour of the x-component of the beam traversing the first half-system forwards must be identical (without/with inversion for the upper/lower sign) to the behaviour of the y-component of the beam traversing the second half-system forwards.

5.8 Symmetry Groups

We find that the matrices for the second half-system may, for each symmetry type, be calculated directly from the matrix M of the first half-system (or from its inverse M^{-1}) in the following manner:

$$M_t = I_0 M I_0 \qquad M_m = I_1 M^{-1} I_1$$

$$M_{ct}(1) = I_2 M I_2 \qquad M_{cm}(1) = I_3 M^{-1} I_3$$

$$M_{at} = I_4 M I_4 \qquad M_{am} = I_5 M^{-1} I_5$$

$$M_{ct}(2) = I_6 M I_6 \qquad M_{cm}(2) = I_7 M^{-1} I_7$$

where the (1) or (2) with the cross symmetries refer to rotations through $+90^{o}$ or -90^{o}. Here we treat these cross symmetries as if dipoles may be included. The eight symmetries then form a complete symmetry group.

We find that the matrices I_i have values as shown on the next page:

$$I_0 = \begin{bmatrix} 1 & 0 & 0 & 0 & 0 & 0 \\ 0 & 1 & 0 & 0 & 0 & 0 \\ 0 & 0 & 1 & 0 & 0 & 0 \\ 0 & 0 & 0 & 1 & 0 & 0 \\ 0 & 0 & 0 & 0 & 1 & 0 \\ 0 & 0 & 0 & 0 & 0 & 1 \end{bmatrix} \qquad I_1 = \begin{bmatrix} 1 & 0 & 0 & 0 & 0 & 0 \\ 0 & -1 & 0 & 0 & 0 & 0 \\ 0 & 0 & 1 & 0 & 0 & 0 \\ 0 & 0 & 0 & -1 & 0 & 0 \\ 0 & 0 & 0 & 0 & -1 & 0 \\ 0 & 0 & 0 & 0 & 0 & 1 \end{bmatrix}$$

$$I_2 = \begin{bmatrix} 0 & 0 & 1 & 0 & 0 & 0 \\ 0 & 0 & 0 & 1 & 0 & 0 \\ 1 & 0 & 0 & 0 & 0 & 0 \\ 0 & 1 & 0 & 0 & 0 & 0 \\ 0 & 0 & 0 & 0 & 1 & 0 \\ 0 & 0 & 0 & 0 & 0 & 1 \end{bmatrix} \qquad I_3 = \begin{bmatrix} 0 & 0 & 1 & 0 & 0 & 0 \\ 0 & 0 & 0 & -1 & 0 & 0 \\ 1 & 0 & 0 & 0 & 0 & 0 \\ 0 & -1 & 0 & 0 & 0 & 0 \\ 0 & 0 & 0 & 0 & -1 & 0 \\ 0 & 0 & 0 & 0 & 0 & 1 \end{bmatrix}$$

$$I_4 = \begin{bmatrix} -1 & 0 & 0 & 0 & 0 & 0 \\ 0 & -1 & 0 & 0 & 0 & 0 \\ 0 & 0 & -1 & 0 & 0 & 0 \\ 0 & 0 & 0 & -1 & 0 & 0 \\ 0 & 0 & 0 & 0 & 1 & 0 \\ 0 & 0 & 0 & 0 & 0 & 1 \end{bmatrix} \qquad I_5 = \begin{bmatrix} -1 & 0 & 0 & 0 & 0 & 0 \\ 0 & 1 & 0 & 0 & 0 & 0 \\ 0 & 0 & -1 & 0 & 0 & 0 \\ 0 & 0 & 0 & 1 & 0 & 0 \\ 0 & 0 & 0 & 0 & -1 & 0 \\ 0 & 0 & 0 & 0 & 0 & 1 \end{bmatrix}$$

$$I_6 = \begin{bmatrix} 0 & 0 & -1 & 0 & 0 & 0 \\ 0 & 0 & 0 & -1 & 0 & 0 \\ -1 & 0 & 0 & 0 & 0 & 0 \\ 0 & -1 & 0 & 0 & 0 & 0 \\ 0 & 0 & 0 & 0 & 1 & 0 \\ 0 & 0 & 0 & 0 & 0 & 1 \end{bmatrix} \qquad I_7 = \begin{bmatrix} 0 & 0 & -1 & 0 & 0 & 0 \\ 0 & 0 & 0 & 1 & 0 & 0 \\ -1 & 0 & 0 & 0 & 0 & 0 \\ 0 & 1 & 0 & 0 & 0 & 0 \\ 0 & 0 & 0 & 0 & -1 & 0 \\ 0 & 0 & 0 & 0 & 0 & 1 \end{bmatrix}$$

The matrices I_0 through I_3 have previously been derived (KAR76) for only 4 dimensions (x, x´, y and y´).

We find that the eight matrices I_0 through I_7 form the abelian eight-group. As a check on the validity of this statement we have drawn up the group table as follows:

I_0	I_1	I_2	I_3	I_4	I_5	I_6	I_7
I_1	I_0	I_3	I_2	I_5	I_4	I_7	I_6
I_2	I_3	I_0	I_1	I_6	I_7	I_4	I_5
I_3	I_2	I_1	I_0	I_7	I_6	I_5	I_4
I_4	I_5	I_6	I_7	I_0	I_1	I_2	I_3
I_5	I_4	I_7	I_6	I_1	I_0	I_3	I_2
I_6	I_7	I_4	I_5	I_2	I_3	I_0	I_1
I_7	I_6	I_5	I_4	I_3	I_2	I_1	I_0

This group table enables us to read off the product of any two matrices in the group (HAM62).

5.9 Second-order Terms

Symmetrical systems are convenient not only for their first-order properties but also because many second-order terms vanish identically.

We start with Brown's theory (BRO72) and derive additional equations. We then apply the resulting method to symmetrical systems with given properties to find the zero terms.

Brown firstly derives a general vector differential equation describing the trajectory of a charged particle in an arbitrary static magnetic field B possessing midplane symmetry:

$$\begin{aligned} x'' + (1-n)h^2x = {} & h\delta + (2n-1-\beta)h^3x^2 + h'xx' + \tfrac{1}{2}\,h\,x'^2 + (2-n)h^2x\,\delta \\ & + \tfrac{1}{2}\,(h'' - n\,h^3 + 2\,\beta h^3)y^2 + h'yy' - \tfrac{1}{2}\,hy'^2 - h\delta^2 \\ & + \text{higher order terms} \end{aligned} \qquad (5.26)$$

$$y'' + n\,h^2 y = 2(\beta - n)h^3\,xy + h'xy' - h'x'y + hx'y' + n\,h^2 y\delta \qquad (5.27)$$

$$+ \text{higher order terms}$$

$$\text{where} \quad n = -\left[\frac{1}{h\,B_y}\left(\frac{\partial B_y}{\partial x}\right)\right]_{\substack{x=0\\y=0}}$$

$$\beta = \left[\frac{1}{2!h^2\,B_y}\left(\frac{\partial^2 B_y}{\partial x^2}\right)\right]_{\substack{x=0\\y=0}}$$

$$\text{and} \quad h = {}^{1}/_{\rho_0} \qquad (5.28)$$

where ρ_0 is the radius of curvature.

The next step is to express the solutions in a Taylor expansion

$$x = (x|x_0)x_0 + (x|x_0')x_0' + (x|\delta)\delta + (x|x_0^2)x_0^2 + (x|x_0x_0')x_0x_0'$$
$$+ (x|x_0\delta)x_0\delta + (x|x_0'^2)x_0'^2 + (x|x_0'\delta)x_0'\delta + (x|\delta^2)\delta^2 + (x|y_0^2)y_0^2$$
$$+ (x|y_0y_0')y_0y_0' + (x|y_0'^2)y_0'^2 \qquad (5.29)$$

$$y = (y|y_0)y_0 + (y|y_0')y_0' + (y|x_0y_0)x_0y_0 + (y|x_0y_0')x_0y_0' + (y|x_0'y_0)x_0'y_0$$
$$+ (y|x_0'y_0')x_0'y_0' + (y|y_0\delta)y_0\delta + (y|y_0'\delta)y_0'\delta \qquad (5.30)$$

The first-order coefficients have a one-to-one correspondence with the following five characteristic first-order trajectories:

(i) the unit sine-line function $s_x(t)$ in the bend-plane where $s_x(0) = 0$, $s_x'(0) = 1$: $s_x(t)$ corresponds to $(x|x_0')$ and $s_x'(t)$ to $(x'|x_0')$;

(ii) the unit cosine-line function $c_x(t)$ in the bend-plane where $c_x(0) = 1$, $c_x'(0) = 0$: $c_x(t)$ corresponds to $(x|x_0)$ and $c_x'(t)$ to $(x'|x_0)$;

(iii) The dispersion function $d_x(t)$ in the bend-plane where $d_x(0) = 0$, $d_x'(0) = 0$; $d_x(t)$ corresponds to $(x|\delta)$ and $d_x'(t)$ to $(x'|\delta)$;

(iv) the unit sine-like function $s_y(t)$ in the non-bend plane where $s_y(0) = 0$, $s_y'(0) = 1$; $s_y(t)$ corresponds to $(y|y_0')$ and $s_y'(t)$ to $(y'|y_0')$; and

(v) the unit cosine-line function $c_y(t)$ in the non-bend plane where $c_y(0) = 1$, $c_y'(0) = 0$; $c_y(t)$ corresponds to $(y|y_0)$ and $c_y'(t)$ to $(y'|y_0)$.

Figure 5.3 illustrates $s_x(t)$, $c_x(t)$ and $d_x(t)$. $s_y(t)$ and $c_y(t)$ are similar in nature to $s_x(t)$ and $c_x(t)$.

Equations (5.29) and (5.30) are now substituted into equations (5.26) and (5.27) to find differential equations for each first- and second-order coefficient:

$$c_x'' + k_x^2 c_x = 0 \qquad c_y'' + k_y^2 c_y = 0 \tag{5.31}$$

$$s_x'' + k_x^2 s_x = 0 \qquad s_y'' + k_y^2 s_y = 0 \tag{5.32}$$

$$q_x'' + k_x^2 q_x = f_x \qquad q_y'' + k_y^2 q_y = f_y \tag{5.33}$$

where $k_x^2 = (1-n)h^2$ and $k_y^2 = nh^2$.

Equations (5.31) and (5.32), together with initial conditions for c and s, represent the equations of motion for the first-order mono-energetic terms. The solutions to equation (5.33) give the first-order dispersion d_x and the second-order terms, where the driving term f has a characteristic form for each coefficient q. These driving terms are listed by Brown for f_{1ij} and f_{3ij}, corresponding to solutions q_{1ij} (or T_{1ij}) and q_{3ik} (or T_{3ij}) respectively.

The value of q may be found using the Green's function integral

$$q(t) = \int_0^t f(\tau)\, G(t,\tau)\, d\tau \tag{5.34}$$

where

$$G(t,\tau) = s(t)\, c(\tau) - s(\tau)\, c(t) \tag{5.35}$$

leading to

$$q(t) = s(t) \int_0^t f(\tau)\, c(\tau)\, d\tau - c(t) \int_0^t f(\tau)\, s(\tau)\, d\tau \tag{5.36}$$

We also need to know the value of q'. This is:

$$q'(t) = s'(t) \int_0^t f(\tau)\, c(\tau)\, d\tau - c'(t) \int_0^t f(\tau)\, s(\tau)\, d\tau \tag{5.37}$$

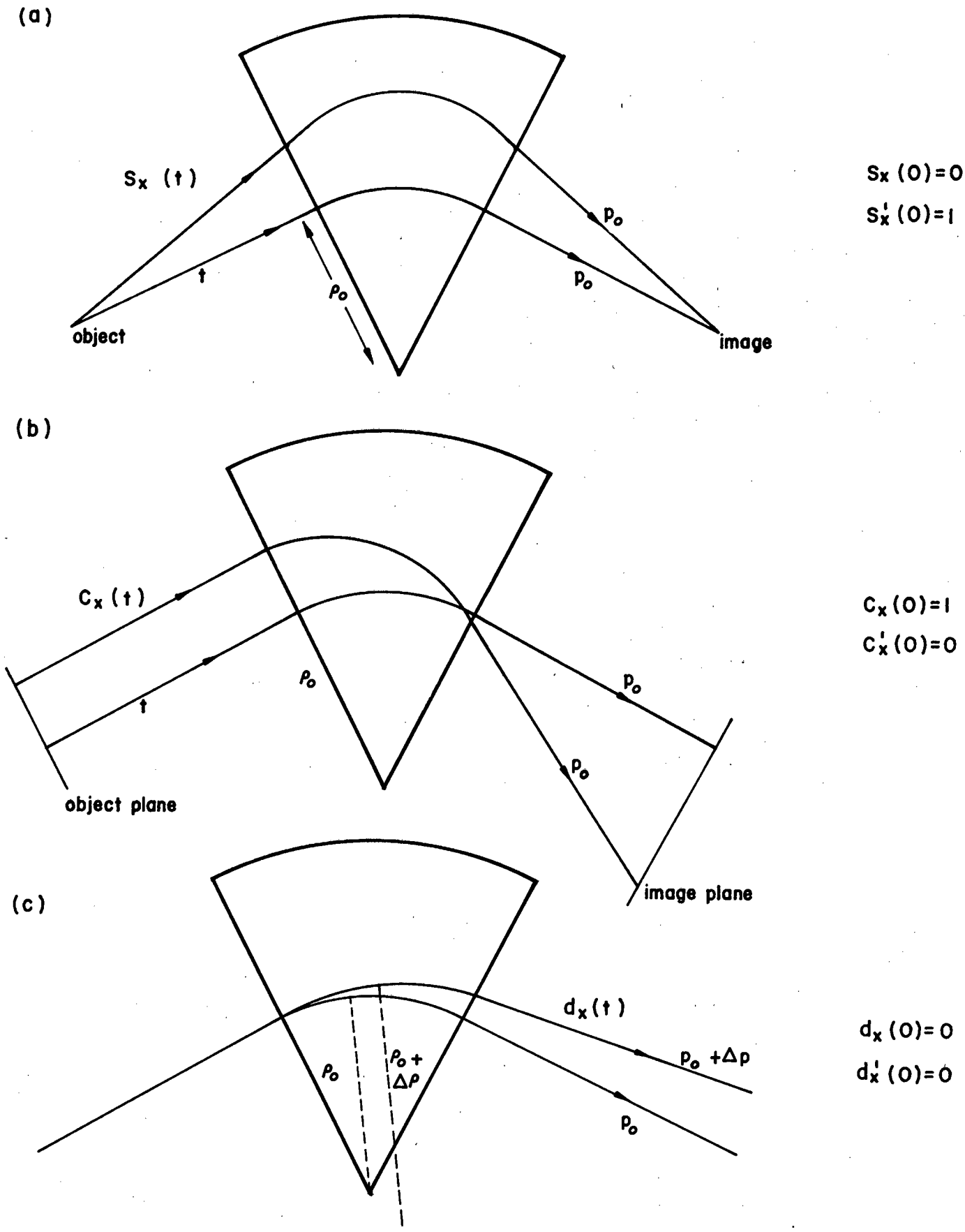

Figure 5.3: The shape of (a) the sine-like function $s_x(t)$,
(b) the cosine-like function $c_x(t)$, and
(c) the dispersion function $d_x(t)$, in the magnetic midplane.

Brown has treated the case of $q(t) = 0$ for mirror symmetry with parallel-to-point imaging at the mid-point and $d' = 0$ (at the midpoint). We will now generalize this treatment to take into account $q'(t) = 0$ as well. We will apply this to several different cases to find which q and q' are zero for each case.

We look at four cases of interest:

(i) if we have point-to-point imaging from the beginning of a system to its end, then $s(t) = 0$ and

$$q(t) = - c(t) \int_0^t f(\tau)\, s(\tau)\, d\tau \tag{5.38}$$

(ii) if we have parallel-to-parallel imaging then $c'(t) = 0$ and

$$q'(t) = s'(t) \int_0^t f(\tau)\, c(\tau)\, d\tau \tag{5.39}$$

(iii) if we have parallel-to-point imaging, then $c(t) = 0$ and

$$q(t) = s(t) \int_0^t f(\tau)\, c(\tau)\, d\tau \tag{5.40}$$

(iv) if we have point-to-parallel imaging, then $s'(t) = 0$ and

$$q'(t) = - c'(t) \int_0^t f(\tau)\, s(\tau)\, d\tau \tag{5.41}$$

If we apply the above four cases to symmetrical systems, then we can state that: a second-order term is identically zero if its relevant integrand $f(\tau)\, s(\tau)$ or $f(\tau)\, c(\tau)$ is an odd function about the midpoint of the system. This has to be calculated for each system under consideration. We can, however, make the following general statement:

> if $c(\tau)$ is an odd/even function, then $c'(\tau)$ and $s(\tau)$ will be even/odd functions and $s'(\tau)$ odd/even. This implies that if a given $q(t)$ is zero, then $q'(t)$ will not be, and vice versa.

We now look at specific cases, state whether the first-order functions are odd or even, and then list the second-order coefficients that are

zero. *

(a i) Mirror symmetry with $M_{11} = M_{22} = M_{33} = M_{44} = M_{26} = 0$ (equations (5.13), (5.14))

$c_x(\tau)$ = odd $s_x(\tau)$ = even $d_x(\tau)$ = even $h(\tau)$ = even
$c_y(\tau)$ = odd $s_y(\tau)$ = even

$c_x'(\tau)$ = even $s_x'(\tau)$ = odd $d_x'(\tau)$ = odd $h'(\tau)$ = odd
$c_y'(\tau)$ = even $s_y'(\tau)$ = odd
$h''(\tau)$ = even

For $f(\tau)$ odd, $q(t) = 0$, i.e.

$T_{112} = T_{116} = T_{211} = T_{222} = T_{226} = T_{266} = T_{134} = T_{233} = T_{244} = 0$
$T_{314} = T_{323} = T_{336} = T_{413} = T_{424} = T_{446} = 0$

(a ii) Mirror symmetry with $M_{12} = M_{21} = M_{34} = M_{43} = M_{26} = 0$ (equations (5.13) and (5.16))

$c_x(\tau)$ = even $s_x(\tau)$ = odd $d(\tau)$ = even $h(\tau)$ = even
$c_y(\tau)$ = even $s_y(\tau)$ = odd

$c_x'(\tau)$ = odd $s_x'(\tau)$ = even $d'(\tau)$ = odd $h'(\tau)$ = odd
$c_y'(\tau)$ = odd $s_y'(\tau)$ = even
$h''(\tau)$ = even

For $f(\tau)$ even, $q(t) = 0$, i.e.

$T_{112} = T_{126} = T_{211} = T_{216} = T_{222} = T_{266} = T_{134} = T_{233} = T_{244} = 0$
$T_{314} = T_{323} = T_{346} = T_{413} = T_{424} = T_{436} = 0$

(b i) Anti-mirror symmetry with $M_{11} = M_{22} = M_{33} = M_{44} = M_{16} = 0$ (equations (5.19) and 5.20))

$c_x(\tau)$ = odd $s_x(\tau)$ = even $d_x(\tau)$ = odd $h(\tau)$ = odd
$c_y(\tau)$ = odd $s_y(\tau)$ = even

$c_x'(\tau)$ = even $s_x'(\tau)$ = odd $d_x'(\tau)$ = even $h'(\tau)$ = even
$c_y'(\tau)$ = even $s_y'(\tau)$ = odd
$h''(\tau)$ = odd

* In the above treatment x' implies $\frac{dx}{dt}$ whereas we usually work with $\theta = \frac{dx}{dz}$. However $\theta = \frac{dx}{dz} = \frac{x'}{z'} = \frac{x'}{1 + hx}$. Thus if $hx \ll 1$ ($x \ll \rho_0$) we can approximate $\theta \simeq x'$. In this high-energy limit we can thus state e.g. $T_{222} = (\theta|\theta_0^2) \simeq (x'|x_0'^2)$.

For $f(\tau)$ odd, $q(t) = 0$, i.e.

$$T_{111} = T_{116} = T_{122} = T_{166} = T_{133} = T_{144} = T_{212} = T_{226} = T_{234} = 0$$
$$T_{313} = T_{324} = T_{336} = T_{414} = T_{423} = T_{446} = 0$$

(b ii) Anti-mirror symmetry with $M_{12} = M_{21} = M_{34} = M_{43} = M_{16} = 0$ (equations (5.19) and (5.22))

$c_x(\tau)$ = even $s_x(\tau)$ = odd $d_x(\tau)$ = odd $h(\tau)$ = odd
$c_y(\tau)$ = even $s_y(\tau)$ = odd

$c_x'(\tau)$ = odd $s_x'(\tau)$ = even $d_x'(\tau)$ = even $h'(\tau)$ = even
$c_y'(\tau)$ = odd $s_y'(\tau)$ = even
$h''(\tau)$ = odd

For $f(\tau)$ even, $q(t) = 0$, i.e.

$$T_{111} = T_{122} = T_{126} = T_{166} = T_{133} = T_{144} = T_{212} = T_{216} = T_{234} = 0$$
$$T_{313} = T_{324} = T_{346} = T_{414} = T_{423} = T_{436} = 0$$

(c) The case of cross-mirror symmetry treated in 5.8 (i.e. only quadrupoles) is identical to mirror symmetry except that only chromatic aberrations will appear. Thus we can state that

(i) for $M_{11} = M_{22} = M_{33} = M_{44} = 0$, we will get

$$T_{116} = T_{226} = T_{336} = T_{446} = 0$$

and (ii) for $M_{12} = M_{21} = M_{34} = M_{43} = 0$, we will get

$$T_{126} = T_{216} = T_{346} = T_{436} = 0$$

In the case of the translational-type symmetries, systems with the properties of

either $M_{11} = M_{22} = M_{33} = M_{44} = 0$, $R_{16} = R_{26} = 0$

or $M_{12} = M_{21} = M_{34} = M_{43} = 0$, $R_{16} = R_{26} = 0$

are very seldom found which do not also belong to the mirror-type symmetry group. Hence we will not treat them separately here.

If we combine more than one symmetrical system into a composite system then we may find that further second-order elements disappear. We examine this arrangement below.

When two elements follow each other, then the total first and second-order transfer matrices are

$$R_{ij}(2) = \sum_k R_{ik}(1)\, R_{kj}(0)$$

and

$$T_{ijk}(2) = \sum_{\ell} R_{i\ell}(1)\, T_{\ell jk}(0) + \sum_{\ell m} T_{i\ell m}(1)\, R_{\ell j}(0)\, R_{mk}(0) \qquad (5.42)$$

Using equation (5.42) we have calculated that in a system with translational symmetry where each half-system has $M_{ij} = 0$ for $i \neq j$, that

$$T_{ijk} = V_{ijk}\,(M_{ii} + M_{jj}\, M_{kk})$$

where V_{ijk} are the second-order terms for the half-system. Thus when $M_{ii} = -1$ for $i = 1, 2, 3, 4$ the only non-zero second-order terms are

$$T_{116},\ T_{126},\ T_{216},\ T_{226},\ T_{336},\ T_{346},\ T_{436} \text{ and } T_{446}$$

i.e. all geometric aberrations disappear, leaving only chromatic aberrations.

When two systems of the type (a i) follow each other, then T_{116}, T_{226}, T_{336} and T_{446} are zero as well. This is also true for two systems of the type (b i) and (c i). Hinterberger (HIN73) quotes this result without derivation or proof for two systems of type (a i). It is possible that he obtained these results from the output of the TRANSPORT computer program for a specific system, as he also quotes $T_{266} \neq 0$. This may have resulted from rounding errors in the calculation. Brown (BRO79) has also derived this result, except that he neglects to state that the transfer matrix of his "unit cell" must be the <u>negative</u> of the identity matrix for x, x′, y and y′. The result is not correct for a <u>positive</u> identity transfer matrix.

Thus we have found that the composite system with the least second-order aberrations consists of two-half systems, one a translation of the other, each made up of one of the following:

(a) a mirror symmetrical system which has (for its half-system)

$$M_{11} = M_{22} = M_{33} = M_{44} = M_{26} = 0$$

(i.e. point-to-parallel and parallel-to-point optics and zero angular dispersion); or

(b) an anti-mirror symmetrical system which has (for its half-system)

$$M_{11} = M_{22} = M_{33} = M_{44} = M_{16} = 0$$

(i.e. optics similar to that of (a) but with zero dispersion, not necessarily zero angular dispersion); or

(c) a cross-mirror symmetrical system of quadrupoles only, with its half-system requirement

$$M_{11} = M_{22} = M_{33} = M_{44} = 0$$

6. QUADRUPOLE SYSTEMS INDEPENDENT OF BEAM PARAMETERS

6.1 Introduction

Within an accelerator facility it is often necessary to transport the beam over quite long distances, and while doing so, to prevent the beam from spreading out. Various combinations of quadrupoles are most commonly used for this purpose. Where possible these quadrupole systems should be independent of the beam parameters. Then the quadrupole settings depend only on the magnetic rigidity of the beam, and may be rapidly altered when a different beam is accelerated (i.e. the beam parameters need not be measured at the entrance to the system before the quadrupole strengths are set).

The quadrupole units used to create many systems are the doublet and the triplet. We will discuss systems made up of two doublets and two triplets. Longer systems may be made up of several of these.

Because we are dealing only with quadrupoles here, we present discussion in terms of the 4 x 4 matrices in x, x′, y and y′. The matrices with the most desirable characteristics are of the form:

$$R = \begin{bmatrix} R_{11} & 0 & 0 & 0 \\ 0 & R_{22} & 0 & 0 \\ 0 & 0 & R_{33} & 0 \\ 0 & 0 & 0 & R_{44} \end{bmatrix} \qquad (6.1)$$

These represent the imaging of the source at the end of the system, with horizontal magnification R_{11}, and vertical magnification R_{33}.

Systems with such transfer matrices represent point-to-point and parallel-to-parallel transfer, and are described as doubly-telescopic (HIN73) i.e. horizontally and vertically. We now examine the optics of such systems, and in particular we discuss two-doublet and two-triplet telescopes.

6.2 Two-Doublet Telescopes

Two doublet telescopes have

$$R_{11} = R_{22} = R_{33} = R_{44} = -1 \qquad R_{ij} = 0 \quad i \neq j \qquad (6.2)$$

i.e. they transport the beam with unit magnification, both horizontally and vertically. The case where $R_{11} = R_{33} = +1$ is not realizable with only four quadrupoles (KAR76).

Two doublet telescopes have been examined by various analytical methods (MOL66a, MOL66b, NOR67, KAR76, DYM64, DYM65a, LEE69). However we develop a method here to determine a solution to the simplest system i.e. that which has equal field strengths in all four quadrupoles (with reverse polarity on two of them) and equal drift lengths at each end of each doublet, as shown in figure 6.1.

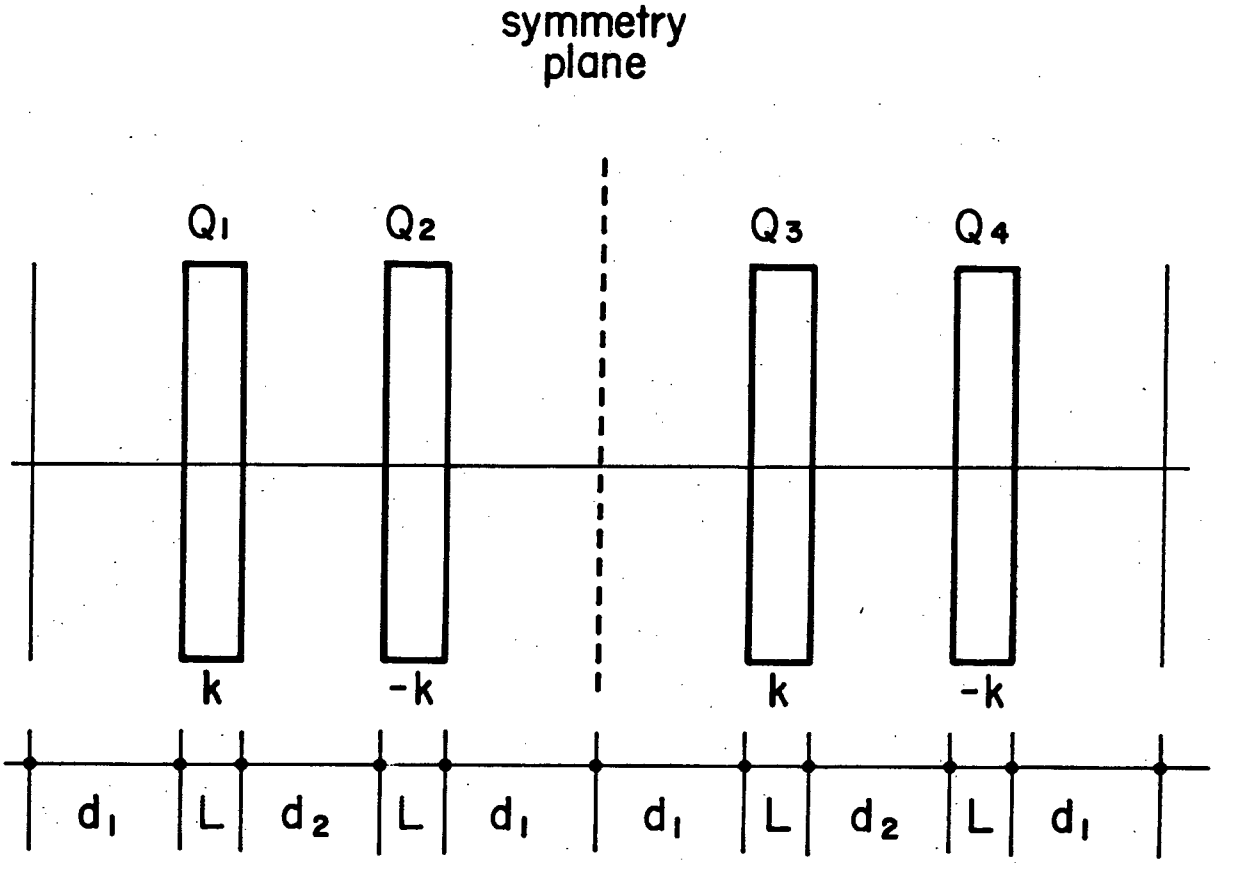

Figure 6.1: A system of two symmetrical doublets with a total length of $2\,(2d_1 + d_2 + 2L)$.

We see that this system has both translational symmetry and cross-mirror symmetry. (The mirror symmetrical arrangement of two doublets does not

produce telescopic optics (KAR76).)

From the translational symmetry requirement for satisfying equation (6.2) we get (from chapter 5)

$$M_{11} + M_{22} = 0 \qquad (5.2a)$$

$$M_{33} + M_{44} = 0 \qquad (5.2b)$$

However for the cross-mirror symmetry requirement we get

$$\begin{aligned} M_{22} &= -M_{44} \\ M_{12} &= M_{34} \\ M_{21} &= M_{43} \end{aligned} \qquad (5.25)$$

which implies, (because det $[M] = 1$) that

$$M_{11} = -M_{33}$$

Thus when equations (5.25) hold, the requirement of (5.2a) automatically implies (5.2b), and we need only restrain the value of $M_{11} + M_{22}$.

On multiplying out the matrices for quadrupoles and drifts, we get

$$M_{11} + M_{22} = 2 \cos kL \cosh kL + k (2 d_1 + d_2)(\cos kL \sinh kL - \sin kL \cosh kL) - 2 d_1 d_2 k^2 \sin kL \sinh kL \qquad (6.3)$$

When we use the series expansion for cos kL, cosh kL, sin kL and sinh kL, we find

$$M_{11} + M_{22} = 2 \left(1 - \frac{k^4 L^4}{6}\right) - \frac{2}{3} k^4 L^3 (2 d_1 + d_2) - 2 d_1 d_2 k^4 L^2 \qquad (6.4)$$

This result is derived by ignoring terms in the sixth, and higher, powers of kL. This is a valid approximation for $kL < 1$. Equation (6.4) may be solved for the field strength of the quadrupoles:

$$B_0 = a (B\rho) k^2 = a (B\rho) \left[\frac{6}{L^4 + 2 L^3 (2 d_1 + d_2) + 6 d_1 d_2 L^2} \right]^{\frac{1}{2}} \qquad (6.5)$$

We applied this solution to a test system with the following parameters:

L = 0,4 m

d_1 = 1,7 m

d_2 = 0,8 m

a = 0,0381 m

and $B\rho$ = 21,496 kG.m.

The resultant field strength for the quadrupoles of 1,4675 kG differs by only 0,04% from the value of 1,4681 kG computed using the program TRANSPORT.

The two doublet telescope is well suited to an initially (nearly) parallel beam, but for an initially highly divergent beam the beam extent becomes large in the horizontal plane in the second quadrupole for a - + - + configuration, in the third for a + - + - configuration, and vice versa for the vertical extent. This is illustrated in figure 6.2.

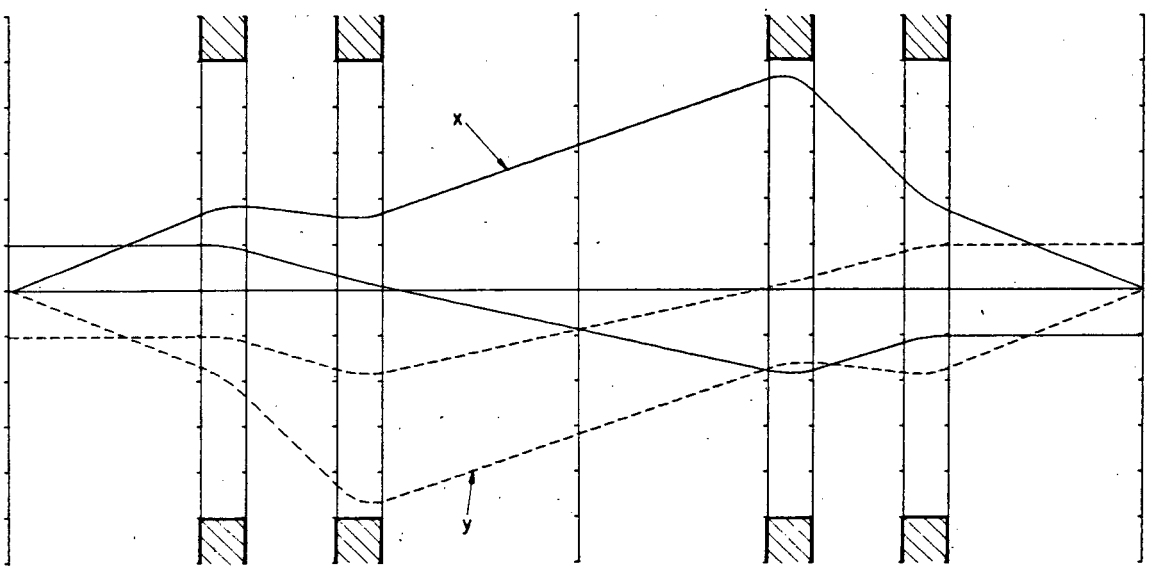

Figure 6.2: Point and parallel rays traced through a two-doublet telescope. When the direction of travel is reversed (or the quadrupole polarities reversed) the horizontal and vertical rays are interchanged.

6.3 Two-Triplet Telescopes with Unit Magnification

The two-triplet arrangement of quadrupoles shown in figure 6.3 may be made telescopic with unit magnification using an arbitrary selection of six quadrupole strengths which will satisfy equation (6.1), i.e. so that

$$R_{11} = R_{33} = \pm 1 \qquad (6.6)$$

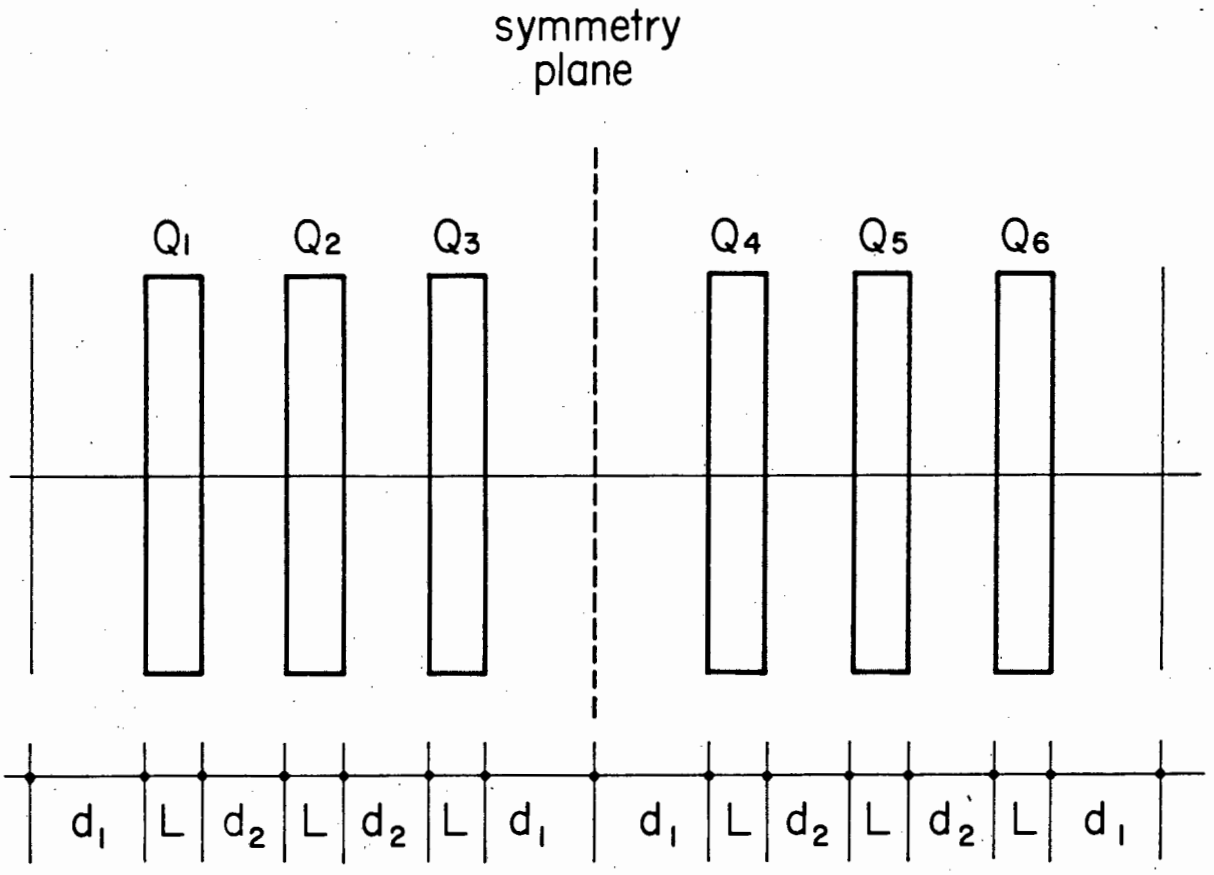

Figure 6.3: A system of two symmetrical quadrupole triplets with a total length of $4\,(d_1 + d_2) + 6L$.

It is, however, preferable to retain the inherent symmetry already in the geometry of the system. We thus look at the four symmetry types applicable to systems of quadrupoles (see chapter 5).

If we examine the half-system M, we can, with some manipulation, show that with only a quadrupole triplet we cannot simultaneously get point-to-point imaging, ($M_{12} = 0$, $M_{34} = 0$) and parallel-to-parallel imaging, ($M_{21} = 0$, $M_{43} = 0$). We can, however, in certain cases get $M_{11} = 0$, $M_{33} = 0$ (parallel-to-point imaging) and $M_{22} = 0$, $M_{44} = 0$ (point-to-parallel imaging). When this occurs we find that for quadrupoles Q_1 and Q_3 their strengths are equal, i.e. $q_1 = q_3$. (This is not, however, the only condition that implies $q_1 = q_3$.) When $q_1 = q_3$ the triplet becomes mirror symmetrical magnetically as well as geometrically.

We now consider the cases where the two half-systems are related by translational, mirror, cross-translational and cross-mirror symmetry, respectively. Thin-lens optics is adequate for investigation of these symmetries and provides a clear understanding of the various solutions which exist, without the complexity of a more exact treatment.

(a) In the case of <u>translational symmetry</u> we have for the quadrupole strengths:

$$q_1 = q_4, \quad q_2 = q_5, \quad \text{and } q_3 = q_6 \tag{6.7}$$

and

$$R = MM$$

To find M we write the focal length of the i^{th} quadrupole f_i as

$$f_i = \frac{1}{g_i} = \frac{1}{k^2 L}$$

and multiply out the matrices of the drift lengths and thin lenses.

There are no solutions to the requirements $R_{11} = R_{33} = +1$, but for $R_{11} = R_{33} = -1$ we require

$$\text{(i)} \quad \begin{aligned} M_{11} + M_{22} &= 0 \\ M_{33} + M_{44} &= 0 \end{aligned} \tag{5.2}$$

This leads to the solution (where d_1 and d_2 are now the drift lengths to the quadrupole centres):

$$g_1 = \frac{-g_3 d_2^3 \pm \left[g_3^2 d_2^6 + (d_1+d_2)\{4g_3^2 d_1^2 d_2^3 - d_2(2d_1+d_2)(d_1+d_2)\}\{ g_3^2 d_2(2d_1+d_2) - 2\}\right]^{\frac{1}{2}}}{d_2\{(2d_1+d_2)(d_1+d_2) - 4g_3^2 d_1^2 d_2^2\}} \tag{6.8}$$

and

$$g_2 = \frac{-2(1 + 2g_1 g_3 d_1 d_2)}{(g_1+g_3)\, d_2\, (2d_1+d_2)} \tag{6.9}$$

Here g_3 is arbitrary, restricted only by the necessity for the quantity in the square brackets in equation (6.8) to be positive.

(ii) A special case of the above solution exists when

$$M_{11} = M_{22} = M_{33} = M_{44} = 0 \qquad (6.10)$$

implying $q_1 = q_3 = q_4 = q_6$

In this case we have two symmetric quadrupole triplets, and equations (6.8) and (6.9) reduce to

$$g_1^2 = g_3^2 = \frac{(2d_1^2+3d_1d_2+2d_2^2) \pm \left[(2d_1^2+3d_1d_2+2d_2^2)^2 - 8d_1^2d_2(d_1+d_2)\right]^{\frac{1}{2}}}{4\, d_1^2 d_2^2} \qquad (6.11)$$

and

$$g_2 = - \frac{1 + 2g_1^2 d_1 d_2}{g_1 d_2 (2d_1 + d_2)} \qquad (6.12)$$

We can thus get four possible configurations i.e. we can start with either positive or negative quadrupole polarities for each of the "strong" or "weak" solutions (upper and lower signs respectively) in equation (6.11). While the weak solution would be used in practice, the strong solution will also be referred to in later sections.

(b) For <u>mirror symmetry</u> we require

$$q_1 = q_6, \quad q_2 = q_5, \quad \text{and } q_3 = q_4 \qquad (6.13)$$

Equation (6.1) can only be solved when equation (6.10) is valid, which implies $q_1 = q_3$. This case then becomes identical to case (a - ii) described above.

(c) For <u>cross-translational symmetry</u> we require

$$q_1 = -q_4, \quad q_2 = -q_5, \quad \text{and } q_3 = -q_6 \qquad (6.14)$$

In solving equation (6.1) we find that equation (6.10) cannot be valid. Instead we require (from equation (5.9)):

$$M_{11} = \pm M_{44}$$

$$M_{22} = \pm M_{33}$$

$$M_{12} = \mp M_{34} \qquad (6.15)$$

and $$M_{21} = \mp M_{43}$$

(i) For the upper sign to be valid ($R_{11} = R_{33} = +1$) and for $M_{12} \neq 0$, $M_{21} \neq 0$, in general, we find

$$q_1 = -q_2 = q_3 \qquad (6.16)$$

for $$g_1^2 = \frac{d_1 + d_2}{d_1 d_2^2} \qquad (6.17)$$

There are two possible configurations of this type corresponding to a polarity sequence and the reverse sequence.

(ii) As a special case of (i) above we can require

$$M_{12} = 0, \quad M_{21} \neq 0$$

i.e. point-to-point but not parallel-to-parallel imaging, for which the restriction $d_1 = d_2$ applies, and equation (6.17) reduces to

$$g_1^2 = \frac{2}{d_1^2} \qquad (6.18)$$

(iii) Another special case of (i) above is for

$$M_{12} \neq 0, \quad M_{21} = 0$$

i.e. parallel-to-parallel, but not point-to-point imaging. We now find $d_1 = \sqrt{2}\, d_2$, and equation (6.17) becomes:

$$g_1^2 = \frac{2 + \sqrt{2}}{d_1^2} \qquad (6.19)$$

(iv) For the lower sign in equation (6.15), leading to $R_{11} = R_{33} = -1$ and for $M_{12} \neq 0$, $M_{21} \neq 0$, we find

$$q_1 = q_3$$

with

$$g_1^2 = \frac{1}{2d_1d_2} \tag{6.20}$$

and

$$g_2 = -\frac{2g_1}{1 + g_1^2 d_2^2} \tag{6.21}$$

As in case (i) there are two possible configurations, corresponding to the two possible polarity sequences.

(v) There are no solutions for the case $M_{12} = 0$, $M_{21} \neq 0$, but for the case

$M_{12} \neq 0$, $M_{21} = 0$

we find the restriction $d_1 = d_2/2$, for which equations (6.20) and (6.21) become

$$g_1 = -g_2 = \frac{1}{2d_1} \tag{6.22}$$

(d) For <u>cross-mirror symmetry</u> we require

$$q_1 = -q_6, \quad q_2 = -q_5, \text{ and } \quad q_3 = -q_4 \tag{6.23}$$

From this we find that equation (6.10) cannot be valid. Instead we need (from equation 5.25):

$$\begin{aligned} M_{11} &= \pm M_{33} \\ M_{22} &= \pm M_{44} \\ M_{12} &= \mp M_{34} \\ M_{21} &= \mp M_{43} \end{aligned} \tag{6.24}$$

which requires $q_1 = q_3$. This symmetry then reduces to the cross-translational symmetry discussed in (c).

In figure 6.4 we show point-to-point and parallel-to-parallel rays through a number of the above systems:

The system described in section (a - ii) and section (b) which has both translational and mirror symmetry is shown for both the strong and the weak solutions in figures 6.4a and 6.4b respectively. The systems with cross-translational symmetry described in sections (c - iv) - with inver=

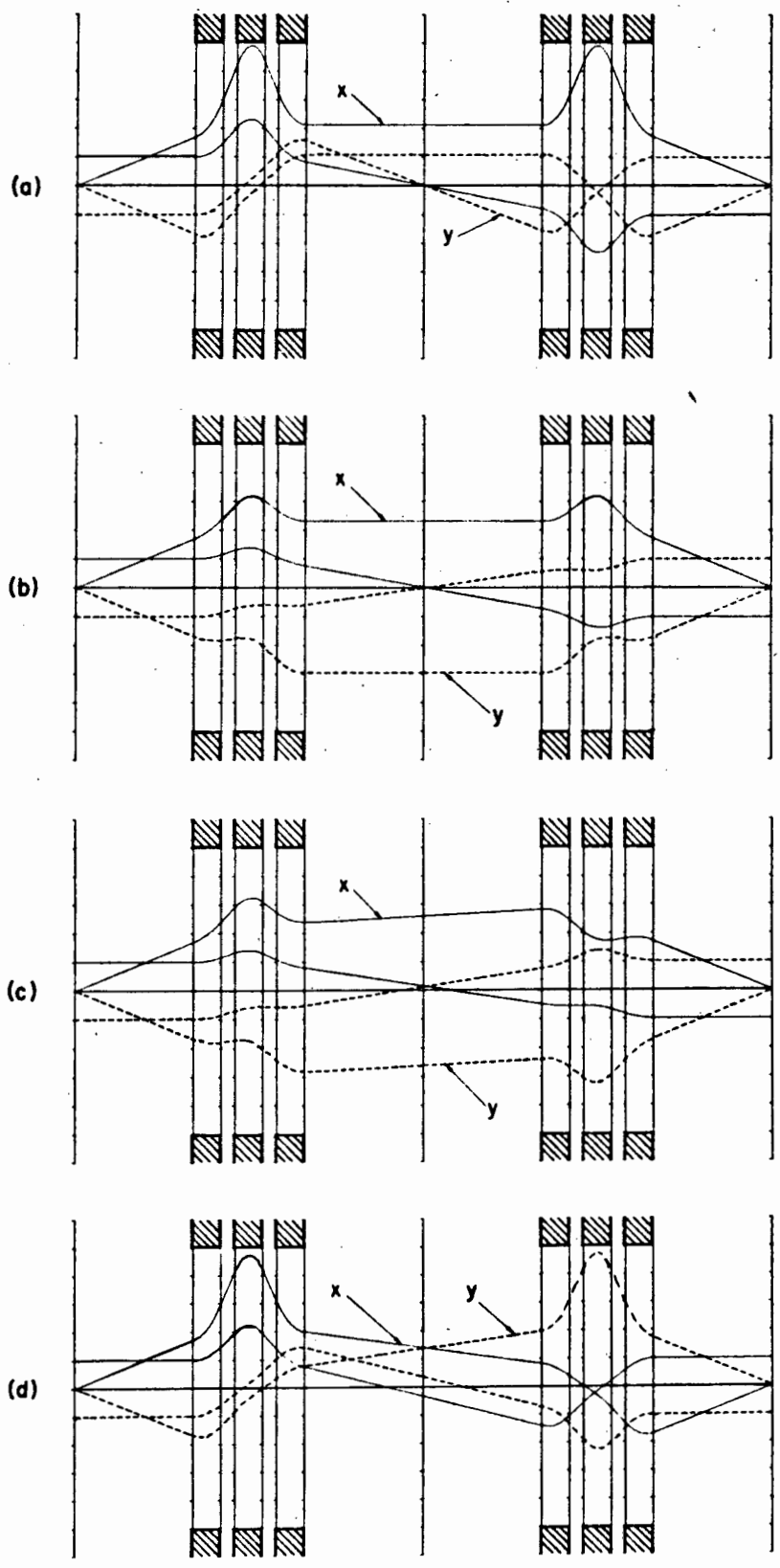

Figure 6.4: Point and parallel rays traced through telescopic systems with unit magnification.

(a) $R_{11} = R_{33} = -1$ translational symmetry, strong solution

(b) $R_{11} = R_{33} = -1$ translational symmetry, weak solution

(c) $R_{11} = R_{33} = -1$ cross-translational symmetry

(d) $R_{11} = R_{33} = +1$ cross-translational symmetry.

sion - and in section (c - i) - without inversion - are illustrated in figures 6.4c and 6.4d respectively. The quadrupole strengths were calculated using the computer program TRANSPORT, with the thin-lens strengths calculated above as starting values (to the fitting routine). These solutions are for a system with the following parameters:

$$d_1 = 1{,}7 \text{ m} \quad d_2 = 0{,}2 \text{ m} \quad L = 0{,}4 \text{ m}$$
$$B\rho = 21{,}495 \text{ kG.m} \quad a = 0{,}0381 \text{ m} \qquad (6.25)$$

Of the results quoted above, those in sections (a - ii) (c - i), (c - ii) and (c - iv) agree with the derivations of reference (KAR76).

6.4 Modified Telescopes

We define "modified telescopes" as quadrupole systems which provide both point-to-point and parallel-to-parallel transfer, and unit horizontal magnification M_x, but variable vertical magnification M_y (or unit M_y and variable M_x) i.e.

$$R_{11} = \pm 1, \quad R_{33} \neq \pm 1 \quad R_{ij} = 0 \quad i \neq j \qquad (6.26)$$

or

$$R_{11} \neq \pm 1, \quad R_{33} = \pm 1 \quad R_{ij} = 0 \quad i \neq j \qquad (6.27)$$

If we reverse the polarity of each quadrupole in the system described by equation (6.26), we then have the other configuration, described by equation (6.27).

As soon as we require either $|R_{11} \neq 1|$ or $|R_{33} \neq 1|$ we lose the symmetry of the quadrupole strengths which exist for a telescope, and the equations (6.26) or (6.27) become too unwieldy for analytical treatment. In the thin-lens approximation they take the form:

$$V_s + \sum_{i=1}^{6} a_{si} g_i + \sum_{i,j,k} b_{sijk} g_i g_j g_k + \sum_{i,j,k,l,m} c_{sijklm} g_i g_j g_k g_l g_m = 0$$

and

$$W_s + \sum_{i,j} d_{sij}\, g_i g_j + \sum_{ijkl} e_{sijkl} g_i g_j g_k g_l + f_s g_1 g_2 g_3 g_4 g_5 g_6 = 0$$

for s = 1, 2 and 3 (6.28)

where $V_1 = \frac{R_{33} - R_{11}}{2}$, $V_2 = V_3 = 0$

and

$$W_1 = 1 - \frac{R_{11} + R_{33}}{2}, \quad W_2 = W_3 = 0$$

and a, b, c, d, e and f are functions of d_1 and d_2 only.

In practice it is much simpler to solve equations (6.26) or (6.27) numerically, using the complete transfer matrix for each quadrupole and not the thin-lens approximation. Two methods of solution are discussed in section 6.6.

We have six equations to solve, i.e.

$$R_{11} = \pm 1, \qquad R_{33} = M_y,$$
$$\text{and} \quad R_{12} = R_{21} = R_{34} = R_{43} = 0 \tag{6.29}$$

and the six unknown quadrupole strengths, so we expect 6 solutions for R_{11}, $R_{33} < 0$ and a further 6 for R_{11}, $R_{33} > 0$. We have calculated these using the system parameters given in equation (6.25). We present these solutions in figures 6.5 and 6.7 for $|R_{33}| \geq 1$ only. We can obtain the results for $|R_{33}| < 1$ directly from these by traversing the system backwards which gives the inverse magnifications.

For unit horizontal and vertical magnification, these systems are simple unit telescopes, with symmetries discussed in section 6.3. Thus in figure 6.5 we show the six solutions for $R_{11} = -1$, $R_{33} \leq -1$ in the form of plots of quadrupole strengths as functions of R_{33}. Where the curves pass through $R_{33} = -1$, the quadrupole strengths for figures 6.5a, b, c and d are those determined for both translational and mirror symmetry in section 6.3 (a - ii), while for figures 6.5e and f they are those found in section 6.3 (c - iv) for cross-translational symmetry. It may be seen that the curves in figures 6.5c join with those in figure 6.5e at their turning points, i.e. at maximum magnification. Figures 6.5d and 6.5f are similarly linked. This linking is further illustrated in figure 6.6 in which the excursions of the individual quadrupole field strengths are plotted separately. Here the curves of figure 6.5c - e are linked, and also extended beyond unit magnification to include the reciprocal magnifications which would be obtained by traversing the system backwards.

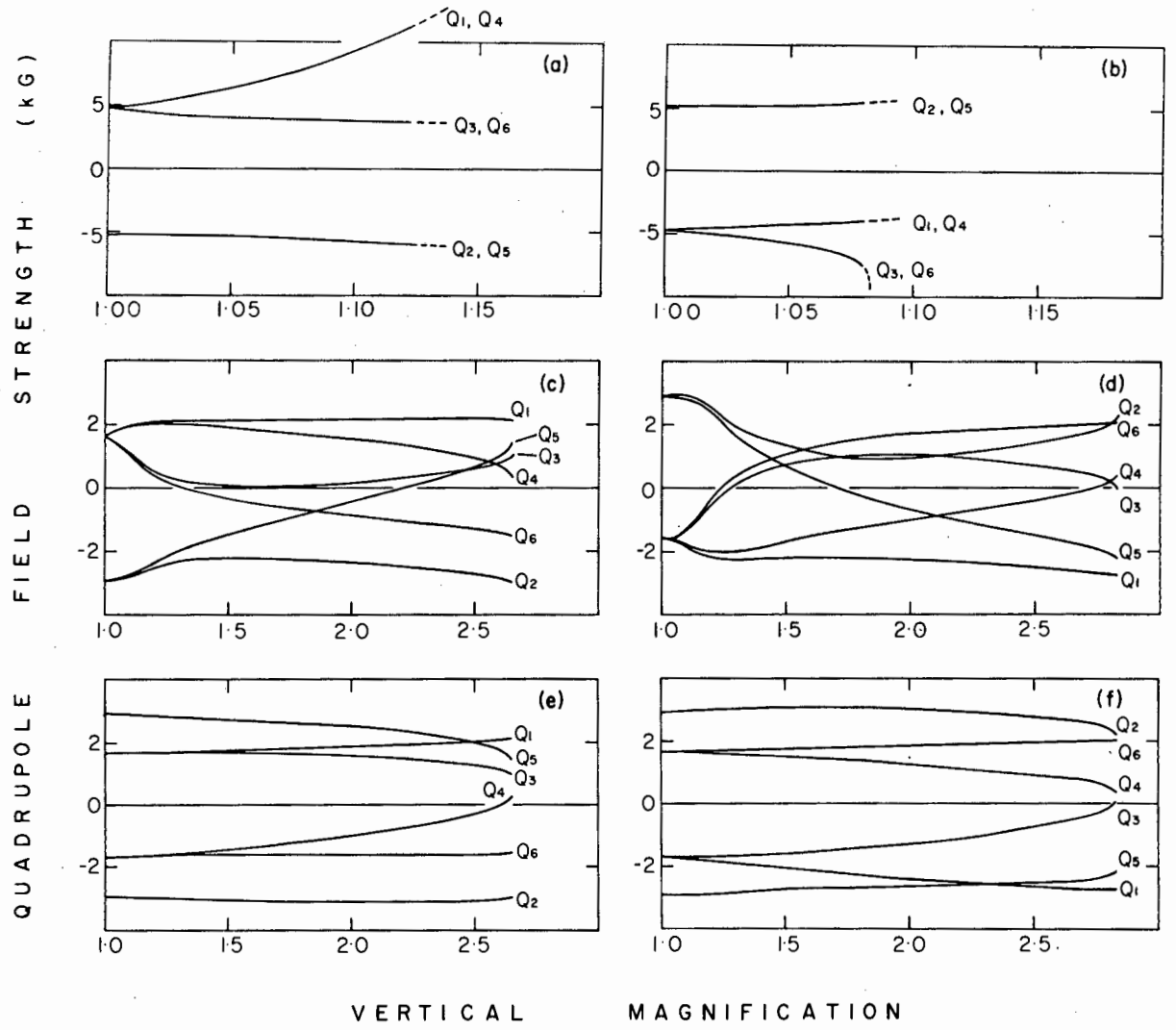

Figure 6.5: Sets of quadrupole field strengths as a function of R_{33} for the modified telescope case $R_{11} = -1$, $R_{33} \leq -1$. Note that the curves in (c) link with those in (e) and the curves in (d) link with those in (f). The curves (a) and (b) originate at the strong solution to the telescope, and are plotted on a different scale to the others.

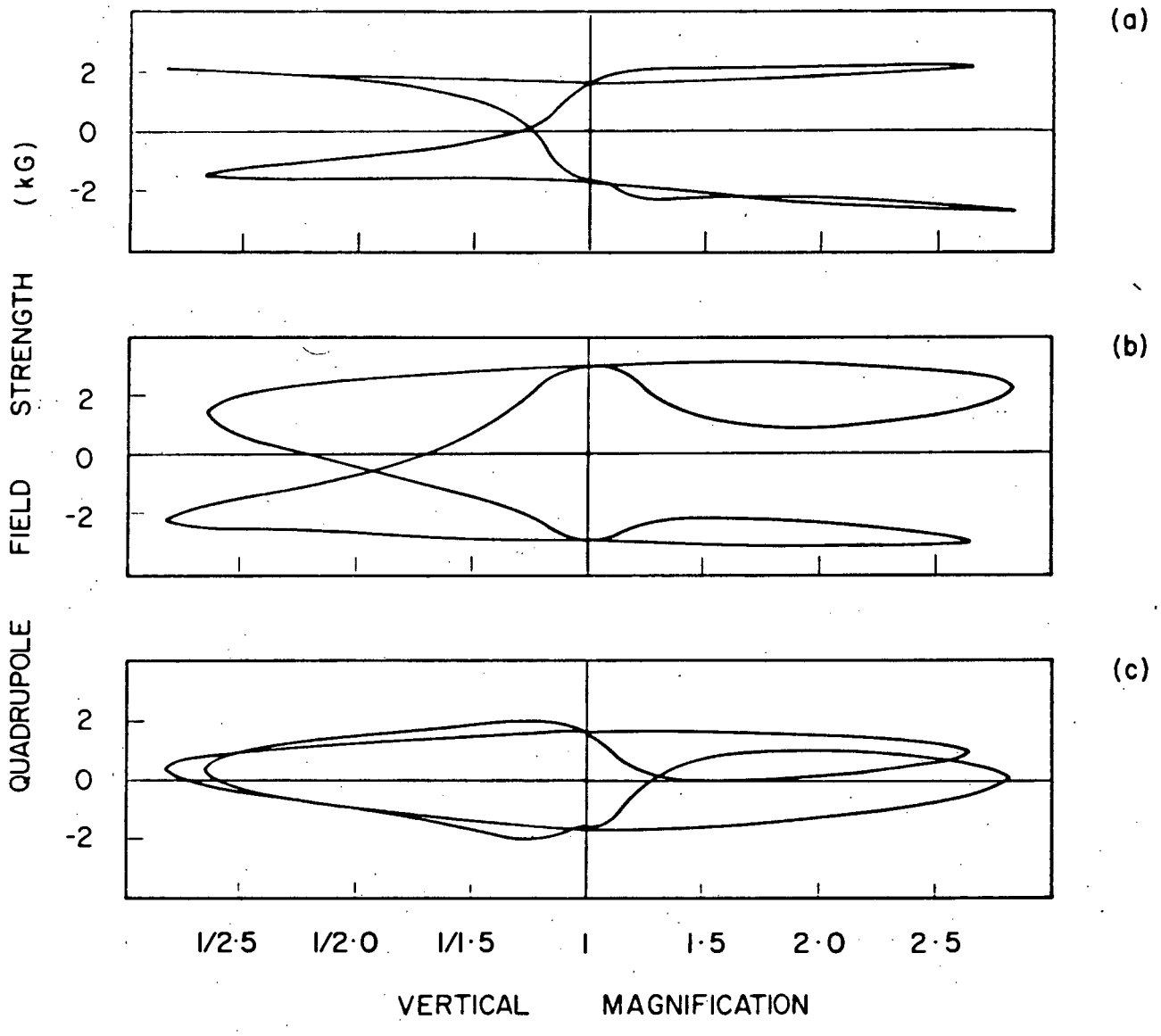

Figure 6.6: The quadrupole field strengths of (a) Q1, (b) Q2 and (c) Q3 as functions of magnification. Note the inverse scale used for values of $|R_{33}|<1$. The mirror images of these curves are the plots of Q6, Q5 and Q4 respectively. These curves are taken from figures 6.5(c) through (f).

Figure 6.7 shows the six solutions for $R_{11} = +1$, $R_{33} \geq +1$. The points $R_{33} = +1$ in figures 6.7a and b were predicted by the calculations of section 6.3 (c - i) for cross-translational symmetry, but these points in figures 6.7c, d, e and f are not accounted for by thin-lens theory because it is not valid for high quadrupole fields. However, the curves in figure 6.7a join with those in 6.7c at their turning points, and similarly for figures 6.7b and d.

Although a wide range of magnifications is made available, the quadrupole strengths tend to be large at the extremes of this range. If we restrict the quadrupole fields to $\leq$ 10 kG. for the example considered here, we can still obtain $0{,}125 < |R_{33}| < 8$. This is particularly useful in the situation where the vertical beam extent is limited (by a dipole aperture for example) early in the beamline, but a large vertical beam is required further on, e.g. at a target.

6.5 Zoom Lenses

We define "zoom lenses" as quadrupole systems which provide both point-to-point and parallel-to-parallel transfer, with equal, variable horizontal and vertical magnifications. This is thus analogous to the properties of the optical "zoom lens".

In the zoom lens system of $R_{11} = R_{33} \neq \pm 1$ reversal of quadrupole polarities does not affect the transfer matrix. Thus of the six possible solutions to the set of equations

$$\begin{aligned} R_{11} &= R_{33} = M_x \equiv M_y \\ R_{12} &= R_{21} = R_{34} = R_{43} = 0 \end{aligned} \tag{6.30}$$

only three are unique for each of $R_{11} < 0$ and $R_{11} > 0$. The method of solution of these equations is similar to that for equations (6.29), and is discussed in section 6.6.

We have calculated these solutions for the system with parameters defined in equation (6.25). The results for negative magnification are shown in figure 6.8, and those for positive magnification in figure 6.9.

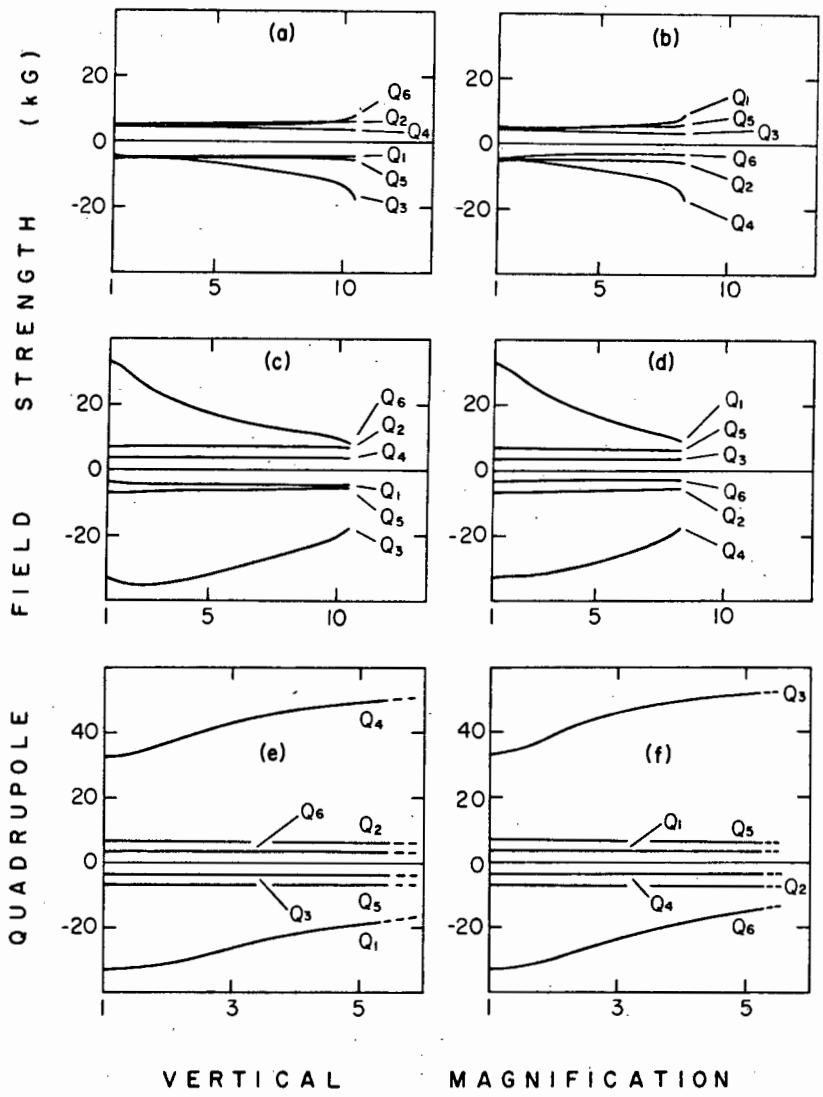

Figure 6.7: Sets of quadrupole field strengths as a function of R_{33} for the modified telescope case $R_{11} = +1$, $R_{33} \geq +1$. Note that the curves in (a) link with those in (c), and the curves in (b) link with those in (d). The scale is different for the set (e) (f).

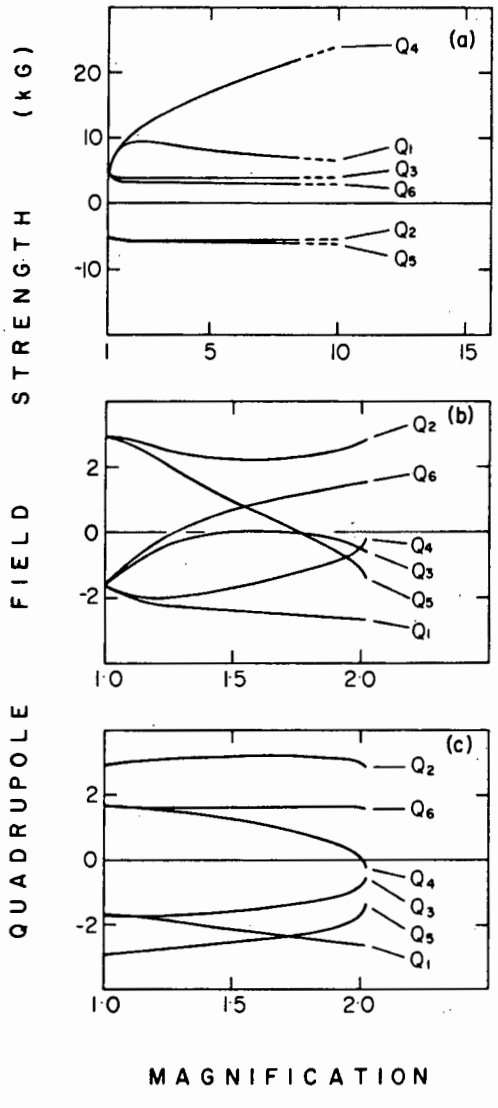

Figure 6.8: Three sets of quadrupole field strengths as a function of magnification for the zoom lens case $R_{11} = R_{33} \leq 1$. Note that the curves in (b) link with those in (c). Curves in (a) are plotted on a different scale. These originate at the strong solution to the telescope.

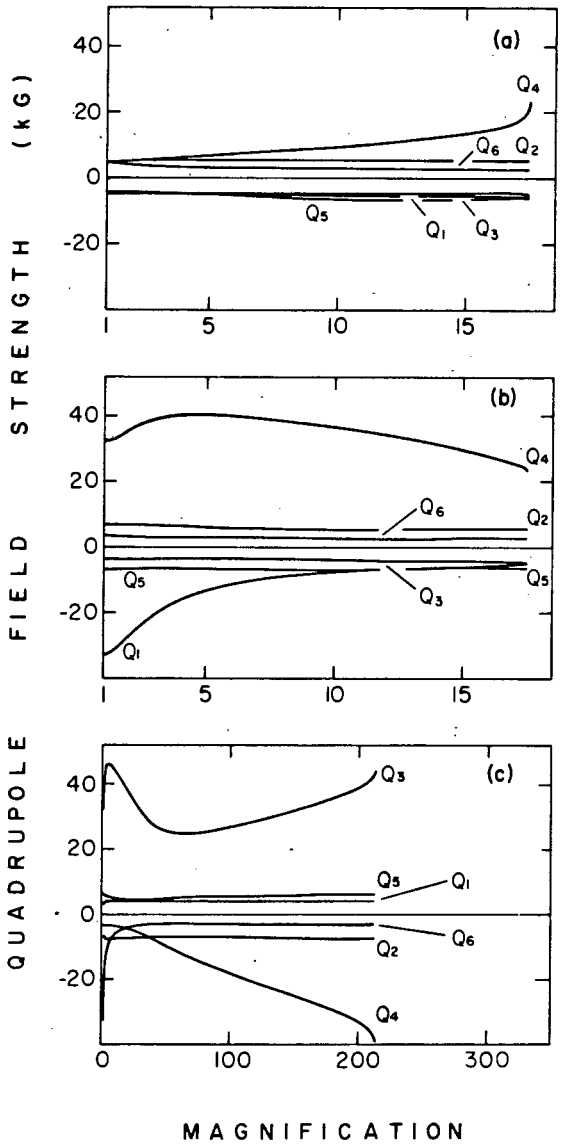

Figure 6.9: Three sets of quadrupole field strengths as a function of magnification for the zoom lens case $R_{11} = R_{33} \geq 1$. Note that the curves in (a) link with those in (b). The scale differs for plot (c).

The quadrupole field strengths at unit magnification are identical to the values found for the modified telescope in section 6.4. Thus the field strengths for unit magnification in figure 6.8a correspond to those of figures 6.5a and b, while those of figure 6.9a, for example, correspond to unit magnification in figures 6.7a and b. At maximum magnification the curves in figure 6.8b join with those of figure 6.8c, and similarly for figures 6.9a and b.

If, in the example given here, we limit the maximum quadrupole strengths to less than 10 kG.we can still achieve magnifications in the range $0{,}1<|R_{11}|<10$, which is more than adequate for most beamline applications.

6.6 Methods of Solution to Modified Telescope and Zoom Lens Systems

We have used two methods of finding the quadrupole strengths as a function of magnification for the modified telescope and zoom lens systems (i.e. solutions to equations (6.29) and (6.30)). In both of them a single solution for a given magnification is found after supplying an initial guess as to the possible quadrupole strengths. This initial guess will be similar to the solutions to the unit telescope for magnifications close to unity, and in the case of magnifications very different from unity, will be based on the adjacent solutions already found. The methods are described below.

(a) Computer Program TRANSPORT

The computer program TRANSPORT is used with constraints on R_{11}, R_{12}, R_{21}, R_{33}, R_{34} and R_{43}, allowing the quadrupole strengths to be varied until these constraints are satisfied. This program uses a method of non-linear least-squares with differential correction (BR071) to find the desired solution. We found that very often it would fit

$$R_{12} = R_{21} = R_{34} = R_{43} = 0 \qquad R_{11} = \pm 1$$

giving arbitrary values of the vertical magnification R_{33}, but when we required a specific value of $R_{33} = M_y \neq 1$, it would put

$$R_{33} = M_y + \lambda$$

This is also a point on the modified telescope curve of R_{33} vs. quadrupole strength, so it was of use in constructing the curve. For the zoom lens calculation, however, it was most unsatisfactory, as we would get

$$R_{11} = M + \gamma \qquad R_{33} = M + \lambda$$

and in most cases the errors γ and λ were too different to be able to use the result. (An error of 0,1% was considered acceptable.) Hence the need for an alternative method.

(b) Computer Program QUADS

We have written a computer program QUADS which uses an IMSL (IMSL: International Mathematical and Statistical Library) routine for solving the six simultaneous non-linear equations (6.29) or (6.30). The method employed in the routine is at least quadratically convergent, (BRO69), and requires 27 function evaluations per iterative step. We found this program satisfactory, especially for evaluating the zoom lens.

6.7 Conclusions

The two-doublet telescope provides a convenient method of transferring a beam over long distances with direct imaging of the initial beam. However it does have disadvantages:

(i) the beam may become large inside the quadrupoles if it is highly divergent initially;

(ii) the magnification is fixed at unity, and cannot easily be altered;

(iii) there are no vanishing second-order chromatic aberrations ($T_{116} = T_{226} = T_{336} = T_{446} \neq 0$, $T_{126} = T_{346} \neq 0$, $T_{216} = T_{436} \neq 0$).

If a two-doublet telescope is used, then sufficient space should be left between the quads in each pair. If necessary, the system may later be

upgraded to a two-triplet telescope by the addition of the two extra quads.

We see that the two-triplet telescope is an extremely versatile system. By altering only the quadrupole field strengths we can vary the magnifications obtainable in either the horizontal plane or the vertical plane, or both simultaneously. The ease with which we can change R_{11}, R_{33} from positive to negative values (or vice versa) is particularly useful when matching a beam to a spectrometer (see chapter 10). An additional advantage is that the chromatic aberration terms T_{116}, T_{226}, T_{336}, T_{446} vanish (in the mirror symmetrical systems).

In practice a table of quadrupole field strengths as a function of magnification may be drawn up for any given two-triplet configuration. These results depend only on the geometry of the system and the magnetic rigidity of the beam, but are easily scaled to a change in the latter. The initial beam parameters do not affect the system at all.

7. ORTHOGONAL QUADRUPOLE SYSTEMS

7.1 Introduction

In most beamlines, whether between pre-accelerator and main accelerator or between accelerator and target area, elements are required to enable the size and shape of the beam to be varied. As we have mentioned before, quadrupole lenses have suitable focussing properties. Unfortunately, however, the action of a quadrupole is focussing in one plane but defocussing in the other, and various combinations of quadrupoles must be used to achieve overall focussing in both planes. As a result, the changes to the beam shape in one plane are difficult to decouple from changes in the other.

In an idealised situation we would like to have these beam shaping quadrupoles restricted to a short section of beamline, probably between two sets of slits, and operating in waist-to-waist mode. In such a section we then require a minimum of four quadrupoles to transform a double waist at the initial slit into another double waist of given size at the final slit. With four quadrupoles, however, altering the field strength of any one or more quadrupoles to vary the size of the beam in the horizontal plane unavoidably affects the beam in the vertical plane, and vice versa i.e. the shaping in x and y is not independent, and all quadrupoles must be adjusted in a complicated manner. However, by using an additional two quadrupoles, we can separate the shaping in x and y, making them independent of each other. The quadrupoles which control the x-shaping are then said to be "orthogonal" to those which control the y-shaping. This principle has been incorporated into the transfer beamline at SIN (MAR75), and discussed by Joho (JOH75) but the quadrupoles are distributed throughout the transfer beamline, and their operation is not as simple as in the specialised waist-to-waist section we propose here.

7.2 Concept

The way in which we propose to operate the system is shown in figure 7.1. Here we represent the quadrupoles by thin lenses and the initial waist by a point source. The rays drawn are those of maximum divergence at the initial waist for x and y respectively. The quadrupoles Q_3 and Q_5 (con-

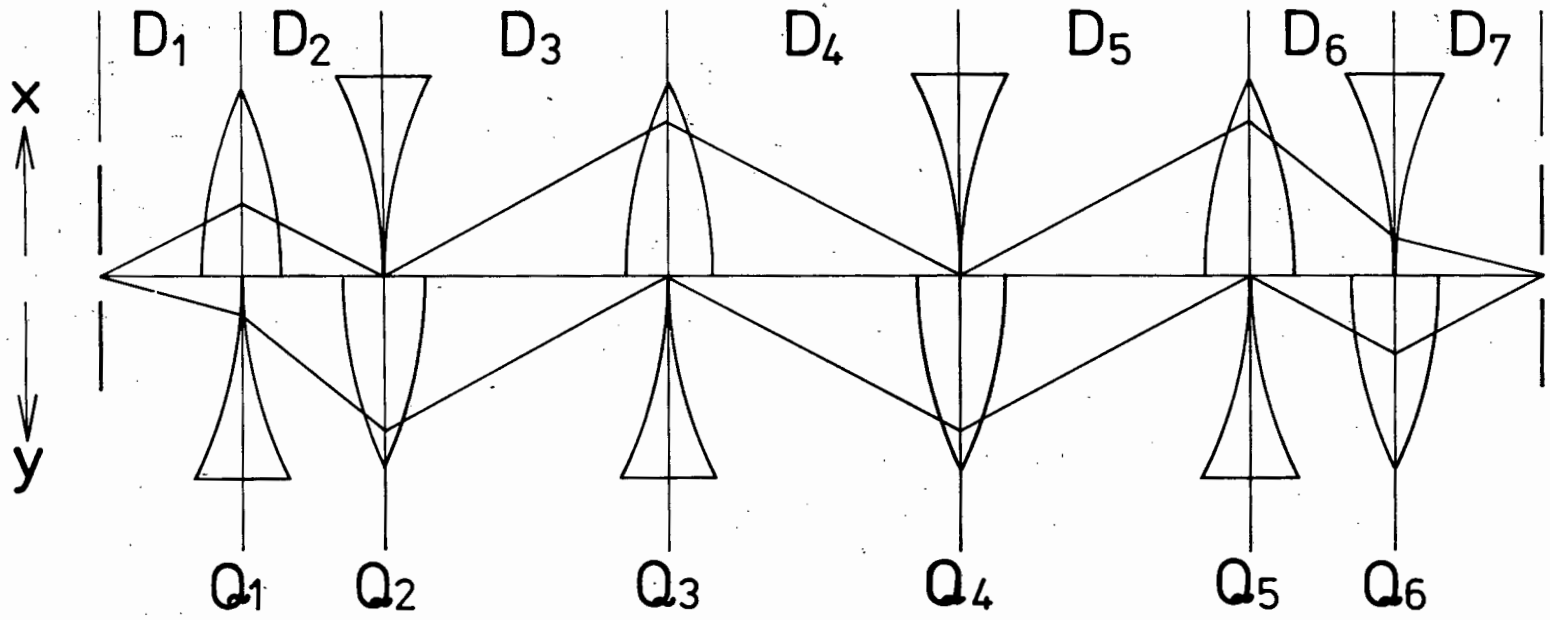

Figure 7.1: A system of six quadrupoles (represented as thin-lenses) in an orthogonal arrangement. The rays shown have maximum initial and final divergences both horizontally (x) and vertically (y).

trolling x only) are orthogonal to Q_2 and Q_4 (controlling y only). The quadrupoles Q_1 and Q_6 serve only to separate x and y into "orthogonal" modes.

Thin lenses and point sources are, of course, only theoretical approximations, and we might expect to achieve only approximate orthogonality in practice. However we shall show that the independence of x and y is remarkably good.

We have mentioned that the beam should not become too large inside the quadrupoles to avoid the cost of large aperture quads. From figure 7.1 we can see that the horizontal beam size becomes large in Q_3 and Q_5, and the vertical size large in Q_2 and Q_4. The optimum solution for limiting the size will be such that x in Q_3 should equal x in Q_5, this size being equal to y in Q_2 and Q_4. We can determine the placing of the quadrupoles in the system, to achieve this optimum sizing, using thin-lens optical theory, as follows:

We stated in chapter 4 that the focal length of a quadrupole in the focussing plane is

$$f_c = \frac{1}{k \sin kL}, \qquad (4.10)$$

and in the defocussing plane it is

$$f_d = \frac{1}{k \sinh kL} \qquad (4.13)$$

The (first-order) approximation for thin lens optics was given in equation (4.14)

i.e. $f_c = -f_d = 1/k^2L$

where c refers to focussing, and d to defocussing actions. If we put $f_0 = 1/k^2L$, we can then apply the more realistic (second-order) approximation (REG67):

$$f_c = f_0 + L/6 \qquad (7.1)$$

$$f_d = f_0 - L/6 \qquad (7.2)$$

We now apply equations (7.1) and (7.2) to the quadrupoles in figure 7.1 to find the optimum spacing for the quadrupoles. The equations in the

following two sections will be fully derived in Appendix D: only the more important steps are shown as equations (7.4) - (7.35).

It should be noted that the drift lengths D_1 through D_7 are measured to the centres of the quadrupoles, such that

$$\sum_{i=1}^{7} D_i = T \qquad (7.3)$$

where T is the total length of the system.

7.3 Double Waist

We first treat the case where both x and y are at a waist initially. This treatment applies to a double waist at the end of the system as well. We assume a point source, so that we may apply point-to-point optics. This is a valid approximation if the waists are narrow, i.e. if x is small compared to x´, and y small compared to y´. With this assumption we find that the only beam parameters entering the calculation are the initial divergences x_i' and y_i', and the final divergences x_f' and y_f', as well as the magnetic rigidity of the beam.

The thin-lens equation for the rays affected by Q_1, is, for x:

$$\frac{1}{D_1} + \frac{1}{D_2} = \frac{1}{f_c} = \frac{1}{f_0 + L/6} \qquad (7.4)$$

which specifies an x cross-over at the centre of Q_2. Introducing the distance from the initial waists to the centre of Q_2 as the parameter $E = D_1 + D_2$ leads to

$$f_0 = \frac{D_1(E - D_1)}{E} - \frac{L}{6}. \qquad (7.5)$$

Similarly for y we have

$$\frac{1}{D_1} - \frac{1}{r} = \frac{1}{f_d} = \frac{1}{\frac{L}{6} - f_0} \qquad (7.6)$$

where the distance r is defined in figure 7.2 . Also shown in the figure is y_2, which, from geometrical considerations, can be calculated as

$$y_2 = y_i'\left[\frac{D_1 D_2}{r} + D_1\right]. \qquad (7.7)$$

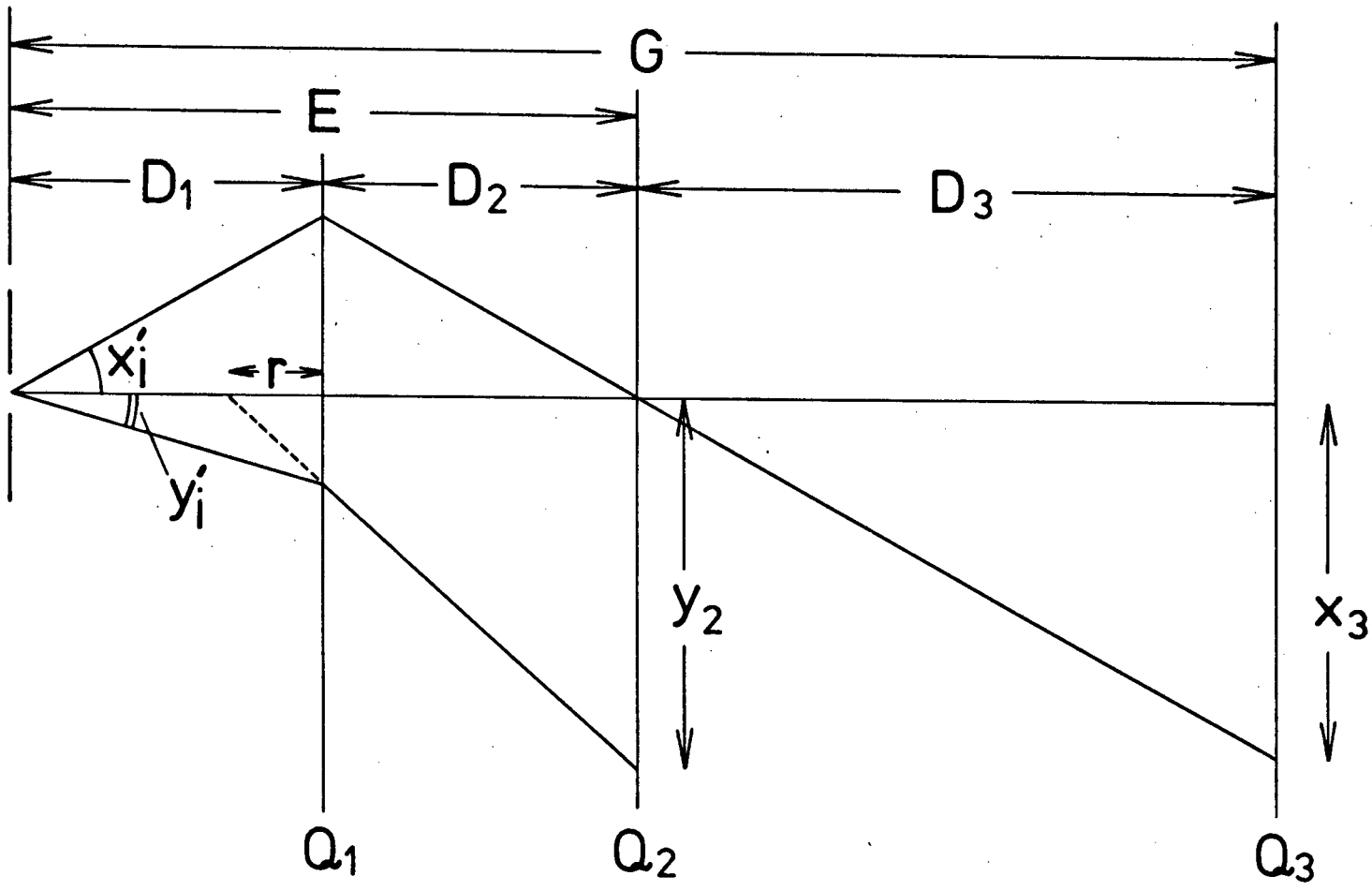

Figure 7.2: Schematic representation of the first three quadrupoles of figure 7.1 showing the size of the beam in Q2 and Q3, for the case of an initial double waist.

When we combine equations (7.5), (7.6) and (7.7), we find

$$y_2 = y_i' E \left[1 + \frac{3D_1(E-D_1)}{3D_1(E-D_1)-EL} \right] . \qquad (7.8)$$

We want y_2 to be a minimum (to restrict the beam size in Q_2). Hence, differentiating and putting $dy_2/dD_1 = 0$, together with equations (7.5) and (7.8), we find

$$D_1 = D_2 = \frac{E}{2} \qquad (7.9)$$

and

$$f_0 = \frac{D_1}{2} - \frac{L}{6} . \qquad (7.10)$$

We also require the horizontal beam size x_3 in quadrupole Q_3 to be of the same order as y_2. From figure 7.2 it can be seen that x_3 is directly proportional to D_3. Equation (7.8) can be re-written using equation (7.9) giving

$$y_2 = y_i' 4D_1 \left[\frac{3D_1 - L}{3D_1 - 2L} \right], \qquad (7.11)$$

which, for small L and putting $D_1 + D_2 + D_3 = G$ becomes

$$y_2 \approx 2y_i'(G-D_3) \qquad (7.12)$$

i.e., y_2 is proportional to the difference between the composite length G and the drift length D_3. Thus y_2 decreases with increasing D_3, while x_3 increases with D_3. The minimum quadrupole aperture is thus reached when D_3 is chosen such that they are equal, i.e., $x_3 = y_2$, giving

$$D_3 = \frac{y_2}{x_i'} . \qquad (7.13)$$

If we want the same (minimum) beam size in Q_4 and Q_5 as well, we find from the symmetry shown in figure 7.1 that

$$D_3 = D_4 = D_5 . \qquad (7.14)$$

Equations (7.9) and (7.11) will also apply to a double waist at the end of the system as well, and we find that

$$D_6 = D_7 \qquad (7.15)$$

and

$$D_5 = \frac{x'_f}{y'_f} 4D_7 \left[\frac{3D_7 - L}{3D_7 - 2L}\right]. \qquad (7.16)$$

Thus, using equations (7.3), (7.9) and (7.11) to (7.16), we can solve for all the drift lengths in terms of the initial and final divergences. For the special case of equal ratios of horizontal to vertical divergences initially and finally, i.e.,

$$\frac{y'_i}{x'_i} = \frac{y'_f}{x'_f} = 1 \qquad (7.17)$$

then $D_1 = D_7$ (7.18)

and $4D_1 + 3D_3 = T$ (7.19)

which leads to $48D_1^2 - (20L + 3T)D_1 + 2LT = 0,$ (7.20)

giving two solutions for D_1. In many cases it will be found that the smaller value is less than the quadrupole length L, and the larger solution has to be used.

7.4 Waist in One Dimension Only

The treatment below is a general one, in that even if the system under consideration does not start at a waist, we may theoretically always increase (or decrease) D_1 until a waist in at least one dimension is reached.

Then we extend it further a distance P (as shown in figure 7.3) until a waist in the other dimension is found. Equation (7.4) still holds true, but equation (7.6) now becomes

$$\frac{1}{D_1 + P} - \frac{1}{r} = \frac{1}{f_d} = \frac{1}{\frac{L}{6} - f_0} \qquad (7.21)$$

and equation (7.8) becomes

$$y_2 = y'_i \left[E + P + \frac{3E(PE + D_1E - D_1P - D_1^2)}{3D_1(E - D_1) - LE}\right]. \qquad (7.22)$$

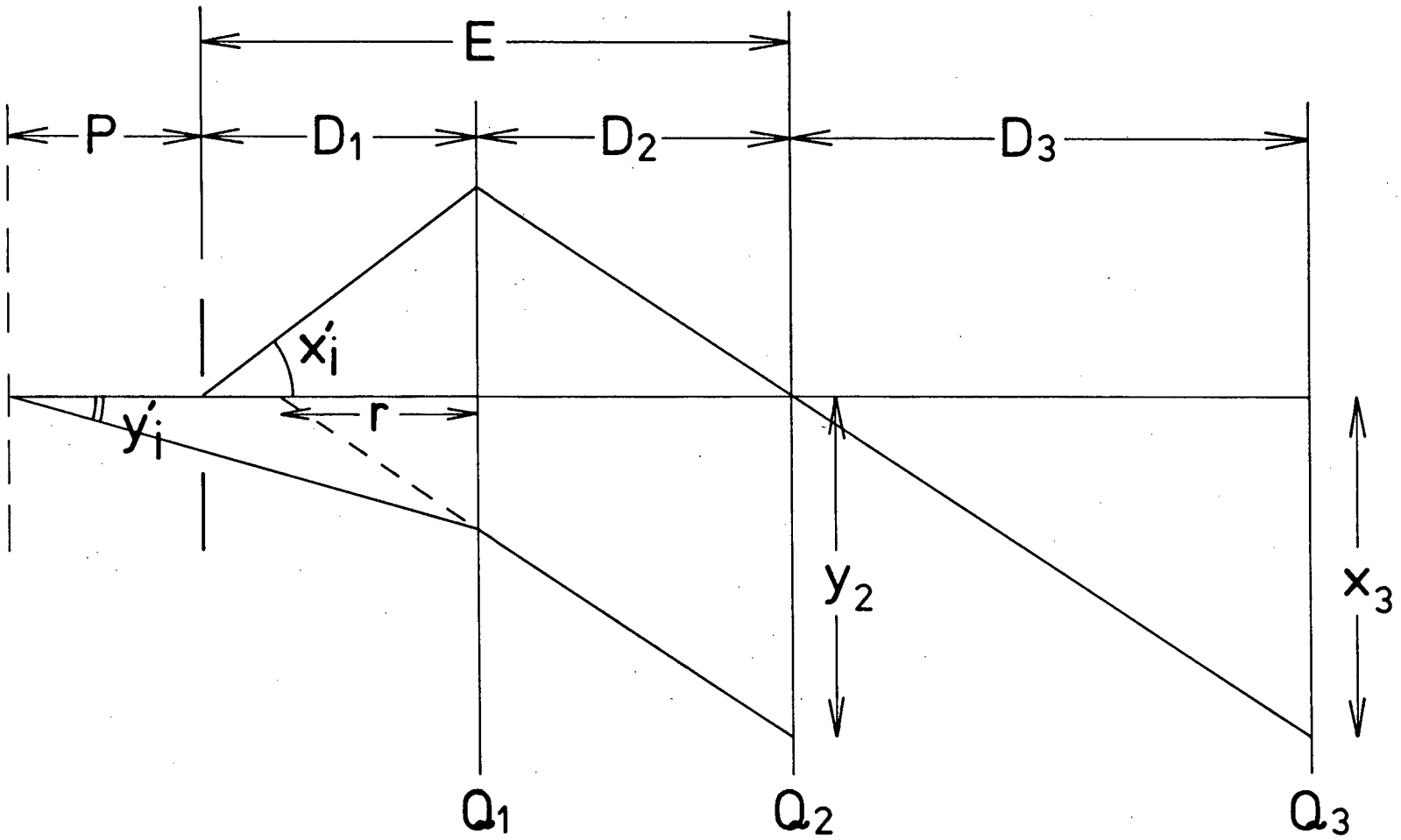

Figure 7.3: Schematic representation of the first three quadrupoles of figure 7.1 for the case where the initial y waist is at a distance P behind the initial x waist.

Putting $dy_2/dD_1 = 0$ as before, now leads to the result

$$D_1 = E + \frac{EL}{3P}\left[1 - \left(1 + \frac{3P}{L} + \frac{3P^2}{EL}\right)^{\frac{1}{2}}\right] \qquad (7.23)$$

and thus

$$y_2 = y'_i\left[2E + P + \frac{3P^2}{3P + 2L\left\{1 - \left(1 + \frac{3P}{L} + \frac{3P^2}{EL}\right)^{\frac{1}{2}}\right\}}\right] \qquad (7.24)$$

Putting $x_3 = y_2$ as before we now find

$$D_3 = \frac{y_2}{x'_i}\,\frac{D_2}{D_1} = \frac{y_2}{x'_i}\,\frac{E - D_1}{D_1} \qquad (7.25)$$

If we assume that we have a double waist at the end of the system, then equations (7.14) to (7.16) will be valid. These, together with equations (7.3) and (7.23) to (7.25) completely define the system.

We have written a computer program ORTHO to calculate the following quantities:

$$D_1 = E + \frac{EL}{3P}\left[1 - \left(1 + \frac{3P}{L} + \frac{3P^2}{EL}\right)^{\frac{1}{2}}\right], \qquad (7.26)$$

$$D_3 = \frac{y'_i}{x'_i}\left[2E + P + \frac{3P^2}{3P + 2L\left(1 - \left(1 + \frac{3P}{L} + \frac{3P^2}{EL}\right)^{\frac{1}{2}}\right)}\right]\left[\frac{E - D_1}{D_1}\right] \qquad \ldots (7.27)$$

$$D_7 = \frac{4L + 3\frac{y'_f}{x'_f}D_3 \pm \left[16L^2 - 72\frac{y'_f}{x'_f}LD_3 + 9\left(\frac{y'_f}{x'_f}\right)^2 D_3^2\right]^{\frac{1}{2}}}{24} \qquad \ldots (7.28)$$

$$A = E + 3D_3 + 2D_7 - T \qquad (7.29)$$

The input to the program consists of: L, T, P, y'_i/x'_i and y'_f/x'_f.

A range of values for E is used, for each of which D_1, D_3, D_7 and A are calculated. Those values which result in A = 0 give a solution to the system. Some solutions may be discarded in practice because of the restriction that $D_i > L$ for i = 1, ..., 7, i.e. all seven drift lengths must

be somewhat larger than the effective length of a quadrupole. Other solutions, while physically possible, give equal maximum values of x and y which do not necessarily correspond to the smallest maxima obtainable. These should also be discarded.

Having found the inter-quadrupole spacing, we can find the focal lengths of the quadrupoles (and hence the field strengths) from the following equations.

$$f_1 = \frac{D_1 (E - D_1)}{E} - \frac{L}{6} \tag{7.5}$$

$$f_2 = \frac{D_3 \{ EC_2 + PC_2 + 3P (E - D_1)^2 \}}{D_3 (C_2 + 3D_1^2 + 3PE) + EC_2 + PC_2 + 3P(E - D_1)^2} - \frac{L}{6} \tag{7.30}$$

where $C_2 \equiv 6D_1 (E - D_1) - LE$ (7.31)

$$f_3 = f_4 = \frac{D_3}{2} - \frac{L}{6} \tag{7.32}$$

$$f_5 = \frac{2 D_3 D_7 C_5}{D_3 (3D_7^2 + C_5) + 2D_7 C_5} - \frac{L}{6} \tag{7.33}$$

where $C_5 \equiv 6 D_7^2 - 2 D_7 L$ (7.34)

and $f_6 = \frac{D_7}{2} - \frac{L}{6}$ (7.35)

The polarities of the quadrupoles have not been incorporated into these equations yet. Either the set f_1, f_3 and f_5 or the set f_2, f_4 and f_6 require negative signs. The method of choosing polarities is discussed in the next section.

7.5 Quadrupole Polarities

We define the "normal" quadrupole polarities for any given system as those which result in minimum beam width in the quadrupoles. This implies that if $x'_i > y'_i$ then Q_1 should be positive (x-focussing). The subsequent quadrupoles always have alternate polarities (see figure 7.1). Conversely, if $x'_i < y'_i$ then the normal polarity of Q_1 is negative. If $x'_i = y'_i$ the normal polarity sequence is then determined in a similar manner by the ratio y'_f/x'_f. If this is greater than unity, the normal polarity for Q_6 is negative and the alternate polarity sequence implies Q_1

positive. If, however, we wish to change x_f and y_f from their optimum values so that $y'_f/x'_f < 1$, than we should use the reverse polarity sequence. We may do this because $x'_i = y'_i$ sets no normal polarity for Q_1. However, if x'_i is very different from y'_i, conflicting requirements at the initial and final quadrupoles may result in large beam extent in the quadrupoles.

7.6 Results

We have used the program TRANSPORT to test the validity of our approximations. We used equations (7.30) to (7.34) to find initial estimates for the quadrupole strengths. The results of our investigation are discussed below and summarized in Table 7.1.

We consider both the case P = 0 (initial waists in x and y coincident) and the case P ≠ 0 (initial waists not coincident) in a system which we have chosen to be 13 m long, with quadrupoles of effective length L = 0,40 m.

(a) P = 0

We examine a special case where $y'_i / x'_i = (y'_f/x'_f)^{-1}$ and we choose $y'_i/x'_i = 0{,}75$ and thus $y'_f/x'_f = 1{,}33$. From the results of program ORTHO we find:

$$D_1 = D_2 = D_6 = D_7 = 0{,}86667 \text{ m and } D_3 = D_4 = D_5 = 3{,}17777 \text{ m.}$$

For an emittance of 3π mm.mrad, we have selected initial values:

$$x_i = 0{,}5 \text{ mm}, \quad x'_i = 6 \text{ mrad}, \quad y_i = 0{,}667 \text{ mm}, \quad y'_i = 4{,}5 \text{ mrad.}$$

Using the calculated distances between quadrupole centres, we then used TRANSPORT to fit waists at succeeding quadrupoles, and so to form a final double waist. In figure 7.4 we show the beam envelope plotted through this system. From this we can see that x in Q_3 and Q_5 is nearly identical to y in Q_2 and Q_4. The actual ratio y'_f/x'_f is 1,23, compared with the design value of 1,33 used in the thin-lens treatment. The plot shows optimum values of x_f and y_f, i.e., for which the system is properly orthogonal.

TABLE 7.1: A range of final beam parameters obtainable for the special case discussed in the text.

Quadrupole polarities	x_f (mm)	y_f (mm)	$\frac{y'_f}{x'_f}$	Figure
Normal	0,64	0,52	1,23[a]	7.4
Normal	7,00	0,52	13,46	7.5(a)
Normal	0,64	0,32	2,00	7.5(b)
Reversed	0,40	0,88	0,454	-
Reversed	0,40	7,00	0,057	7.6(a)
Reversed	0,35	0,88	0,398	7.6(b)

[a] Thin-lens design value = 1,33

If we alter only Q_3 and Q_5 to change x_f from its optimum value of 0,64 mm to 7,0 mm, y_f is unaffected and remains equal to 0,52 mm. This is demonstrated in figure 7.5(a). If, instead, we alter Q_2 and Q_4 to change y_f from 0,52 mm to 0,32 mm, x_f is completely unaffected and remains equal to 0,64 mm as shown in figure 7.5(b). If each of these two cases the final ratio y'_f/x'_f is increased relative to the thin-lens design value (refer to Table 7.1). The system as designed works well for $y'_f/x'_f > 1$. For $y'_f/x'_f < 1$ the system should be used with the quadrupole polarities reversed. This is illustrated in figure 7.6(a), where x now behaves similarly to y in figure 7.5(a); and in figure 7.6(b) where x behaves like y in figure 7.5(b). In the reverse polarity cases illustrated, the ratio y'_f/x'_f is decreased relative to the design value.

With these two modes of operation of the system, a very wide range of sizes of the final waists can be obtained. The range can in principle be extended even further than shown above, but the size of the beam in the fourth or fifth quadrupole may become large, depending on the emittance. The position of the waists also shifts slightly: for example, in figure 7.5(a) where x_f is much greater than the thin-lens design size, the beam becomes large in Q_5 and the x-waist is no longer in the middle of Q_4. This implies that any subsequent alteration to y_f will also slightly affect x_f. This defect is exaggerated in figure 7.6(a) because reverse polarities are less favourable for the case illustrated where $x'_i > y'_i$.

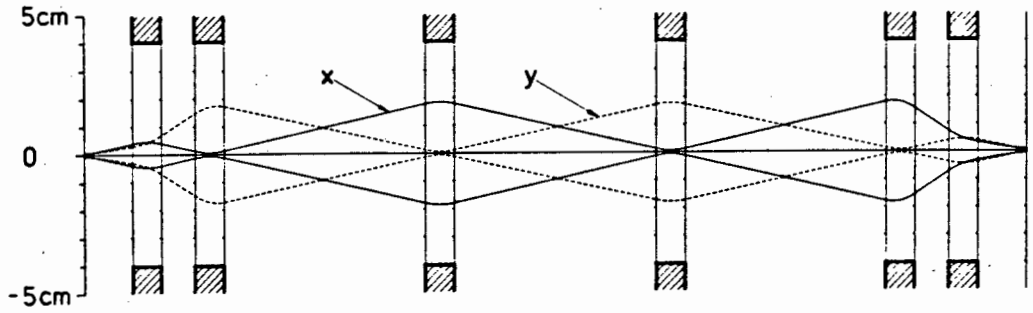

Figure 7.4: Beam envelope plot for a system designed for $y_i'/x_i' = 0{,}75$ and $y_f'/x_f' = 1{,}33$ showing optimum values of x_f and y_f.

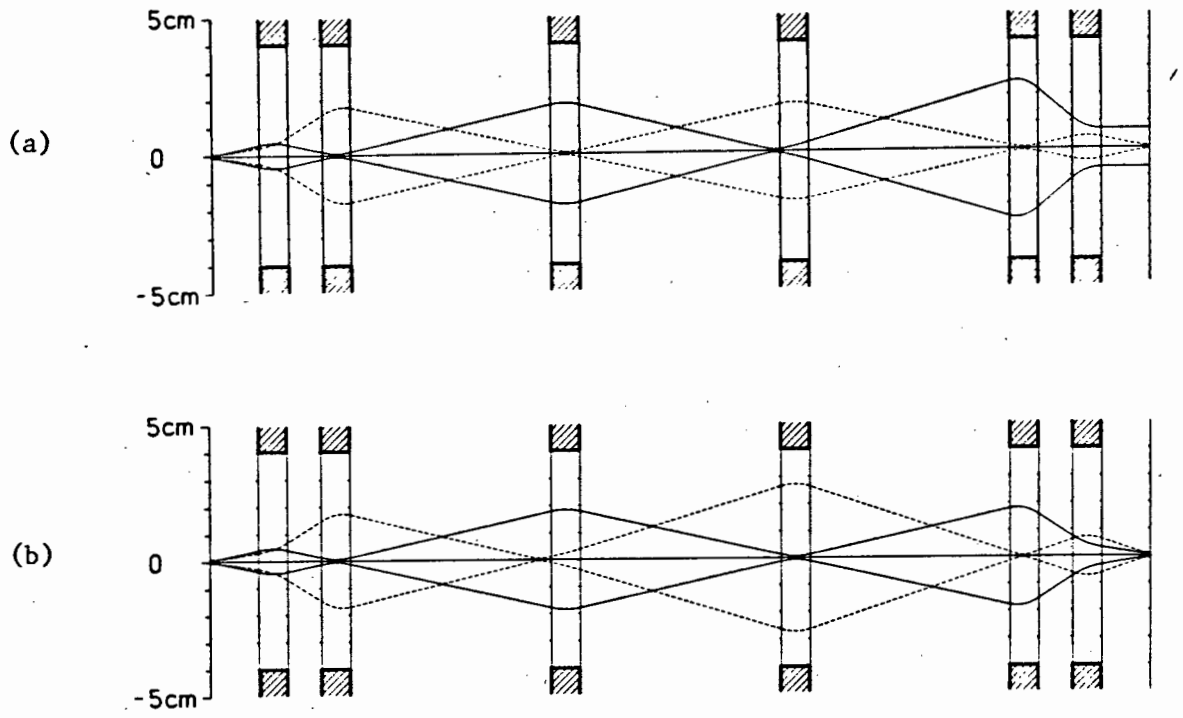

Figure 7.5: Beam envelope plots for the system shown in figure 7.4 with:
(a) x_f increased to 7 mm and y_f unaltered; and
(b) y_f decreased to 0,32 mm and x_f unaltered.

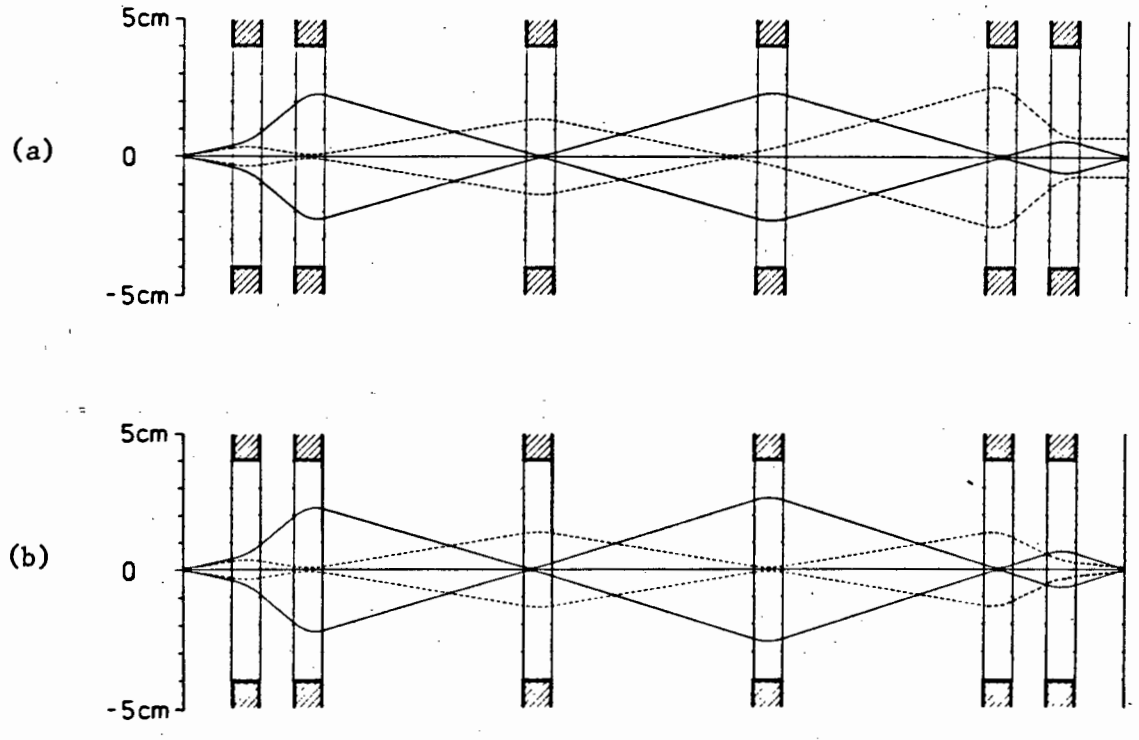

Figure 7.6: Beam envelope plots for the system shown in figure 7.4, but with reverse polarities, giving

(a) y_f = 7 mm and x_f unaltered from the optimum value for this polarity sequence;

(b) x_f = 0,35 mm and y_f unaltered from the optimum value for this polarity sequence.

If the input beam is such that y'_i/x'_i is larger than the thin-lens design value, then the maximum value of y in the quadrupoles increases and that of x decreases, and vice versa for smaller y'_i/x'_i. This effect may be seen in figure 7.7, plotted for $y'_i/x'_i = 1,0$ instead of 0,75. The orthogonality of the quadrupoles is not affected, however.

(b) $P \neq 0$

Here we consider a system designed for P = 0,5 m, $y'_i/x'_i = 0,6$ and $y'_f/x'_f = 2,5$.

Figure 7.8 gives the beam envelope plot for an emittance of 3π mm.mrad, with x'_i = 6 mrad and y'_i = 3,6 mrad, with the vertical waist 0,5 m before the horizontal waist. Note that D_1 is no longer equal to D_2. The actual ratio y'_f/x'_f is 2,492 — very close to the thin-lens design value of 2,500.

In all the above cases we have started with x small compared to x', and the orthogonality of the quadrupoles is very good. If we start with larger x_i and y_i (implying smaller x'_i and y'_i respectively for any given emittance) we find larger waists within quadrupoles Q_2 to Q_5 and there is thus more effect on one dimension when the other is varied (i.e., the orthogonality becomes degraded). However, this only becomes noticeable when x or y (in mm) is larger than x' or y' (in mrad) respectively.

7.7 Conclusion

We have demonstrated that the orthogonal quadrupole system gives excellent independent control over the horizontal and vertical focussing properties for both coincident and non-coincident initial waists. While it is in principle possible to accomplish the same focussing with only four quadrupoles, using a computer-linked control system and look-up tables, for example, this also requires very precise knowledge of the initial beam parameters. In practice these are rarely so well-defined, and manual tuning is almost always required. The orthogonal quadrupole

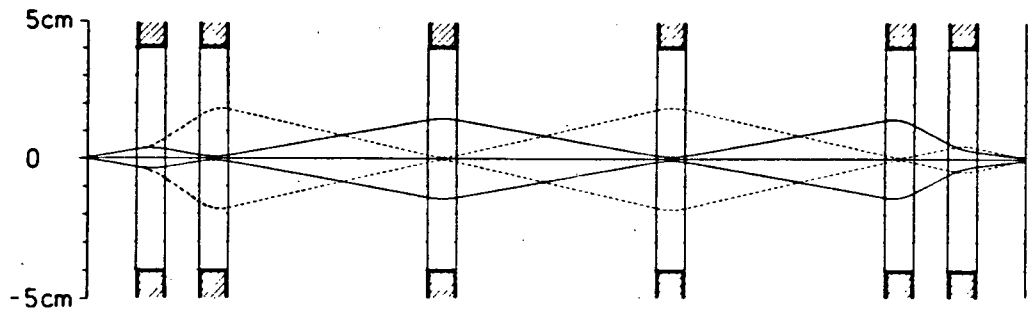

Figure 7.7: Beam envelope plot for the system shown in figure 7.4 with $y_i'/x_i' = 1$ (i.e., larger than the design value) showing the larger maximum y in the quadrupoles which is obtained.

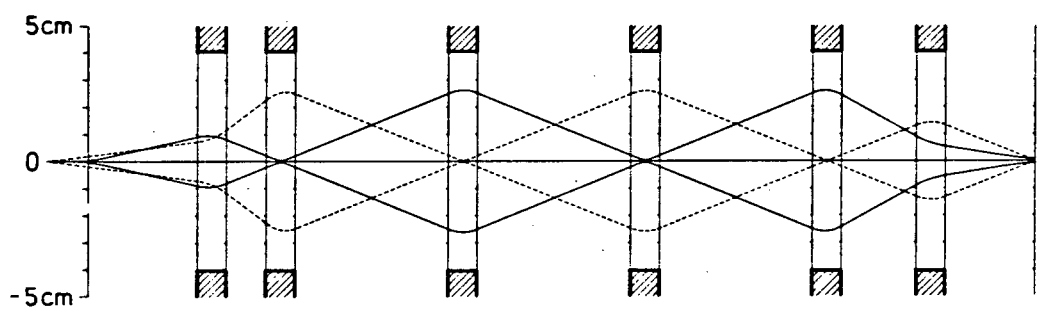

Figure 7.8: Beam envelope plot for a system with P = 0,5 m, $y_i'/x_i' = 0,6$ and $y_f'/x_f' = 2,5$.

system described here is considered to provide sufficiently improved ease of operation to warrant the cost of the two additional quadrupoles.

The advantage of the orthogonal quadrupole system over the two-triplet telescope (with modified telescope and zoom lens capabilities) is the ease with which the system may be tuned, expecially when the waist size is to be altered in only one dimension. The range of possible magnifications is also greater, with lower quadrupole field strengths. A disadvantage of the orthogonal quadrupole system is its dependence on initial beam parameters. This system should therefore only be used in such sections of beamline where:

(i) the initial conditions are unlikely to vary greatly, and
(ii) we require the beam leaving the system to be easily adjustable.

Examples of such sections are given in chapters 9 and 10. A further disadvantage of the orthogonal quadrupole system is that no chromatic aberration terms vanish. However if a two-triplet telescope is used with non-unit magnifications, then the symmetry of the system is lost and all chromatic aberration terms are also present.

8. DIPOLE SYSTEMS

8.1 Introduction

Dipoles are used in beam transport systems for one or more of the following reasons:

(i) to send the beam in the desired direction;
(ii) to achromatise a dispersed beam, or
(iii) to disperse an achromatic beam.

We are not concerned here with situations in which dipoles are used only to bend the beam. We will discuss the behaviour of the off-momentum rays in two-dipole systems only, as 3 or more dipoles are rarely used for dispersion matching. (A single-dipole system is described in section 9.8.)

Of interest are the situations where

(a) a beam with arbitrary dispersion is to be achromatised. The reverse of this situation gives arbitrary dispersion to an achromatic beam;

(b) the momentum spread of a beam is to be reduced by removal of the rays with extreme momenta. This is achieved by placing a "momentum-selecting" slit to cut out the dispersed rays at a position of horizontal focus (of the central-momentum rays)(REE69). This situation may occur together with (a).

We introduce here the concept of resolving power. The resolving power R1 expresses the capability of a system to separate particles of different momenta, and is defined as the ratio of horizontal momentum dispersion to image size (BRO67):

$$R1 \equiv \frac{R_{16}}{2R_{11}\, x_0} \qquad (8.1)$$

where x_0 is the half-width of the source slit. The higher the resolving-power, the more effective the action of the momentum-selecting slit becomes. To increase R1, we require a large dispersion R_{16}, a small magnification R_{11} and a small object slit. This implies that the horizontal rays should travel in a point-to-point mode between object slit and momentum-selecting slit.

Although systems consisting of only dipoles can achieve this point-to-point mode (LIV69, HIN69, ENG67) we examine systems which contain quadrupoles as well. Quadrupoles add versatility to a system, and are essential if we wish to achieve (a) above. Quadrupoles situated between the dipoles affect the dispersed rays. It is often convenient to locate at least one quadrupole at (or near) a waist in both x and y so that the dispersed rays may be controlled without affecting the central momentum rays. Quadrupoles may also be placed before the first dipole and after the last dipole to control the optics of these central momentum rays (e.g. to ensure that the vertical beam height is not too large in the dipoles). Telescopic optics for the system is often desirable.

We examine systems which have either mirror or anti-mirror symmetry. These are easily achromatised:

> mirror symmetrical systems are achromatic if the dispersed ray is parallel to the central ray at the symmetry plane, $M_{26} = 0$ (see equation (5.13))
> anti-mirror symmetrical systems are achromatic if the dispersed ray crosses the central axis at the symmetry plane, $M_{16} = 0$ (see equation (5.19)).

The anti-mirror symmetrical system cannot be used with a momentum-selecting slit at its symmetry plane because of the zero dispersion there.

8.2 One Quadrupole between Two Dipoles

The system with one quadrupole between two dipoles is the simplest one in which an initially achromatic beam may be made achromatic at the exit to the system (except the case of a deflection through 360^{o} which requires no quadrupoles). It has been discussed by various authors (PEN61, STE65, ENG67, LIV69, JOH75). We examine the system here because it illustrates the principles of achromatising in a relatively simple way.

The mirror-symmetrical case is shown in figure 8.1a, and the anti-mirror symmetrical one in figure 8.1b. The transfer matrix of the half-system M is calculated as follows:

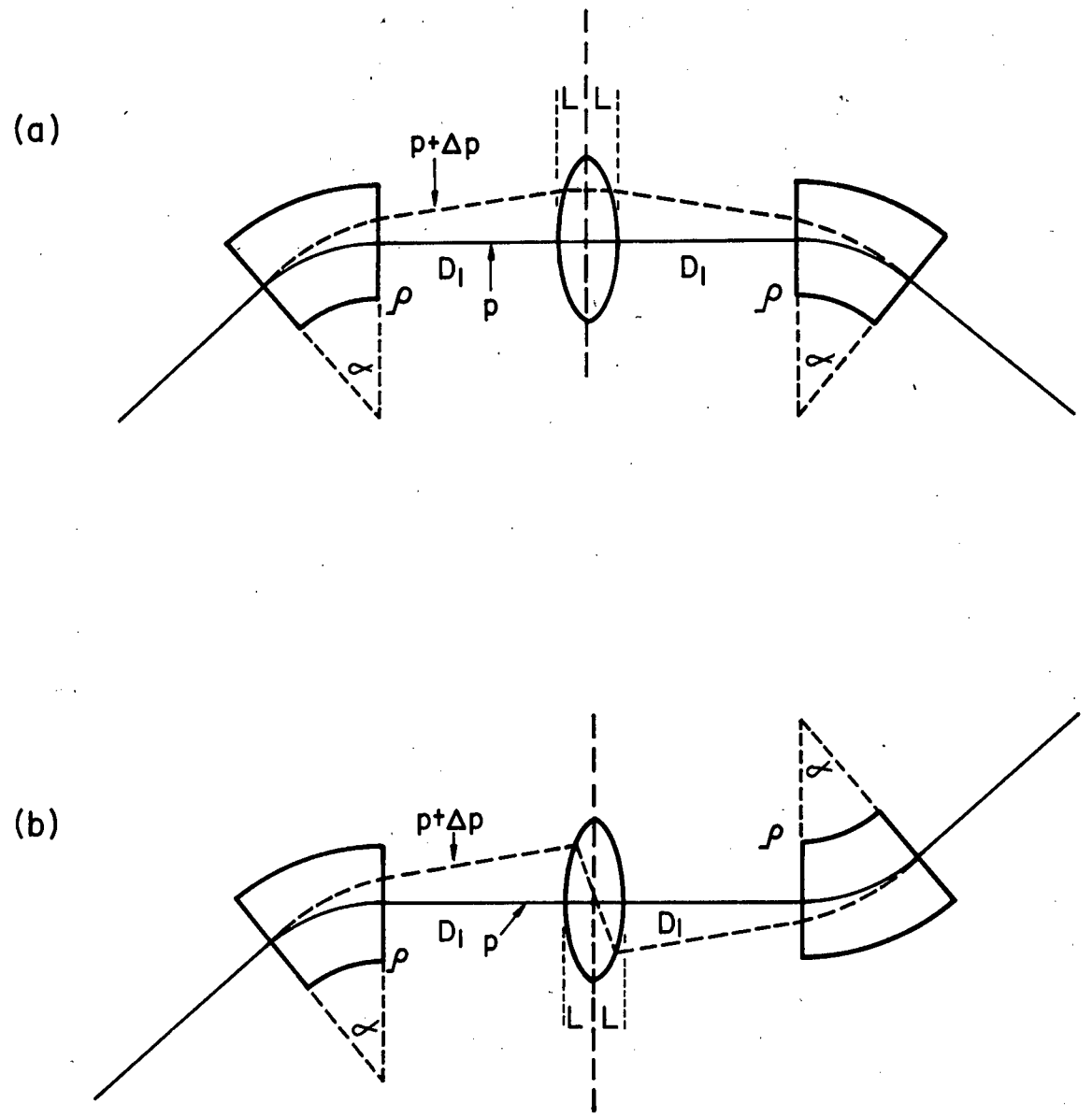

Figure 8.1: Achromatic systems with
(a) a mirror symmetrical arrangement
(b) an anti-mirror symmetrical arrangement
of one quadrupole between two dipoles.

$$M = \begin{bmatrix} \cos kL & \frac{\sin kL}{k} & 0 & 0 \\ -k \sin kL & \cos kL & 0 & 0 \\ 0 & 0 & 1 & 0 \\ 0 & 0 & 0 & 1 \end{bmatrix} \begin{bmatrix} 1 & D_1 & 0 & 0 \\ 0 & 1 & 0 & 0 \\ 0 & 0 & 1 & 0 \\ 0 & 0 & 0 & 1 \end{bmatrix} \begin{bmatrix} \cos\alpha & \rho\sin\alpha & 0 & \rho(1-\cos\alpha) \\ -\frac{\sin\alpha}{\rho} & \cos\alpha & 0 & \sin\alpha \\ -\sin\alpha & -\rho(1-\cos\alpha) & 1 & \rho(\alpha-\sin\alpha) \\ 0 & 0 & 0 & 1 \end{bmatrix} \quad \ldots (8.2)$$

We have made the following assumptions:

(i) the dipole has a uniform field i.e. n = 0, and
(ii) the dipole has zero edge angles.

These assumptions imply that the vertical extent of the beam is not affected by the dipole, and we have thus not included the terms affecting (y, y´) in equation (8.2).

The expression for dispersion and angular dispersion at the symmetry plane are (for a quadrupole of length 2L):

and $$M_{16} = \cos kL\,(\rho - \rho\cos\alpha + D_1 \sin\alpha) + \frac{\sin kL}{k} \sin\alpha \qquad (8.3)$$

$$M_{26} = \cos kL \sin\alpha - k \sin kL\,(\rho - \rho\cos\alpha + D_1 \sin\alpha) \qquad (8.4)$$

From equation (8.3) we see that we cannot get $M_{16} = 0$ except with a very strong quadrupole ($kL > \pi/2$) for $\alpha < 180^{o}$. In practice this excludes the case of anti-mirror symmetry with one quadrupole for many achromatic deflection sys= tems (for high energy beams at least).

We can find the condition for achromatic transfer in mirror symmetrical systems by putting equation (8.4) equal to zero. Then

$$k \tan kL = \frac{\sin\alpha}{\rho(1 - \cos\alpha) + D_1 \sin\alpha} \qquad (8.5)$$

and the resultant dispersion at the symmetry plane is

$$M_{16} = \rho(1 - \cos\alpha) + (D_1 + L/2) \sin\alpha \qquad (8.6)$$

for quadrupole strength

$$B_0 = \frac{a\,(B\rho)}{L} \quad \frac{\sin\alpha}{\rho(1 - \cos\alpha) + D_1 \sin\alpha} \qquad (8.7)$$

Equations (8.6) and (8.7) are derived from (8.5) with the assumption that $kL < 1$.

Edge angles on the dipoles may be necessary for the control of the vertical extent of the beam. If the angles on the edges facing the symmetry plane are both β, then equation (8.7) becomes

$$B_0 = \frac{a\,(B\rho)}{L} \quad \frac{\tan\beta\,(1 - \cos\alpha) + \sin\alpha}{(\rho + D_1 \tan\beta)(1 - \cos\alpha) + D_1 \sin\alpha} \qquad (8.8)$$

We cannot place a momentum selecting slit exactly at the position of maximum dispersion because of the presence there of the quadrupole. Nor can we use this system to achromatise a beam with arbitrary dispersion because we have only one control over the dispersion - we need two if we are to correct both the position and the direction of the dispersed ray entering the second dipole. However, the system is useful for deflection of achromatic beams when the achromatism is to be maintained (HIN75a).

8.3 Two Quadrupoles between Two Dipoles

This system is similar to the one with only one quadrupole between the dipoles, but has several advantages over it:

(i) for mirror-symmetrical systems a momentum-selecting slit may be placed at the symmetry plane, (or anywhere between the two quadrupoles) where the dispersion is greatest;

(ii) for anti-mirror symmetrical systems the quadrupoles can steer the dispersed ray correctly without having to be too strong, especially if the distance between the quadrupoles is relatively large;

(iii) with two controls over the position and direction of the dispersed ray we can recombine an arbitrarily dispersed beam, or give an initially achromatic beam an arbitrary dispersion.

The system is shown in figure 8.2a for mirror symmetry, and in figure 8.2b for anti-mirror symmetry.

The expressions for M_{16} and M_{26} are now:

$$M_{16} = \cos kL\,(\rho - \rho\cos\alpha + D_1 \sin\alpha) + \frac{1}{k}\sin kL \sin\alpha + D_2\left[\cos kL \sin\alpha - k \sin kL\,(\rho - \rho\cos\alpha + D_1 \sin\alpha)\right] \qquad (8.9)$$

and

$$M_{26} = \cos kL \sin\alpha - k \sin kL\,(\rho - \rho\cos\alpha + D_1 \sin\alpha) \qquad (8.10)$$

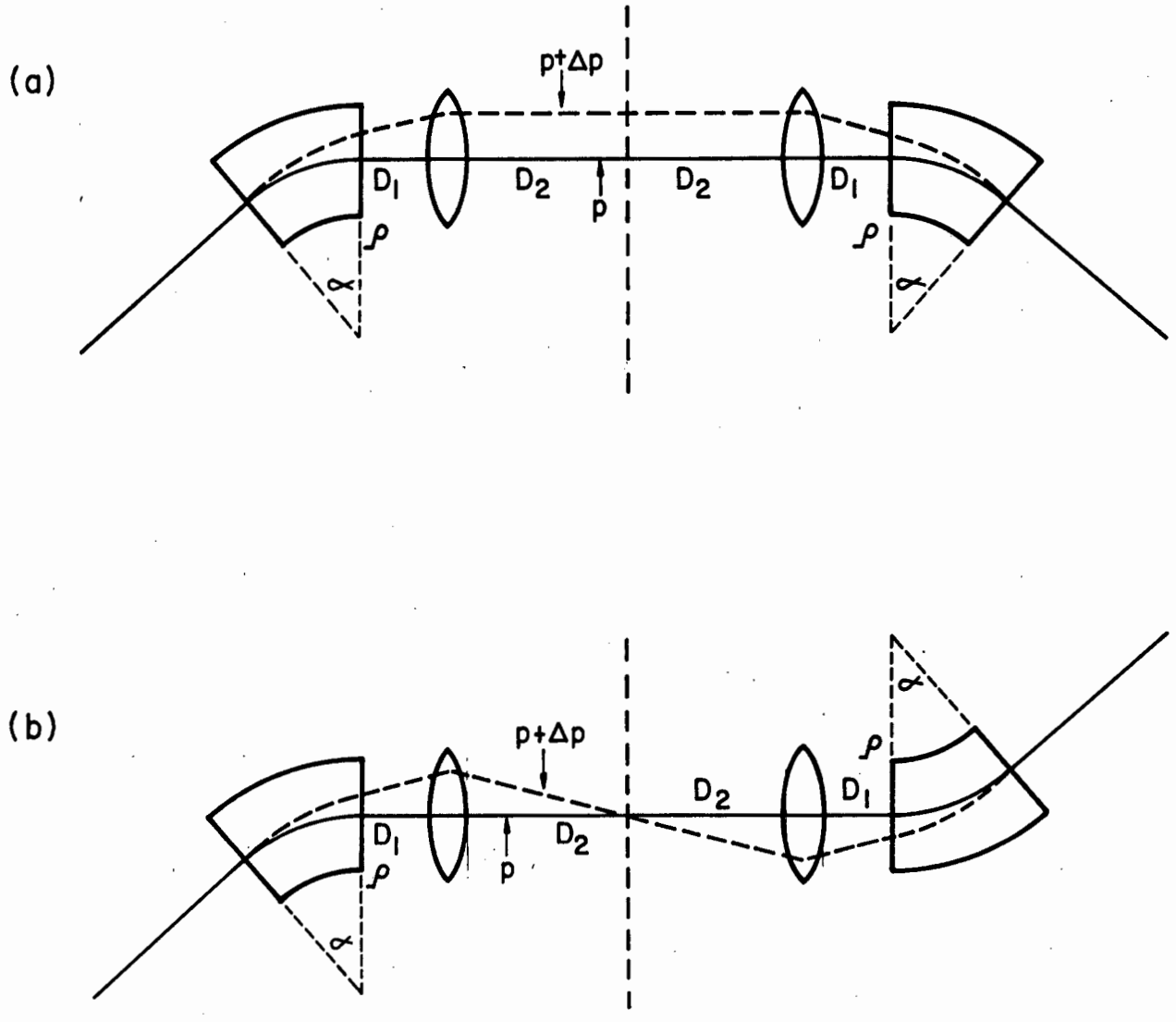

Figure 8.2: Achromatic systems with two quadrupoles between two dipoles in
(a) a mirror symmetrical arrangement
(b) an anti-mirror symmetrical arrangement

Equation (8.10) is independent of D_2 and for the case of mirror symmetry D_2 may be chosen to suit the optics of the central momentum rays.

If we apply the thin-lens approximation, then $M_{16} = 0$ implies that the quadrupole field strength

$$g = k^2 L$$

$$= \frac{1}{D_2} + \frac{\sin \alpha}{\rho(1 - \cos \alpha) + D_1 \sin \alpha}$$

This is the condition for the anti-mirror symmetric system to the achromatic.

These systems have not been widely used in the past. However, we feel that the mirror symmetric system is particularly useful as the length of beamline required is limited and the number of elements needed is small while great versatility is available. These properties are useful for beam transfer lines between accelerators. We will discuss the mirror symmetric system further in this context in chapter 9.

We note in passing that after private communication between ourselves and the group at ICPR in Japan, such a two-dipole two-quadrupole system is incorporated into their published beamline between an existing linear accelerator and their proposed separated-sector cyclotron (WAD79).

8.4 Systems with Many Quadrupoles

Increasing the number of quadrupoles in a two dipole system does not change the principles illustrated in figures 8.2a and 8.2b about the position or direction of the dispersed ray at the symmetry plane. The versatility of the system does however improve with the number of quadrupoles, e.g. the mirror symmetric system described in (JOH75) with four quadrupoles between two dipoles has a much higher resolving power than the system with only two quadrupoles. Probably the maximum number of quadrupoles required is nine, as in the "double-monochromator" proposed by Hinterberger (HIN74a, HIN74b) and now in use at Hahn-Meitner Institute (VICKSI). If the second bend is to be far removed from the first bend, then further systems of either two-doublet or two-triplet telescopes may be used in addition to the nine quadrupoles.

The VICKSI double-monochromator is shown in figure 8.3. It is a mirror-symmetrical system consisting of two double-focussing dipoles, separated by three quadrupole triplets. With suitable quadrupole settings any one

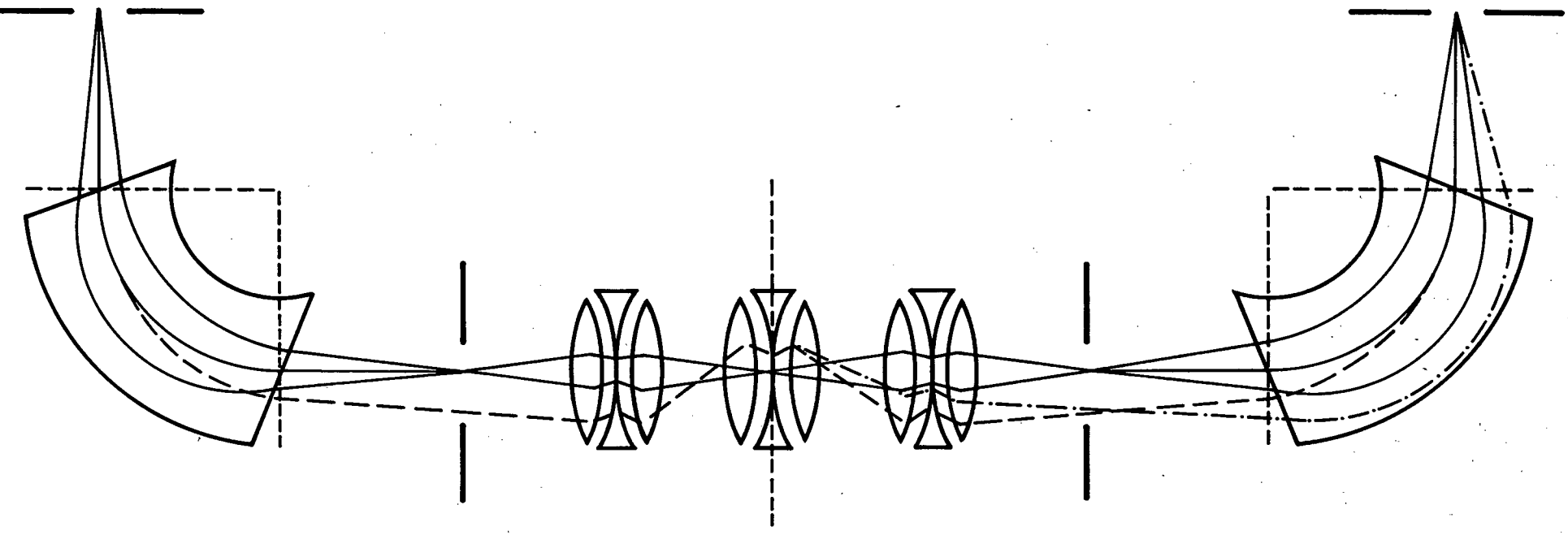

Figure 8.3a: Double-monochromator showing (schematically) the horizontal point rays (solid lines), for
(i) achromatic mode - the off-momentum rays are drawn ----
(ii) non-dispersive mode - the off-momentum rays are drawn -·-·-·-·-
Based on a figure in reference (HIN74a)

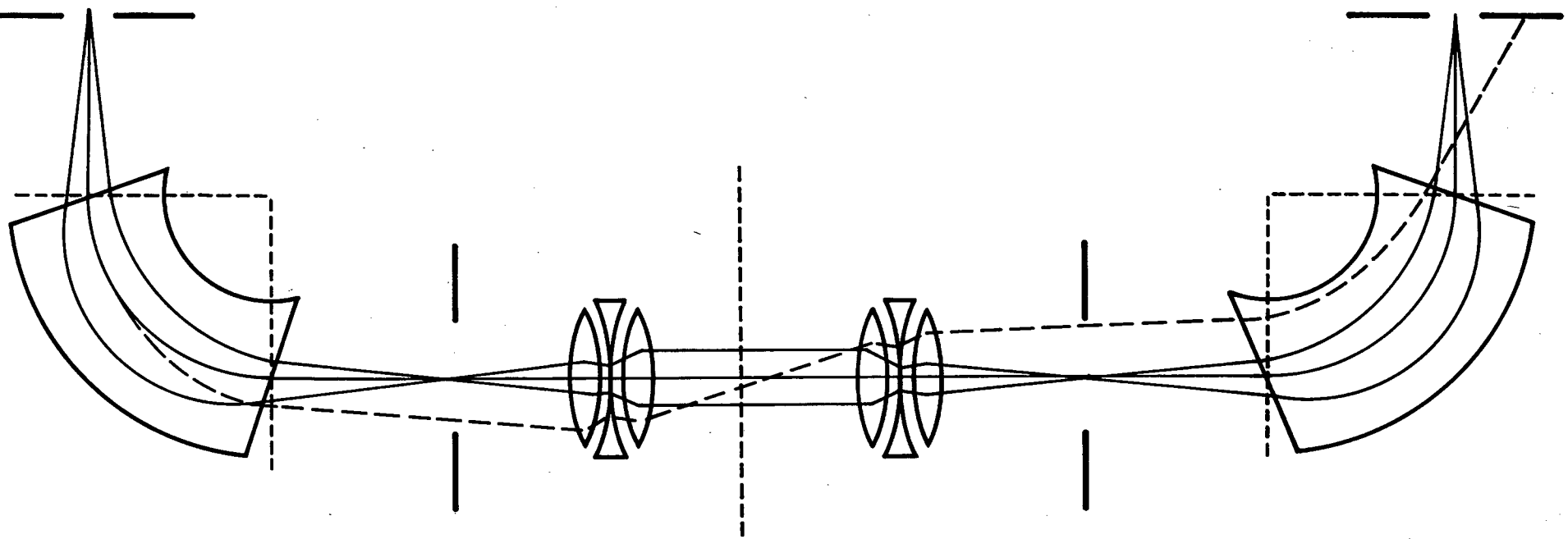

Figure 8.3b: Double-monochromator with central triplet switched off, showing (schematically) the horizontal point rays and the off-momentum rays (drawn ----) for double-dispersive mode. Based on a figure in reference (HIN74a).

of the following modes may be obtained:

(a) doubly-telescopic, non-dispersive, with

$$M_{12} = M_{21} = M_{33} = M_{44} = 0$$

resulting in

$$R_{11} = R_{22} = +1, \quad R_{33} = R_{44} = -1, \quad R_{16} = 0, \; R_{26} \neq 0$$

This is shown in figure 8.3a.

(b) double dispersive, with

$$M_{22} = M_{44} = 0$$

resulting in

$$R_{11} = R_{22} = R_{33} = R_{44} = -1, \quad R_{16} \neq 0, \quad R_{26} \neq 0$$

This is shown in figure 8.3b. The central triplet is not used in this mode. However if we do use the central triplet we can also get

$$M_{11} = M_{22} = M_{34} = M_{43} = 0,$$

resulting in

$$R_{11} = R_{22} = -1, \quad R_{33} = R_{44} = +1, \quad R_{16} \neq 0, \quad R_{26} = 0$$

(c) doubly-telescopic, achromatic, with

$$M_{12} = M_{21} = M_{33} = M_{44} = M_{26} = 0$$

resulting in

$$R_{11} = R_{22} = 1, \quad R_{33} = R_{44} = -1, \quad R_{16} = R_{26} = 0$$

This is shown in figure 8.3a.

(d) approximately doubly-telescopic, isochronous, with

$$M_{16}M_{26} = M_{56}$$

resulting in

$$R_{56} = 0$$

In this mode the normal pulse stretching due to the momentum spread of the beam is compensated for by making the particles with higher momenta take longer paths through the second dipole. Negative values of R_{56} may also be set, which is most useful when the beam is being matched to a time-of-flight spectrometer.

A corresponding anti-mirror symmetrical double monochromator similar to the mirror-symmetrical one can also be constructed by flipping either dipole through 180^{o} (HIN74a).

The double monochromator is well suited to beams being prepared for external targets where a high resolution is required. This is dis= cussed in chapter 10. It is inevitably a fairly large system, and is thus unlikely to find a place in transfer beamlines between accelerators.

9. BEAM TRANSFER BETWEEN CYCLOTRONS

9.1 Introduction

The function of the transfer beamline linking a pre-accelerator and a main accelerator is at least two-fold:

(i) it physically transfers the beam from the extraction elements of the pre-accelerator to the injection elements of the main accelerator, (which is usually in a different room) and

(ii) it has to match the characteristics of the beam extracted from the pre-accelerator to those required for optimal acceleration in the main accelerator in all six dimensions of phase space.

The first of these functions is easily achieved with dipoles of the correct deflecting angle together with some quadrupoles to transport the beam. However the second function is only accomplished with careful planning. This matching may be very difficult to accomplish if the positions of the two accelerators are fixed with a limited length of beamline allowed (for example where an existing building is used to house the accelerators.)

A further requirement of the transfer line is that it be easily tuned for optimum matching. This is necessary because the quality of the beam extracted from the pre-accelerator is not always readily reproducible, and whatever the quality extracted on any given occasion it still has to be matched to the requirements of the main accelerator without delay. If the pre-accelerator is to provide many different types of beams (e.g. variable energy beams and/or several different types of particles) then the ease of tuning would facilitate rapid changes of beam.

The best method to provide ease of tuning is to separate the beamline into sections, each of which affect only one phase space variable (BEC75), or one pair of canonical variables. Where this is not possible, as with horizontal and vertical beam extent, then within a section the variable beam element parameters should only affect the beam in one plane at a time. This separation of variables will be discussed in more detail later.

Another aid to rapid tuning of the system is the provision of a diagnostic line (DEV75, JOH75). If the beam may be readily switched between this line and the transfer line, then the characteristics of the beam may be easily checked, and the common beamline tuned, without possible damage to later elements or to the main accelerator. The diagnostic line is also likely to have more space available for diagnostic equipment than the main line.

9.2 Design of a Transfer Beamline

The separation of variables necessary for convenient beamline tuning requires that the beam be achromatic during its size control and bunch length control. This implies that we need an achromatizing section earlier in the beamline, and a dispersing section later in the beamline. The beamline may thus be divided as follows:

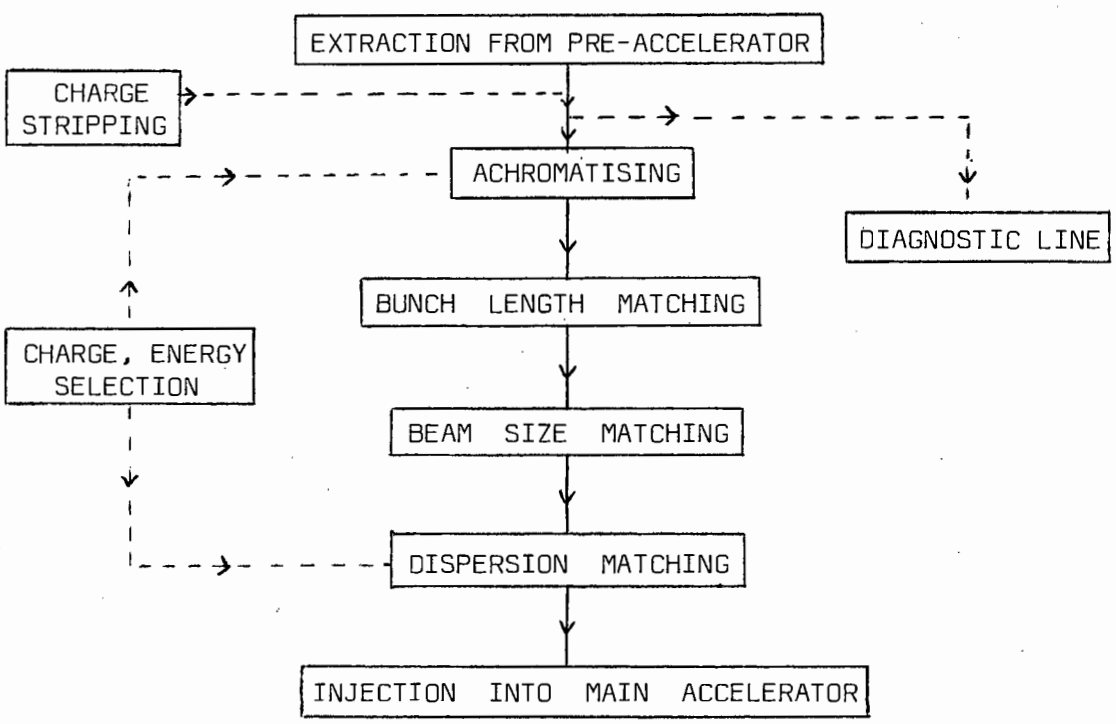

The dashed lines show possible positions of the stripper, diagnostic line and selection of energy and/or charge states.

In addition to this division of beamline functions, we will also require some focussing elements between extraction and achromatising, and between dispersion matching and injection. A possible arrangement of a transfer line is shown in figure 9.1.

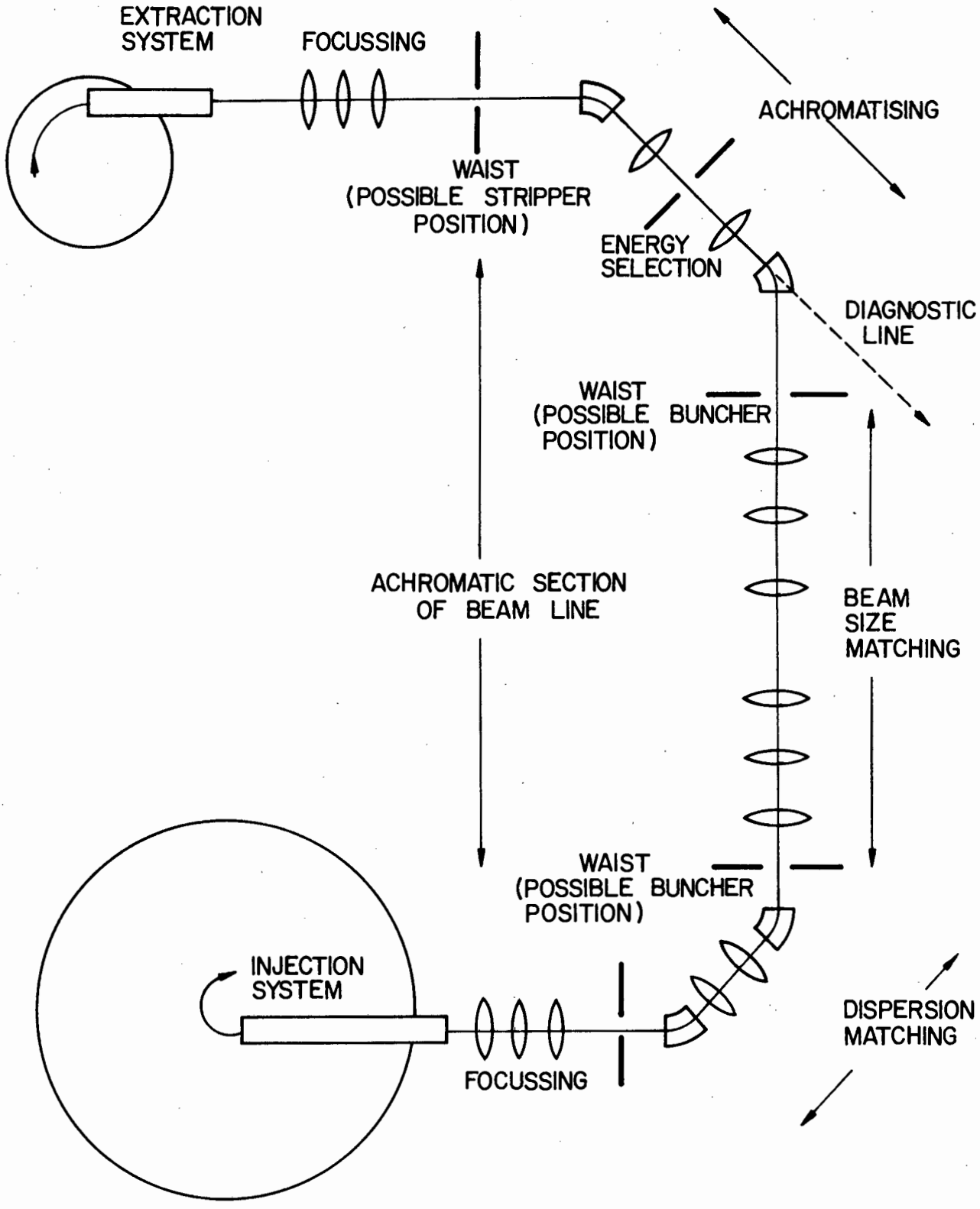

Figure 9.1: Possible layout of a transfer beamline showing separate functions of each section. Quadrupoles shown are schematic only, to indicate certain functions. Others may be necessary in any practical system.

9.3 Application to a Specific Transfer Beamline

As an illustration of the principles which we have described in this and preceding chapters, we apply them to the design of a specific transfer beamline.

This beamline will be used between the solid-pole injector cyclotron (SPC1) and the main separated-sector cyclotron (SSC) at present being designed and constructed at Faure in the Western Cape by the National Accelerator Centre of the Council for Scientific and Industrial Research. The characteristics of the cyclotrons and a description of the facility may be found in references (TEC76, ANN78, ANN79).

SPC1 will be used to accelerate light ions with a maximum proton energy of 8 MeV. At a later stage a second solid-pole cyclotron (SPC2) will be designed to pre-accelerate heavy ions, with a maximum energy/nucleon of 40 MeV.

The transfer line between SPC1 and the SSC is shown in figure 9.2. We now describe the various stages of the beamline design.

9.4 Parameters of the Beam from an Injector Cyclotron

At this stage the properties of the beam extracted from SPC1 are uncertain, and we have made the assumption that the emittances of a 100 μA, 4 MeV proton beam in the horizontal (x, x′) and vertical (y, y′) planes are identical and equal to 12 π mm. mrad. We assume that these are the maximum emittances of any beam to pass through the beamline. For calculation purposes, however, we have used an 8 MeV (i.e. maximum energy) beam with these emittances, as all the beamline elements must also be able to handle the higher energy particles. In practice the 8 MeV proton beam will be limited to approximately 10 μA, with correspondingly smaller emittances.

We begin by considering the representative particles distributed round the relevant eigen-ellipse at the deflection radius of SPC1. These particles placed on a centered, accelerated orbit, are followed through a possible set of deflection elements and out into the fringing field

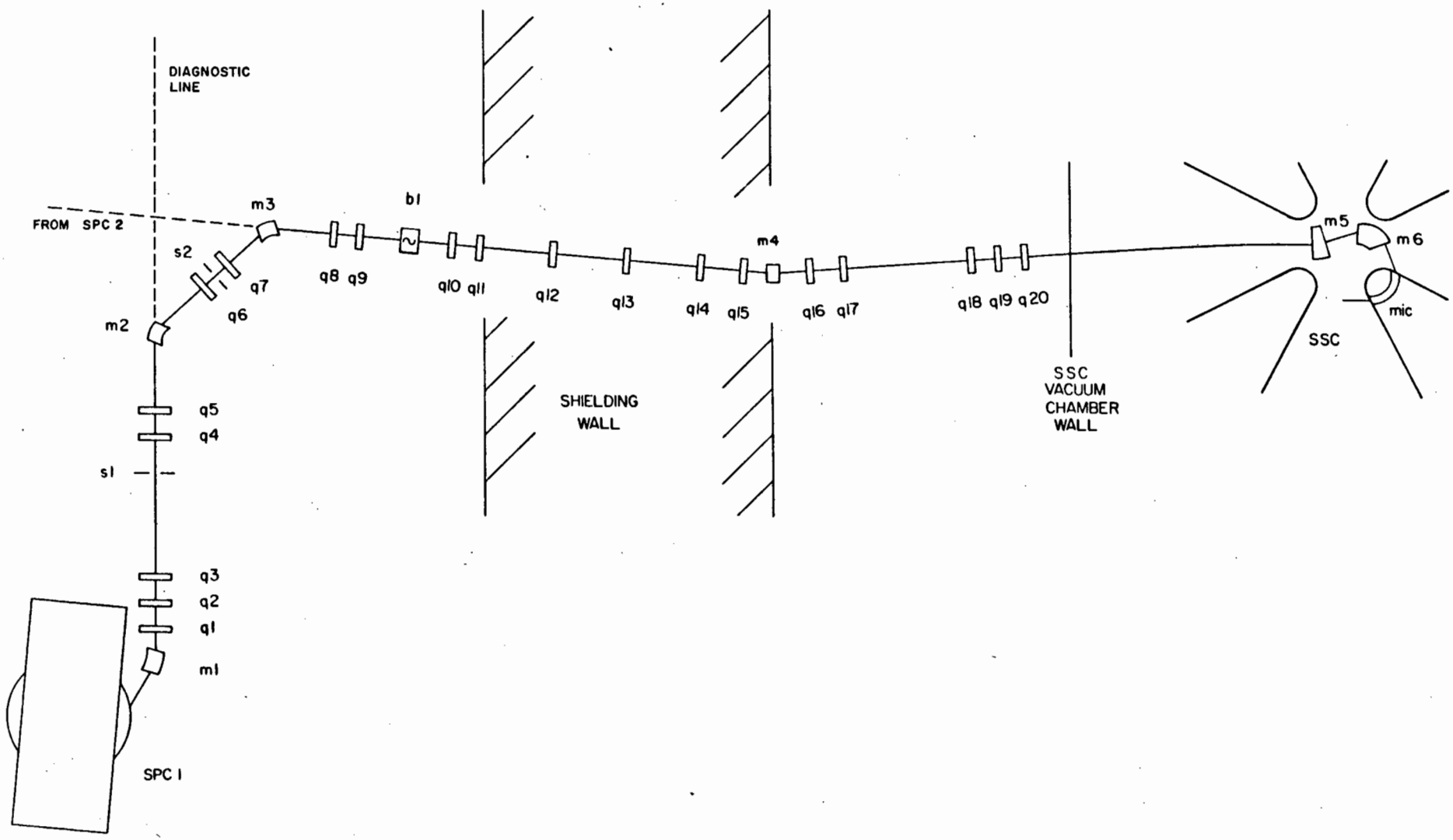

Figure 9.2: Diagram of the transfer beamline from the light-ion injector SPC1 to the SSC.

by means of the ray-tracing computer code GOBLIN. A momentum spread of 0,5% half-width is assumed, and particles with the central momentum ± 0,5% are displaced both radially and longitudinally from the central particle and similarly followed out of the injector. The information thus obtained enables us to construct, by the method described in Appendix C, a phase ellipsoid of a fairly realistic beam in 6-dimensional phase space.

The angle at which the beam is extracted from SPC1 is not convenient for our beamline, so we alter the beam direction using dipole m1 (see figure 9.2). We use the quadrupole triplet q1 - q3 to focus the beam to a double waist at slit s1. This may be seen from figure 9.3a, in which the horizontal and vertical beam envelopes are plotted. It may be seen (from figure 9.2) that the distance from m1 to s1 is quite large. This assists us in focussing any (reasonable) beam extracted from SPC1 to a waist. In theory we require only two quadrupoles to focus both x and y to waists but the addition of the third quadrupole allows us to choose the size of the horizontal waist as well. From the description of the next section of beamline we will see that we prefer a small x-waist at s1. This is also a possible location of a foil stripper, and a waist is required to minimise the effect of beam broadening caused by the stripper (HIN75b).

9.5 Making the Beam Achromatic

This section of beamline stretches from s1 to the buncher b1. Its purpose is both to make the beam achromatic, and to separate the dispersion from its x-like behaviour so that a momentum-selecting slit can operate efficiently. It is this latter purpose that necessitates the inclusion of two dipoles, m_2 and m_3, rather than only the one necessary to achromatize a dispersed beam.

We have chosen a mirror-symmetrical system, with two quadrupoles between the dipoles. (This system is discussed in chapter 8.) The anti-mirror symmetrical system would not be suitable here because the momentum-selecting slit could not be placed at the position of maximum dispersion (see figure 8.2).

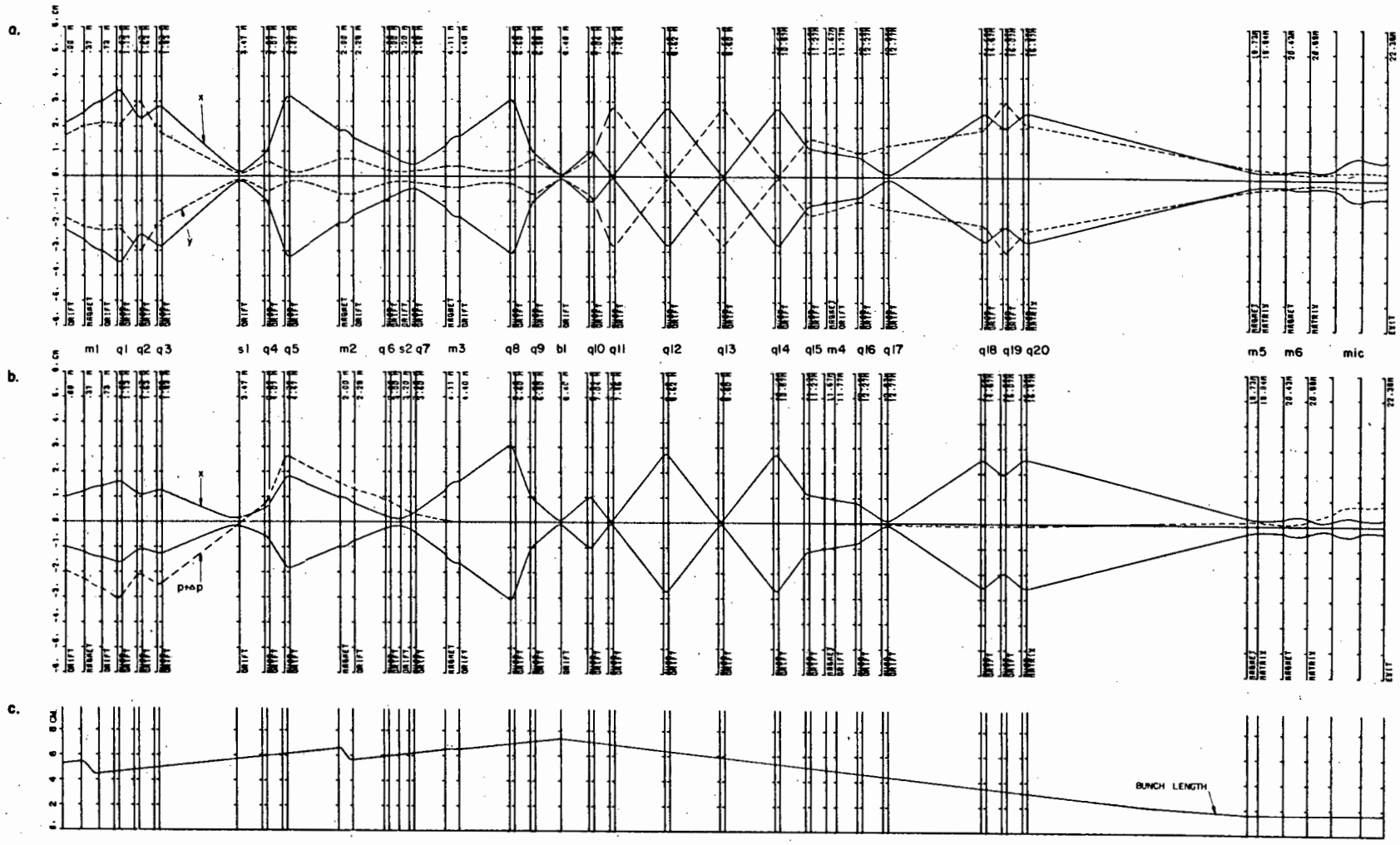

Figure 9.3: (a) Total beam envelope (horizontal and vertical) plotted for an 8 Mev, 12 π mm.mrad proton beam through the transfer beamline.

(b) Horizontal beam envelope without momentum spread. Also shown is the dispersion path.

(c) Plot of bunch half-length along the transfer beamline.

When this system is operated in achromatic mode it will make an initially achromatic beam achromatic again after the second dipole: hence we call it an "achromat". In the mode of operation shown in figures 9.3a and b however, the beam has a positive initial dispersion (i.e. before m2). The quadrupoles between the dipoles, q6 and q7, are adjusted to steer the dispersed beam correctly into the second dipole so that the beam recombines after m3. However with a different beam from SPC1, (e.g. a redesign of the extraction elements of SPC1 could alter the beam drastically) the dispersion before m2 could be negative. Then the symmetry of the system implies that it would be as easy to achromatize such a beam as one with the initial dispersion positive, as the system is only slightly perturbed from its achromatic mode.

For the optimum operation of the momentum-selecting slit, s2, we require a high resolving power, as defined in equation (8.1). This implies that we should aim for small x-waists both at s1 and at s2. The small x-waist at s2 has another advantage, in that the horizontal component of the beam is then hardly affected by the settings of the dispersion-handling quadrupoles. For this reason we focus y to a waist at s2 as well (see figures 9.3a and b).

We could use double-focussing edge-angles on dipoles m2 and m3 to achieve this point-to-point operation in x and y between s1 and s2, and between s2 and b1. However the double-focussing distance for symmetrical 45^{o} dipoles is 4.828 times the dipole radius and this is too long for our system. Another reason for not using double-focussing dipoles is that the quadrupoles between the dipoles disturb the double-focussing action. We have therefore used quadrupole doublets before m2 and after m3 (still preserving mirror symmetry). These accomplish the focussing of both x and y to waists at the symmetry plane and at the end of the system.

If the beam from SPC1 is not very dispersed, the symmetry of the achromat is fairly high. For highly-dispersed beams the system operates less like an achromat, and its symmetry is somewhat degraded.

9.6 Buncher

If a flat-topping resonator is not installed in the SSC initially, then a fairly short bunch length (of less than 4^{o} phase half-width) will be

needed at injection if single-turn extraction in the SSC is desired (TEC76). A buncher is thus required in the transfer beamline to compress the bunch length to at least this value.

We can decouple the control of the bunch length from the other parameters by placing the buncher at a narrow achromatic double-waist, as shown in figure 9.3a. The achromatism ensures that the dispersed rays are not affected by the buncher settings, and the radial defocussing action of the buncher becomes negligible because the beam is narrow in both x and y. (See section 4.4.) The buncher may thus be tuned after the other beamline parameters are set without disturbing them. This is very important for tuning up the beamline correctly, with and without the buncher on.

The extraction elements of SPC1 are highly non-isochronous, so that although we assume a phase of 4^{o} half-width (i.e. ℓ_0 = 16,6 mm) in the last orbit in SPC1, by the time the beam has reached the slit s1 the bunch length is already greater than 56 mm (half-width). The dipoles m2 and m3 do, however, help to focus the bunch length somewhat. The nett result is that placing the buncher at the position marked b1 in figure 9.2 is equivalent to placing it approximately in the centre of a longer beamline with an average bunch length growth rate in the first half equal to the actual bunch length growth rate immediately before the buncher. This may be seen from the equal, but opposite, slopes to the plot of bunch length in figure 9.3c. This placing of the buncher ensures minimum buncher strength.

We can calculate the focal length of the buncher, f_b, if we know the transfer matrix A of the beamline prior to the buncher, and the transfer matrix C of the beamline after the buncher. Then the total 4-dimensional transfer matrix R of the system is (ignoring radial defocussing effects):

$$R = \begin{bmatrix} C_{11} & C_{12} & 0 & C_{16} \\ C_{21} & C_{22} & 0 & C_{26} \\ C_{51} & C_{52} & 1 & C_{56} \\ 0 & 0 & 0 & 1 \end{bmatrix} \begin{bmatrix} 1 & 0 & 0 & 0 \\ 0 & 1 & 0 & 0 \\ 0 & 0 & 1 & 0 \\ 0 & 0 & -1/f_b & 1 \end{bmatrix} \begin{bmatrix} A_{11} & A_{12} & 0 & A_{16} \\ A_{21} & A_{22} & 0 & A_{26} \\ A_{51} & A_{52} & 1 & A_{56} \\ 0 & 0 & 0 & 1 \end{bmatrix}$$

... (9.1)

We may now find the final beam σ from the initial beam σ^0 and R. Thus:

$$\begin{aligned}\sigma_{56} = {} & R_{51}R_{61}\sigma_{11}^{0} + R_{52}R_{62}\sigma_{22}^{0} + R_{55}R_{65}\sigma_{55}^{0} + R_{56}R_{66}\sigma_{66}^{0} \\ & + (R_{51}R_{62} + R_{52}R_{61})\sigma_{12}^{0} + (R_{51}R_{65} + R_{55}R_{61})\sigma_{15}^{0} \\ & + (R_{51}R_{66} + R_{56}R_{61})\sigma_{16}^{0} + (R_{52}R_{65} + R_{55}R_{62})\sigma_{25}^{0} \\ & + (R_{52}R_{66} + R_{56}R_{62})\sigma_{26}^{0} + (R_{55}R_{66} + R_{56}R_{65})\sigma_{56}^{0} \\ = {} & 0 \qquad \text{for an upright ellipse in } \ell, \delta \text{ space} \end{aligned} \tag{9.2}$$

If we substitute the elements R_{ij} from equation (9.1) into (9.2) we find a quadratic equation in $1/f_b$. The two solutions for f_b are both physical and correspond to the conditions of waist and bust formed by focussing elements in the horizontal or vertical planes. The bunch length for the waist is smaller, but results in a slightly increased energy spread, whereas the bust condition leads to a large bunch length, parallel in the sense that it is only slowly varying, with a much reduced momentum spread. We may find this setting very useful for reducing the momentum spread in the SSC when the introduction of a flat-topping resonator makes a large bunch length acceptable. The parameters for the two cases are tabled below.

	Focal length f_b (m)	Bunch length at valley (mm)	$\frac{\Delta p}{p}$ at valley (%)
Waist	7,467	16,39	0,521
Bust	14,537	72,79	0,114

The bunch length along the beamline is plotted for the waist case in figure 9.3c.

9.7 Beam Shaping

We control the size of the beam with the six quadrupoles q10 through q15 shown in figure 9.2. We put the beam shaping quadrupoles in an achromatic section of beamline so that the beam shaping may be independent of

dispersion, and the dispersion control independent of the beam shaping. We can further separate the control of the variables by using an orthogonal quadrupole system, described in chapter 7. This allows us to control the horizontal beam extent independently of the vertical beam extent and vice versa.

The orthogonal quadrupole system as shown in figure 9.3a does not operate in point-to-point mode, but focusses x down to a narrow waist beyond the dipole m4. The reason for the waist only after m4 will be discussed in the next section. The system focusses y down to a fairly broad bust (also after m4). This is not a departure from the orthogonal quadrupole system, but merely an alternative mode, as may be seen from figure 7.6a. In practice the last quadrupole in an orthogonal quadrupole system may be given one of two values, each of which will achieve $r_{12} = 0$ if the polarity is positive, or $r_{34} = 0$ if the polarity is negative. The one setting will produce a final x (or y) waist, and the other a final x (or y) bust.

9.8 Dispersion Matching

The beam injected into a cyclotron requires the higher momentum particles to have a larger radius for optimal acceleration. This implies that the beam should be dispersed. The exact amount of dispersion required in the cyclotron may be calculated by means of the eigen-ellipse theory which we developed in chapter 3.

The beam in our transfer line is, however, still achromatic just beyond q15, and we now need to introduce dispersion. A convenient system for doing this is the mirror-symmetrical system consisting of two dipoles separated by two quadrupoles. This system would allow us to tune the dispersion very conveniently, and provides the beam qualities, at the symmetry plane, suitable for a momentum-selecting slit. However we already have a momentum-selecting slit in our system (at s2). We choose, therefore, to introduce the dispersion by means of one dipole, m4, and to control it by means of the quadrupoles q16 and q17. A slight variation in the field strengths of these quadrupoles has a relatively large effect on the final dispersion due to the long distance the beam travels through the SSC vacuum chamber to the injection elements.

We focus the beam to a y-waist in q16 and an x-waist in q17 to minimize the effect of the dispersion control on the horizontal and vertical size. In practice y is a bust rather than a waist, but the fact that $r_{34} = 0$ helps to minimize the effect of adjacent elements.

9.9 Injection into a Separated-Sector Cyclotron

The injection elements of the SSC consist of two dipoles, m5 and m6, and a magnetic inflection channel (mic) in the first sector magnet. These are not variable beamline elements, but must be considered as fixed sections of our beamline. We need to find the required beam behaviour through these elements, and to do this we take the following steps:

(i) we use the magnetic field of the SSC to calculate, using program STRAY, the eigen-ellipse of the equilibrium orbit at injection energy. This we do using the method we described in chapter 3;

(ii) we trace this eigen-ellipse back from the midline of the first magnetic field valley, (i.e. midway between two sector magnets) through the mic, and the stray field around it to the dipole m6. This is also done with STRAY, and results in a transfer matrix for the section from SSC valley midline to m6. Similarly we find the transfer matrices for the section from m6 to m5 and from m5 to beyond the SSC valley vacuum chamber. For this latter section we pay particular attention to the direction of the central particle, and adjust the dipole m5 to bend the beam in the required direction;

(iii) we combine the transfer matrices of the various sections with those of m6 and m5 to find the required beam outside the valley vacuum chamber.

We can now design the system consisting of the quadrupole triplet q18, q19 and q20. This system provides an interface between the separated-function beamline and the beam required at the first magnetic valley. (It is analogous to the quadrupole triplet q1, q2 and q3, in reverse.) In practice the settings of the dispersion-handling quadrupoles q16 and q17 are also determined using the reverse direction beam i.e. they are chosen such that the beam is achromatic after having passed through m4 in reverse.

9.10 Conclusions

We have designed a transfer beamline capable of matching a wide range of beam parameters to those required for optimum beam transmission through a separated-sector cyclotron.

The beamline provides flexibility and independent tuning of the bunch length, the dispersion, the horizontal beam size, and the vertical beam size.

Provision is made for a diagnostic line (see figure 9.2) and a future link with a beamline from SPC2 (also shown in figure 9.2) so that common beamline elements may be used. The number of elements in the beamline is close to the minimum possible number (see figure 9.1) so that the beamline is, in spite of its versatility, also an economic one - always a major factor in beamline design.

10. EXTERNAL BEAMLINES

10.1 Introduction

If the beam extracted from the main accelerator is to be used for one specific purpose only, then the layout of the beamline will be determined by the particular beam parameters to be matched at the target. If, however, the extracted beam is to be used for a variety of purposes, then we recommend that the beamline has certain characteristics:

(i) as much of the beamline as possible should be common to all branches - this saves on beamline elements;

(ii) the first step should be to make the beam achromatic: the subsequent steps are then independent of the momentum-spread of the accelerator;

(iii) a beam shaping section early in the beamline is most convenient - for example, an orthogonal quadrupole system (see chapter 7) allows independent horizontal and vertical beam control over a wide range of magnifications;

(iv) if a high resolution is required at one or more targets, then a double-monochromator should be included in the beamline.

10.2 Application to a Specific External Beamline

We illustrate the matching of an extracted beam to various types of targets by means of the beamlines we have designed for the National Accelerator Centre. These external beamlines are shown in figure 10.1.

The shape of the extracted beam is found by tracking the eigen-ellipse out through the extraction elements of the SSC.

We start by making the beam achromatic: the quadrupoles QX1 and QX3 direct the dispersed ray correctly into dipole MX2 so that the beam emerging from MX2 is achromatic. The angles of bend of the septum magnet (SM) and dipoles MX1 and MX2 are dictated by the geometry of the SSC. Thus the system from MX1 to MX2 is not quite anti-mirror symmetric. However it operates in a manner similar to the anti-mirror symmetric system described in section 8.3 and shown in figure 8.2b. We do not require a momentum-selecting slit here as we have a double-monochromator further along the beamline in which to place this slit. The point where the dispersed ray

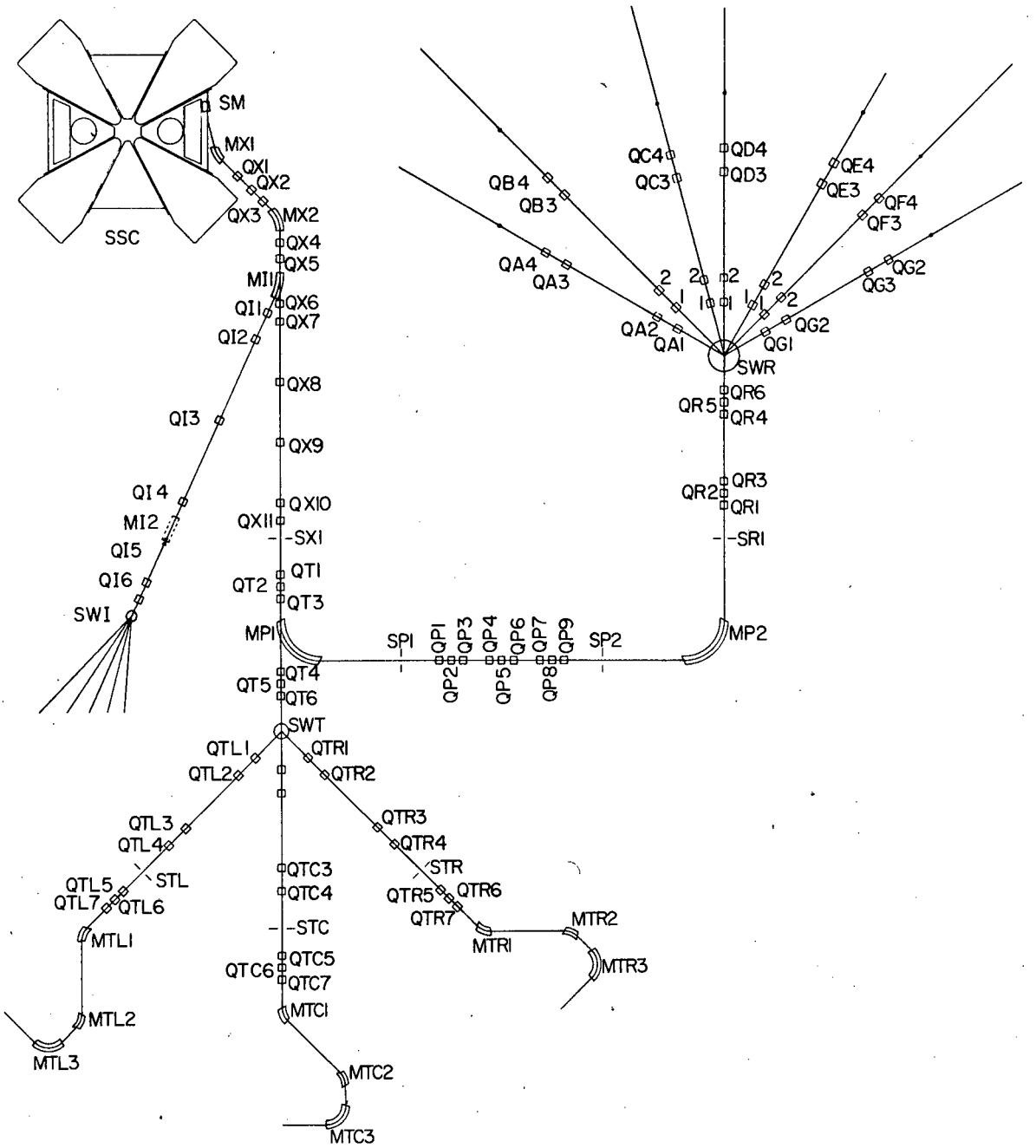

Figure 10.1: Proposed layout of the beamlines from the SSC to the isotope production areas, radiotherapy vaults and experimental areas.

crosses the central trajectory is thus a convenient place for a y-focussing quadrupole i.e. QX2. The quadrupole doublet QX4 and QX5 focusses the beam to a double waist in the centre of the switching magnet MI1. This mode of operation results in the minimum dispersion introduced by MI1 (TEC76). This dipole is activated when the beam is to be sent to the isotope production area. The beamline to this area is described in section 10.3.

From the double-waist in the centre of the (switched off) dipole MI1, the beam enters the orthogonal quadrupole system consisting of the six quadrupoles QX6 through QX11. This system controls the size of the beam entering either the radiotherapy area or the double-monochromator en route to the experimental area.

At slit SX1 we have thus an achromatic beam of the desired size, which we can proceed to match to target requirements.

10.3 Beamlines to Isotope Production Area

The beamlines to the isotope production area consist of a group of five horizontal lines and one vertical line. The 90^{o} dipole, MI2, when activated, deflects the beam downwards through the floor into a basement vault. This vertical beam can be used when liquids (or solids of low melting point) are to be irradiated. A target-changing system will enable a number of different types of target to be irradiated. When MI2 is switched off, the beam passes through to the switching magnet, SWI, which directs the beam along one of five possible lines to the targets.

The six quadrupoles (QI1 through QI6) in the horizontal line are arranged in an orthogonal quadrupole system to permit beam shaping. The quadrupoles are not, however, used in this optimum mode because this would result in a very large beam size in the dipole MI2. Enough flexibility remains, though, to vary the beam size on target in the horizontal lines from as little as 0,6 cm (half-width in x and y) to as much as 5,0 cm, while still keeping the beam half-width in MI2 below 1,2 cm. This is illustrated in figures 10.2(a) and (b) respectively.

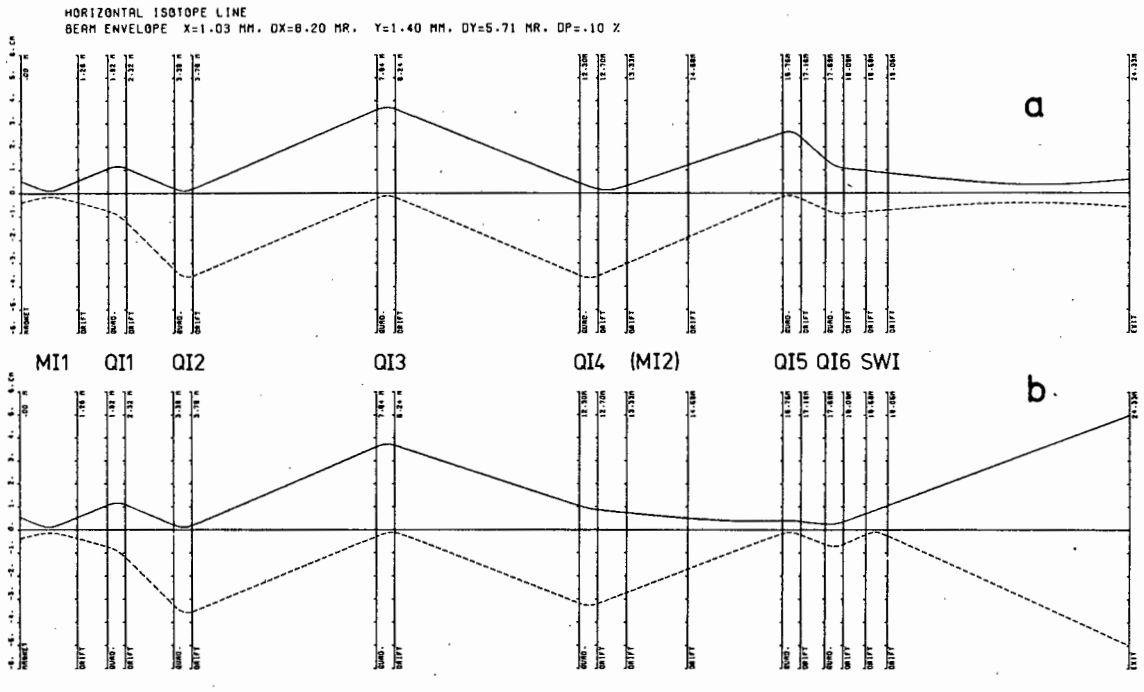

Figure 10.2: Beam envelope plots along a horizontal isotope production beamline for 100 MeV protons and 8 π mm.mrad, showing

(a) minimum beam size on target;

(b) maximum beam size on target.

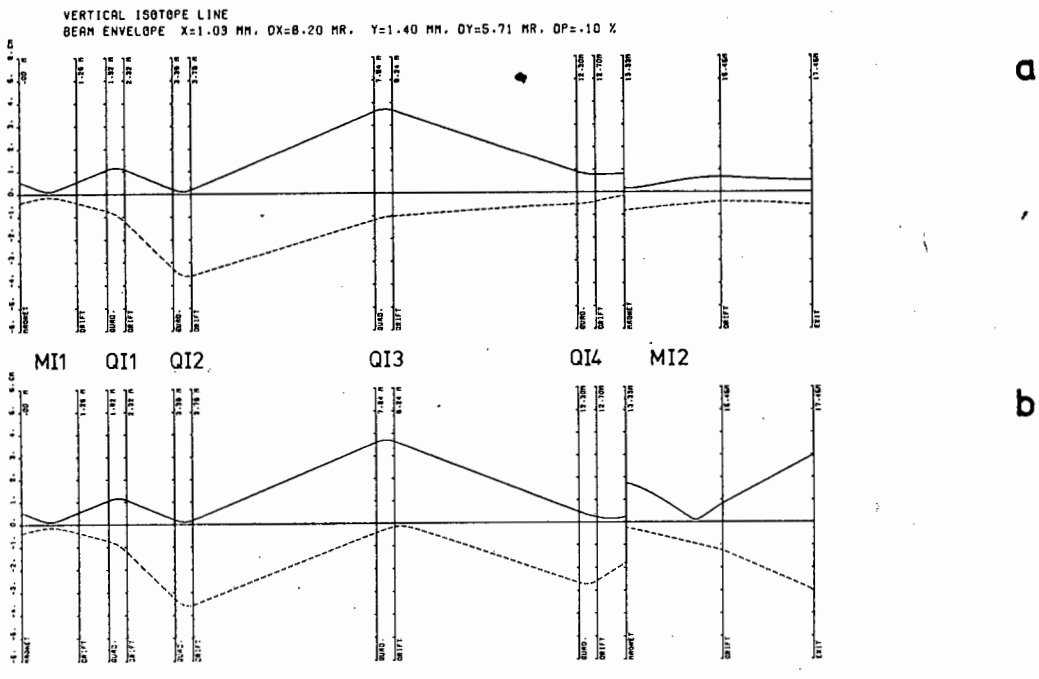

Figure 10.3: Beam envelope plots along the vertical isotope production beamline for 100 MeV protons and 8 π mm.mrad, showing

(a) minimum beam size on target;

(b) maximum beam size on target.

Note that the x and y plots are interchanged at the start of the vertical bend.

The vertical beam has only four quadrupoles to shape it, but again this is quite adequate as may be seen in figures 10.3(a) and (b), which show respectively a minimum beam size of less than 0,6 cm (half-width in x and y), and a maximum beam size of 3,0 cm. The beam height in MI2 still remains less than 1,2 cm. (Note the interchange of the x and y plots due to the 90^{o} vertical plane deflection.) The maximum size required for the vertical beam is smaller than that of the horizontal beam be= cause of the different types of targets to be used in the two areas.

Where only the final size of the beam (and not divergence or correlation) is of importance, as in this case, then one x-focussing quadrupole at a y-waist, and one y-focussing quadrupole at an x-waist are in theory suffi= cient to shape the beam. This is virtually the case in the vertical beam. In the case of the horizontal beam we have a longer beamline, and require a limited beam-height through the switching magnet, SWI. Hence the need for the extra two quadrupoles.

We have specified that in the first part of the beamline we obtain a nar= row waist in the centre of MI1. This will ensure that MI1 introduces the minimum amount of dispersion. We do not, however, attempt to make the beams achromatic on the targets, as this is not necessary for isotope pro= duction.

10.4 Transport to the Radiotherapy Units

The radiotherapy area is divided into three treatment rooms. At present neutron therapy is planned, with a maximum beam energy of 60 MeV deuterons at a maximum beam current of 100 µA on target. Our calculations are done for this beam, with an assumed emittance of 8 π mm.mrad. The possibility of using one of these treatment rooms for proton therapy is under conside= ration.

From the slit SX1 the beam to the radiotherapy area passes undeflected through the dipole MP1. We arrange a quadrupole triplet on either side of this dipole so that the six quadrupoles QT1 through QT6 form a unit telescope (see section 6.3) between SX1 and the centre of the switching magnet SWT. This switching magnet, when activated, deflects the beam

through 45^{o} to the left or to the right, and when switched off allows the beam through undeflected. Here again the waist in the centre of SWI ensures that minimum dispersion is introduced by the dipole (DRA66). Some angular dispersion is introduced, however, but this can be accommodated.

In each of the three beamlines we then arrange a two-doublet telescope (see section 6.2) to transfer the beam from the switching magnet to a slit (STL, STC or STR for the left, centre, or right beams respectively).

We arrange the subsequent quadrupole triplet to provide a beam with equal horizontal and vertical extent. This symmetrical beam enters the isocentric unit, pictured in figure 10.4a, which consists of two 45^{o} dipoles, bending in opposite directions, and a 90^{o} dipole. The unit may in principle be rotated about its axis through 360^{o} for patient irradiation from all angles. The edge angles on the dipoles are chosen to provide equal horizontal and vertical beam extent on the target, as well as zero dispersion. The beam spot size on the target is then invariant under rotation of the isocentric unit. The beam envelope plotted in figure 10.4b shows the beam shaping by the orthogonal quadrupole system (from MI1 to SX1) and the beam passing through the two-triplet unit telescope (from SX1 to the centre of SWT), the 2-doublet telescope (from the centre of SWT to STC), the quadrupole triplet (from STC to the entrance to MTC1) and the isocentric system (MTC1 to the target 20 cm beyond MTC3).

The beam envelope plots for the left- and right-hand units after the switcher SWT are very similar.

10.5 Transport to the Experimental Area

The philosophy for the beamlines to the experimental area is that the beam-spot size and shape be determined at the entrance slit SX1 of the double-monochromator system. (This system encompasses the two 90^{o} dipoles, MP1 and MP2, and the nine quadrupoles, QP1 through QP9, in between. The operation of the system is described in section 8.4.) The orthogonal quadrupole system may be readily tuned to deliver this beam spot size. The beam should then be transported by telescopic systems with unit transfer matrix to the target points, except for dispersion and energy selection in the double-monochromator.

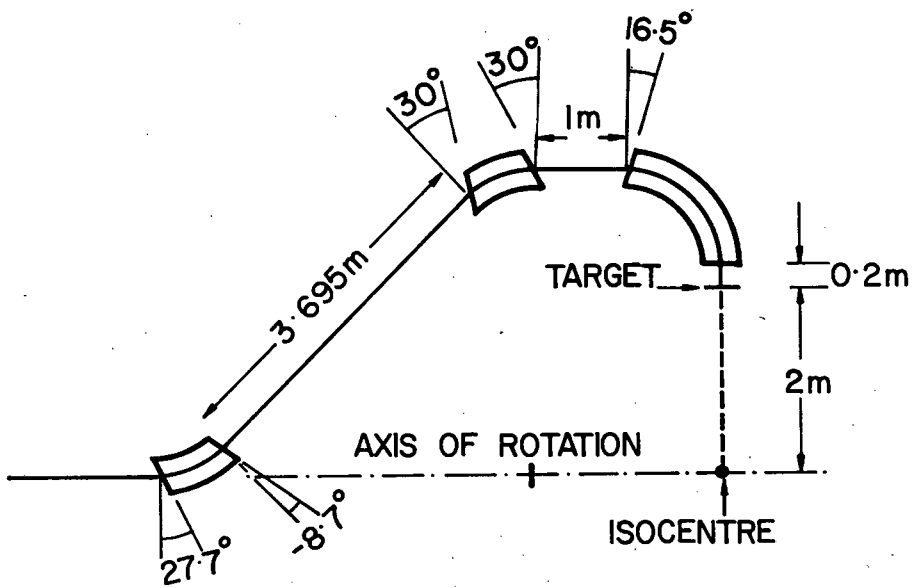

Figure 10.4a: Dimensions and edge-angles for a possible 3-magnet iso= centric unit for neutron therapy.

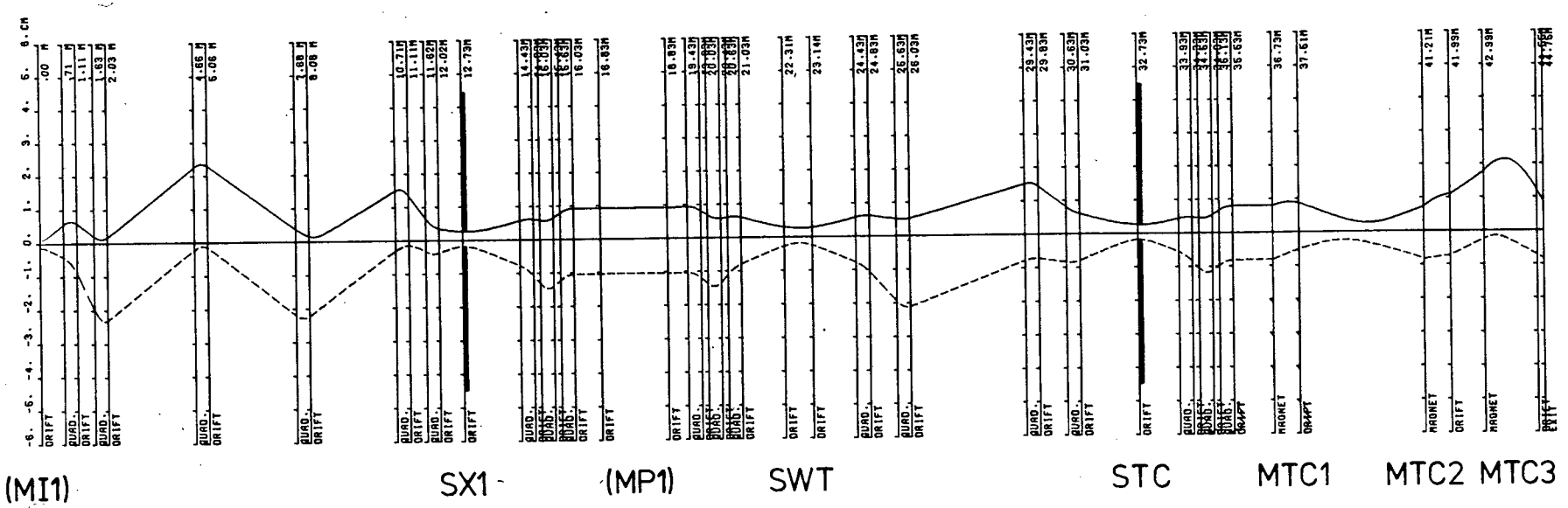

Figure 10.4b: Beam envelope plotted for 60 MeV deuterons, (8 π mm.mrad) shaped by the orthogonal quadrupole system, passing straight through MP1 to the switcher, and then on to the isocentric system.

If, however, a beam spot is required with y<2,5 mm or y>4,5 mm, (assuming a vertical emittance of 3 π mm.mrad.) then the beam will not fit through the 25 mm gap of the dipoles MP1 and MP2. In this case we operate the two quadrupole triplets (QR1 through QR6) in modified telescope mode. This has been described in section 6.4. The system can also be operated in zoom lens mode (see section 6.5) if both x and y are required to be either especially large, or especially small, at the target.

The switching magnet SWR can direct the beam into one of six lines. In each of these a two doublet-telescope (see section 6.2) transports the beam from the waist at the centre of the switcher to the target point.

Although not shown in figure 10.1, we plan to extend the beamline beyond dipole MP2 to another 90^{o} dipole, MP3. This beamline requires a triplet on either side of MP2 for telescopic transfer, and a further two-triplet telescope to transport the beam over the long distance to MP3. After MP3 we can use seven quadrupoles to match the beam to a magnetic spectrometer. A similar extension to the beamline may be made to a time-of-flight spectrometer.

The matching of the beam parameters to the requirements for high resolution in various types of experimental systems has been thoroughly described by various authors, especially (LEH78), also (HIN79, MAI79, ABD75, HEN74, SMI79, BLO71, LAU79, FAL76, SCH76, REI75, ENG79). These experimental systems include magnetic spectrometers, time-of-flight spectrometers, energy-sensitive detectors and optical spectrometers (for beam-foil spectroscopy).

We have made preliminary calculations using the characteristics of a possible magnetic spectrometer and time-of-flight spectrometer (MER79) and have arrived at the conclusion that the beamline as presently designed should be able to match all reasonable beam parameters required on target, including dispersion matching.

11. CONCLUSIONS

Although the field of beam transport is not a new one, we have developed a number of new techniques and systems which should be of use to the beamline designer. We summarize these below.

We have developed a method of solving for the eigen-ellipsoid in all six dimensions of phase space. This information is necessary in two cases, i.e. where

(a) the beam under consideration is extracted from a cyclotron and it is necessary to know the shape of the beam entering the beam transport system, or

(b) the beam is to be injected into a cyclotron and it is necessary to know the requirements to which the beam must be shaped.

We have developed a method of calculating the extracted beam ellipsoid in 6-dimensional phase space when central momentum particles have been tracked through the extraction elements of an accelerator in 4-dimensional (x, x', y, y') phase space, and the particle with higher momentum is also followed through. This is relatively easy with the E-matrix formalism, which we have expanded from a 2-dimensional treatment to a 6-dimensional formalism.

We found it necessary (in the above two methods) to derive the symplectic conditions for both the σ-matrix and the E-matrix formalisms.

We have described the eight possible symmetry types of beam transport systems and examined their group properties.

We have examined the second-order aberrations in these systems and drawn conclusions about the systems with the least number of aberrations.

Although the two-triplet unit telescope is well known, we have examined methods of using this system to achieve variable magnification in either one or both planes, independently of the beam parameters.

Quadrupoles affect both the horizontal and vertical components of a beam. We have, however, been able to separate the horizontal and vertical beam control by means of an orthogonal quadrupole system. We have calculated the optimum spacing and field strengths of the quadrupoles in this system, which is useful for beam shaping, either in a transfer beamline, or soon after extraction in an external beamline.

We have proposed a dipole system with two quadrupoles between two di= poles as the one requiring the least number of elements and the shortest length of beamline necessary
(a) to control both dispersion and angular dispersion and
(b) to allow a good placing of a momentum-selecting slit.

This system is useful in a transfer beamline for making the initial beam achromatic while simultaneously cutting out the particles with momentum which is too high or too low.

We have discussed the principles of transfer beamline design and illustrated these by means of the design of a specific transfer beamline. The methods used also illustrate the new techniques we have described above.

The design of a specific external beamline is also described, which in= cludes beamlines to isotope production units, radiotherapy treatment rooms and experimental areas. Again, the methods used illustrate the new tech= niques we have developed.

APPENDIX A

DERIVATION OF SYMPLECTIC EQUATIONS FOR BEAM MATRICES

Using the symplectic equations of the transfer matrix elements:

$$R_{51} = R_{16} R_{21} - R_{26} R_{11} \tag{2.9}$$

$$R_{52} = R_{16} R_{22} - R_{26} R_{12} \tag{2.10}$$

we can find interrelationships between the beam matrix elements.

(a) σ-matrix notation

We start with an uncorrelated ellipoid ($\sigma_{ij}^{o} = 0 \quad i \neq j$) and apply a transfer matrix R, then

$$\sigma = R\sigma^{o} R^{T}$$

The final beam matrix elements are thus (where $\sigma_{66} = \sigma_{66}^{o}$)

$$\sigma_{16} = R_{16} \sigma_{66} \tag{A.1}$$

$$\sigma_{26} = R_{26} \sigma_{66} \tag{A.2}$$

$$\sigma_{56} = R_{56} \sigma_{66} \tag{A.3}$$

$$\sigma_{15} = R_{11} R_{51} \sigma_{11}^{o} + R_{12} R_{52} \sigma_{22}^{o} + R_{16} R_{56} \sigma_{66} \tag{A.4}$$

$$\sigma_{25} = R_{21} R_{51} \sigma_{11}^{o} + R_{22} R_{52} \sigma_{22}^{o} + R_{26} R_{56} \sigma_{66} \tag{A.5}$$

$$\sigma_{11} = R_{11}^{2} \sigma_{11}^{o} + R_{12}^{2} \sigma_{22}^{o} + R_{16}^{2} \sigma_{66} \tag{A.6}$$

$$\sigma_{12} = R_{11} R_{21} \sigma_{11}^{o} + R_{12} R_{22} \sigma_{22}^{o} + R_{16} R_{26} \sigma_{66}^{o} \tag{A.7}$$

$$\sigma_{22} = R_{21}^{2} \sigma_{11}^{o} + R_{22}^{2} \sigma_{22}^{o} + R_{26}^{2} \sigma_{66} \tag{A.8}$$

We can then solve for elements of R in terms of elements of σ.
From equations (A.1), (A.2) and (A.3) we find

$$R_{16} = \sigma_{16}/\sigma_{66} \tag{A.9}$$

$$R_{26} = \sigma_{26}/\sigma_{66} \tag{A.10}$$

$$R_{56} = \sigma_{56}/\sigma_{66} \tag{A.11}$$

If we substitute equations (A.9) and (A.10) into (2.9) and (2.10) we get

$$R_{51} = (\sigma_{16} R_{21} - \sigma_{26} R_{11})/\sigma_{66} \qquad (A.12)$$

$$R_{52} = (\sigma_{16} R_{22} - \sigma_{26} R_{12})/\sigma_{66} \qquad (A.13)$$

Now using equations (A.9), (A.11) - (A.13) in (A.4) we find

$$\sigma_{15} = (R_{11} R_{21} \sigma_{11}^{o} + R_{12} R_{22} \sigma_{22}^{o})\frac{\sigma_{16}}{\sigma_{66}} - (R_{11}^{2} \sigma_{11}^{o} + R_{12}^{2} \sigma_{22}^{o})\frac{\sigma_{26}}{\sigma_{66}} + \frac{\sigma_{16}\sigma_{56}}{\sigma_{66}}$$

which, incorporating equations (A.6) and (A.7) becomes

$$\sigma_{15} = (\sigma_{12} - \frac{\sigma_{16}\sigma_{26}}{\sigma_{66}})\frac{\sigma_{16}}{\sigma_{66}} - (\sigma_{11} - \frac{\sigma_{16}^{2}}{\sigma_{66}})\frac{\sigma_{26}}{\sigma_{66}} + \frac{\sigma_{16}\sigma_{56}}{\sigma_{66}}$$

$$= \frac{\sigma_{12}\sigma_{16} - \sigma_{11}\sigma_{26} + \sigma_{16}\sigma_{56}}{\sigma_{66}} \qquad (A.14)$$

Similarly, using equations (A.10) - (A.13) in (A.5), we find

$$\sigma_{25} = (R_{21}^{2}\sigma_{11}^{0} + R_{22}^{2}\sigma_{22}^{0})\frac{\sigma_{16}}{\sigma_{66}} - (R_{11} R_{21} \sigma_{11}^{0} + R_{12}R_{22}\sigma_{22}^{0})\frac{\sigma_{26}}{\sigma_{66}} + \frac{\sigma_{26}\sigma_{56}}{\sigma_{66}}$$

which, together with equation (A.7) and (A.8) becomes

$$\sigma_{25} = \frac{\sigma_{22}\sigma_{16} - \sigma_{12}\sigma_{26} + \sigma_{26}\sigma_{56}}{\sigma_{66}} \qquad (A.15)$$

Equations (A.14) and (A.15) can be converted to correlation equations as follows:

dividing equation (A.14) by $(\sigma_{11}\ \sigma_{55})^{\frac{1}{2}}$, we get:

$$r_{15} = (\frac{\sigma_{11}\ \sigma_{22}}{\sigma_{55}\ \sigma_{66}})^{\frac{1}{2}}(r_{12}\ r_{16} - r_{26}) + r_{16}\ r_{56} \qquad (A.16)$$

Similarly equation (A.15) becomes

$$r_{25} = (\frac{\sigma_{11}\ \sigma_{22}}{\sigma_{55}\ \sigma_{66}})^{\frac{1}{2}}(r_{16} - r_{12}\ r_{26}) + r_{26}\ r_{56} \qquad (A.17)$$

(b) E-Matrix Notation

Again, we start with an uncorrelated ellipsoid ($E_{ij} = 0 \quad i \neq j$) and apply a transfer matrix R. Then

$$E = R\, E^0, \tag{A.18}$$

and we find

$$R_{ij} = E_{ij}/E_{jj}^0 \tag{A.19}$$

Substituting equation (2.9) into the expression for E_{51}, i.e.

$$E_{51} = R_{51}\, E_{11}^0 \tag{A.20}$$

and using (A.19), we find

$$E_{51} = \frac{(R_{21}\, E_{16} - R_{11}\, E_{26})}{E_{66}}\, E_{11}^0$$

$$= \frac{E_{21}\, E_{16} - E_{11}\, E_{26}}{E_{66}}$$

But if we choose $E_{21} = 0$, (see equation B.23) then

$$E_{51} = \frac{-\, E_{11}\, E_{26}}{E_{66}} \tag{A.21}$$

Similarly for E_{52}:

$$E_{52} = R_{52}\, E_{22}^0$$

$$= \frac{(R_{22}\, E_{16} - R_{12}\, E_{26})}{E_{66}}\, E_{22}^0$$

$$= \frac{E_{22}\, E_{16} - E_{12}\, E_{26}}{E_{66}} \tag{A.22}$$

The symplectic equations for the beam matrices are thus equations (A.16) and (A.17) (alternatively (A.14) and (A.15))for the σ-matrix, and (A.21) and (A.22) for the E-matrix.

APPENDIX B

RELATIONSHIP BETWEEN THE σ - AND E-MATRICES

We discuss the transformation between the σ- and E-matrices for the four-dimensional phase space in x, x', ℓ and δ, the other two parameters y, y' being independent of these.

We start with matrices E^0 and σ^0 such that

$$\sigma_{ij}^{0} = E_{ij}^{0} = 0 \qquad i \neq j$$

and can then state that (LAR71)

$$\sqrt{\sigma_{ii}} = E_{ii} \qquad i = 1, 2, 3, 4 \qquad \text{(B.1)}$$

The matrices E^0 and σ^0 are then transformed by the matrix R as follows:

$$E = R\,E^0$$

implying:

$$\begin{bmatrix} E_{11} & E_{12} & E_{15} & E_{16} \\ E_{21} & E_{22} & E_{25} & E_{26} \\ E_{51} & E_{52} & E_{55} & E_{56} \\ E_{61} & E_{62} & E_{65} & E_{66} \end{bmatrix} = \begin{bmatrix} R_{11}E_{11}^{0} & R_{12}E_{22}^{0} & 0 & R_{16}E_{66}^{0} \\ R_{21}E_{11}^{0} & R_{22}E_{22}^{0} & 0 & R_{26}E_{66}^{0} \\ R_{51}E_{11}^{0} & R_{52}E_{22}^{0} & E_{55}^{0} & R_{56}E_{66}^{0} \\ 0 & 0 & 0 & E_{66}^{0} \end{bmatrix} \qquad \text{... (B.2)}$$

and $\sigma = R\,\sigma^0\,R^T$

implying

$$\sigma_{11} = R_{11}^{2}\sigma_{11}^{0} + R_{12}^{2}\sigma_{22}^{0} + R_{16}^{2}\sigma_{66}^{0} \qquad \text{(B.3)}$$

$$\sigma_{12} = R_{11}R_{21}\sigma_{11}^{0} + R_{12}R_{22}\sigma_{22}^{0} + R_{16}R_{26}\sigma_{66}^{0} \qquad \text{(B.4)}$$

$$\sigma_{15} = R_{11}R_{51}\sigma_{11}^{0} + R_{12}R_{52}\sigma_{22}^{0} + R_{16}R_{56}\sigma_{66}^{0} \qquad \text{(B.5)}$$

$$\sigma_{16} = R_{16}\sigma_{66}^{0} \qquad \text{(B.6)}$$

$$\sigma_{22} = R_{21}^{2}\sigma_{11}^{0} + R_{22}^{2}\sigma_{22}^{0} + R_{26}^{2}\sigma_{66}^{0} \qquad \text{(B.7)}$$

$$\sigma_{25} = R_{21} R_{51} \sigma_{11}^{0} + R_{22} R_{52} \sigma_{22}^{0} + R_{26} R_{56} \sigma_{66}^{0} \quad (B.8)$$

$$\sigma_{26} = R_{26} \sigma_{66}^{0} \quad (B.9)$$

$$\sigma_{55} = R_{51}^{2} \sigma_{11}^{0} + R_{52}^{2} \sigma_{22}^{0} + \sigma_{55}^{0} + R_{56}^{2} \sigma_{66}^{0} \quad (B.10)$$

$$\sigma_{56} = R_{56} \sigma_{66}^{0} \quad (B.11)$$

$$\sigma_{66} = \sigma_{66}^{0} \quad (B.12)$$

If we now use equations (B.1) and (B.2) in equations (B.3) - (B.12) we get:

$$\sigma_{11} = E_{11}^{2} + E_{12}^{2} + E_{16}^{2} \quad (B.13)$$

$$\sigma_{12} = E_{11} E_{21} + E_{12} E_{22} + E_{16} E_{26} \quad (B.14)$$

$$\sigma_{15} = E_{11} E_{51} + E_{12} E_{52} + E_{16} E_{56} \quad (B.15)$$

$$\sigma_{16} = E_{16} E_{66} \quad (B.16)$$

$$\sigma_{22} = E_{21}^{2} + E_{22}^{2} + E_{26}^{2} \quad (B.17)$$

$$\sigma_{25} = E_{21} E_{51} + E_{22} E_{52} + E_{26} E_{56} \quad (B.18)$$

$$\sigma_{26} = E_{26} E_{66} \quad (B.19)$$

$$\sigma_{55} = E_{51}^{2} + E_{52}^{2} + E_{55}^{2} + E_{56}^{2} \quad (B.20)$$

$$\sigma_{56} = E_{56} E_{66} \quad (B.21)$$

$$\sigma_{66} = E_{66}^{2} \quad (B.22)$$

The submatrix $\begin{bmatrix} E_{11} & E_{12} \\ E_{21} & E_{22} \end{bmatrix}$ contains irrelevant phase information and we choose the phase such that (LAR71)

$$E_{21} = 0 \quad (B.23)$$

From transformation (B.2) we see the following is always true:

$$E_{15} = E_{25} = E_{61} = E_{62} = E_{65} = 0 \quad (B.24)$$

Using equation (B.23) in (B.14), (B.17) and (B.18), we now get

$$\sigma_{12} = E_{12} E_{22} + E_{16} E_{26} \tag{B.25}$$

$$\sigma_{22} = E_{22}^2 + E_{26}^2 \tag{B.26}$$

$$\sigma_{25} = E_{22} E_{52} + E_{26} E_{56} \tag{B.27}$$

The transformation from E to σ is thus completely defined by equations (B.13), (B.15), (B.16), (B.19) - (B.22), and (B.25) - (B.27). We now use these equations to solve for E in terms of σ.

From equations (B.16) and (B.22)

$$E_{16} = \sigma_{16}/\sqrt{\sigma_{66}} = r_{16}\sqrt{\sigma_{11}} \tag{B.28}$$

similarly from (B.19) and (B.22)

$$E_{26} = \sigma_{26}/\sqrt{\sigma_{66}} = r_{26}\sqrt{\sigma_{22}} \tag{B.29}$$

and from (B.21) and (B.22)

$$E_{56} = \sigma_{56}/\sqrt{\sigma_{66}} = r_{56}\sqrt{\sigma_{55}} \tag{B.30}$$

Using equation (B.29) in (B.26):

$$E_{22} = [\sigma_{22} - \sigma_{26}^2/\sigma_{66}]^{\frac{1}{2}} \tag{B.31}$$

$$= [\sigma_{22}(1 - r_{26}^2)]^{\frac{1}{2}}$$

and (B.28) (B.29) (B.31) in (B.25) yields:

$$E_{12} = \frac{\sigma_{12} - \sigma_{16}\sigma_{26}/\sigma_{66}}{[\sigma_{22} - \sigma_{26}^2/\sigma_{66}]^{\frac{1}{2}}} \tag{B.32}$$

$$= \left[\frac{\sigma_{11}}{1 - r_{26}^2}\right]^{\frac{1}{2}} (r_{12} - r_{16} r_{26})$$

The expression for E_{11} is derived from equations (B.13), (B.28) and (B.32):

$$E_{11} = \left[\sigma_{11} - \frac{(\sigma_{12} - \sigma_{16}\sigma_{26}/\sigma_{66})^2}{\sigma_{22} - \sigma_{26}^2/\sigma_{66}} - \frac{\sigma_{16}^2}{\sigma_{66}}\right]^{\frac{1}{2}}$$

$$= \left[\sigma_{11}\{1 - \frac{(r_{12} - r_{16}r_{26})^2}{1 - r_{26}^2} - r_{16}^2\}\right]^{\frac{1}{2}} \qquad (B.33)$$

We use (B.29), (B.30) and (B.31) in (B.27) to find

$$E_{52} = \frac{\sigma_{25} - \sigma_{26}\sigma_{56}/\sigma_{66}}{\left[\sigma_{22} - \sigma_{26}^2/\sigma_{66}\right]^{\frac{1}{2}}}$$

$$= \left[\frac{\sigma_{55}}{1-r_{26}^2}\right]^{\frac{1}{2}} (r_{25} - r_{26}r_{56}) \qquad (B.34)$$

and this result, together with (B.28), (B.30), (B.32) and (B.33) in (B.15) gives

$$E_{51} = \sigma_{15} - \frac{(\sigma_{12} - \sigma_{16}\sigma_{26}/\sigma_{66})(\sigma_{25}-\sigma_{26}\sigma_{56}/\sigma_{66}) - \frac{\sigma_{16}\sigma_{56}}{\sigma_{66}}}{\sigma_{22} - \sigma_{26}^2/\sigma_{66}}$$

$$\left[\sigma_{11} - \frac{(\sigma_{12} - \sigma_{16}\sigma_{26}/\sigma_{66})^2}{\sigma_{22} - \sigma_{26}^2/\sigma_{66}} - \frac{\sigma_{16}^2}{\sigma_{66}}\right]^{\frac{1}{2}} \qquad (B.35)$$

$$= \left[\frac{\sigma_{55}}{1 - \frac{(r_{12} - r_{16}r_{26})^2}{1 - r_{26}^2} - r_{16}^2}\right]^{\frac{1}{2}} \left[r_{15} - \frac{(r_{12}-r_{16}r_{26})(r_{25}-r_{26}r_{56})}{1 - r_{26}^2} - r_{16}r_{56}\right]$$

The expression for E_{55} comes from equation (B.20) using (B.30), (B.34) and (B.35):

$$E_{55} = \left[\sigma_{55} - \frac{(\sigma_{25} - \sigma_{26}\sigma_{56}/\sigma_{66})^2}{\sigma_{22} - \sigma_{26}^2/\sigma_{66}} - \sigma_{56}^2/\sigma_{66}\right.$$

$$\left. - \frac{\{\sigma_{15} - \frac{(\sigma_{12} - \sigma_{16}\sigma_{26}/\sigma_{66})(\sigma_{25} - \sigma_{26}\sigma_{56}/\sigma_{66})}{\sigma_{22} - \sigma_{26}^2/\sigma_{66}} - \frac{\sigma_{16}\sigma_{56}}{\sigma_{66}}\}^2}{\sigma_{11} - \frac{(\sigma_{12} - \sigma_{16}\sigma_{26}/\sigma_{66})^2}{\sigma_{22} - \sigma_{26}^2/\sigma_{66}} - \frac{\sigma_{16}^2}{\sigma_{66}}}\right]^{\frac{1}{2}}. \qquad (B.36)$$

$$= \left[\sigma_{55}\{1 - \frac{(r_{25} - r_{16}r_{56})^2}{1 - r_{26}^2} - r_{56}^2 - \frac{\left[r_{15} - \frac{(r_{12} - r_{16}r_{26})(r_{25} - r_{26}r_{56})}{1 - r_{26}^2} - r_{16}r_{56}\right]^2}{1 - \frac{(r_{12} - r_{16}r_{26})^2}{1 - r_{26}^2} - r_{16}^2}\}\right]^{\frac{1}{2}}$$

The physical significance of the elements of the beam matrices are discussed in chapter 2.

APPENDIX C

CONSTRUCTION OF AN INITIAL BEAM MATRIX

We show here how an initial beam matrix can be constructed from the information available from particle-tracking calculations if that information consists of the following parameters:

(i) horizontal emittance $\pi\varepsilon_x$

(ii) x_{max} in $(x - x')$ plane

(iii) x'_{max} in $(x - x')$ plane

(iv) d, the x-co-ordinate of the particle with maximum momentum

(v) d', the x'-co-ordinate of this particle

(vi) m, the ℓ-co-ordinate of this particle

(vii) ℓ_o, the minimum possible bunch length

(viii) δ, the fractional momentum-spread

(ix) vertical emittance $\pi\varepsilon_y$

(x) y_{max}

(xi) y'_{max}

We initially assume a matrix σ^o in (x, x', ℓ, δ) phase space with no correlations other than r_{12}. Then we can state that

$$\begin{aligned} \sigma_{11}^{o} &= x_{max}^{2} \\ \sigma_{22}^{o} &= x'^{2}_{max} \\ \sigma_{55}^{o} &= \ell_{max}^{2} \\ \sigma_{66}^{o} &= \delta^2 \end{aligned} \qquad (C.1)$$

The emittance in the $(x - x')$ plane is

$$\pi\varepsilon_x = \pi(\sigma_{11}^{o}\,\sigma_{22}^{o} - \sigma_{12}^{o2})^{\frac{1}{2}} \qquad (C.2)$$

which gives the expression for σ_{12}^{o}:

$$\sigma_{12}^{o} = (x_{max}^{2}\, x'^{2}_{max} - \varepsilon_x^{2})^{\frac{1}{2}} \qquad (C.3)$$

We now transform σ^o to the desired matrix σ by means of the transfer matrix R. This matrix must introduce the dispersion, the angular dispersion and the bunch length correlations, but no further skewing of the ellipse in the plane of $(x - x')$ (i.e. the plane in which $\ell = \delta = 0$). Hence R takes the form:

$$R = \begin{bmatrix} 1 & 0 & 0 & R_{16} \\ 0 & 1 & 0 & R_{26} \\ R_{51} & R_{52} & 1 & R_{56} \\ 0 & 0 & 0 & 1 \end{bmatrix} \qquad (C.4)$$

Applying the symplectic equations (2.9) and (2.10) to (C.4), we find

$$R_{51} = -R_{26} \qquad (C.5)$$

$$R_{52} = R_{16} \qquad (C.6)$$

If we now perform the transformation

$$\sigma = R\,\sigma^o\,R^T$$

we find the following expressions for the elements of σ:

$$\sigma_{11} = \sigma_{11}^o + R_{16}^2\,\sigma_{66} \qquad (C.7)$$

$$\sigma_{12} = \sigma_{12}^o + R_{16}\,R_{26}\,\sigma_{66} \qquad (C.8)$$

$$\sigma_{22} = \sigma_{22}^o + R_{26}^2\,\sigma_{66} \qquad (C.9)$$

$$\sigma_{16} = R_{16}\,\sigma_{66} \qquad (C.10)$$

$$\sigma_{26} = R_{26}\,\sigma_{66} \qquad (C.11)$$

$$\sigma_{56} = R_{56}\,\sigma_{66} \qquad (C.12)$$

$$\sigma_{55} = R_{26}^2\,\sigma_{11}^o + R_{16}^2\,\sigma_{22}^o - 2\,R_{16}\,R_{26}\,\sigma_{12}^o + \sigma_{55}^o + R_{56}^2\,\sigma_{66} \qquad \ldots (C.13)$$

From section 2.3 we know that

$$d = r_{16}\sqrt{\sigma_{11}} = \sigma_{16}/\sqrt{\sigma_{66}}$$

From equation (C.10) we then find

$$R_{16} = \sigma_{16}/\sigma_{66} = d/\sqrt{\sigma_{66}} \qquad (C.14)$$

Similarly

$$R_{26} = \sigma_{26}/\sigma_{66} = d'/\sqrt{\sigma_{66}} \qquad (C.15)$$

and $$R_{56} = \sigma_{56}/\sigma_{66} = m/\sqrt{\sigma_{66}} \qquad (C.16)$$

Thus the terms of the desired ellipse are:

$$\sigma_{11} = x_{max}^2 + d^2 \qquad (C.17)$$

$$\sigma_{12} = (x_{max}^2 x_{max}'^2 - \varepsilon_x^2)^{\frac{1}{2}} + dd' \qquad (C.18)$$

$$\sigma_{22} = x_{max}'^2 + d'^2 \qquad (C.19)$$

$$\sigma_{16} = d\,\delta \qquad (C.20)$$

$$\sigma_{26} = d'\delta \qquad (C.21)$$

$$\sigma_{56} = m\,\delta \qquad (C.22)$$

$$\sigma_{55} = (\frac{d'}{\delta})^2 x_{max}^2 + (\frac{d}{\delta})^2 x_{max}'^2 - \frac{2\,dd'}{\delta^2}(x_{max}^2 x_{max}'^2 - \varepsilon_x^2)^{\frac{1}{2}} + \ell_o^2 + m^2 \qquad (C.23)$$

The remaining two terms can be found from the symplectic equations (A.14) and (A.15). They are

$$\sigma_{15} = \frac{d}{\delta}(x_{max}^2 x_{max}'^2 - \varepsilon_x^2)^{\frac{1}{2}} - \frac{d'}{\delta} x_{max}^2 + md \qquad (C.24)$$

and $$\sigma_{25} = \frac{-d'}{\delta}(x_{max}^2 x_{max}'^2 - \varepsilon_x^2)^{\frac{1}{2}} + \frac{d}{\delta} x_{max}'^2 + md' \qquad (C.25)$$

If, however, we choose to represent the beam in terms of the E-matrix, then a more direct method is possible. From section 2.3 we know that

$$E_{11}^2 + E_{12}^2 = x_{max}^2$$

$$E_{22} = x'_{max}$$

$$E_{11}E_{22} = \varepsilon_x$$

Thus $$E_{11} = \varepsilon_x / x'_{max}$$

and $$E_{12} = (x_{max}^2 - \varepsilon_x^2/x_{max}'^2)^{\frac{1}{2}}$$

Also $$E_{16} = d$$

$$E_{26} = d'$$

$$E_{56} = m$$

$$E_{55} = \ell_o$$

$$E_{66} = \delta$$

From the symplectic equations (A.21) and (A.22) we find the remaining two terms:

$$E_{51} = -\frac{d' \varepsilon_x}{\delta \, x'_{max}}$$

and

$$E_{52} = \frac{d \, x'_{max} - d' \, (x_{max}^2 - \varepsilon_x^2 / x'^2_{max})^{\frac{1}{2}}}{\delta}$$

The expressions for the vertical plane can be found in a similar manner:

$$\sigma_{33} = y_{max}^2$$

$$\sigma_{44} = y'^2_{max}$$

$$\sigma_{34} = (y_{max}^2 \, y'^2_{max} - \varepsilon_y^2)^{\frac{1}{2}}$$

and

$$E_{33} = \varepsilon_y / y'_{max}$$

$$E_{44} = y'_{max}$$

$$E_{34} = (y_{max}^2 - \varepsilon_y^2 / y'^2_{max})^{\frac{1}{2}}$$

The relationships between the σ- and E-matrix formalisms can also be used to check the consistency of the values calculated via either one of these methods.

APPENDIX D

DERIVATION OF EQUATIONS FOR ORTHOGONAL QUADRUPOLE SYSTEM

(a) Double Waist

We start with equation (7.4):

$$\frac{1}{D_1} + \frac{1}{D_2} = \frac{1}{f_c} = \frac{1}{f_o + L/6} \tag{7.4}$$

from which (7.5) follows directly, i.e.

$$f_o = \frac{D_1 (E - D_1)}{E} - \frac{L}{6} \tag{7.5}$$

Equation (7.6) is derived directly from optics:

$$\frac{1}{D_1} - \frac{1}{r} = \frac{1}{f_d} = \frac{1}{\frac{L}{6} - f_o} \tag{7.6}$$

To find y_2 we see that (from figure 7.2)

$$\frac{y_2}{D_2 + r} = \frac{y_1}{r} = \frac{D_1 y_i'}{r} \tag{D.1}$$

where y_1 is the extent in Q_1 of the "y-ray". In equation (D.1) we have assumed that y_i' is small so that we may approximate $\tan(y_i')$ by y_i'. From equation (D.1) we find

$$y_2 = \frac{(D_2 + r) D_1}{r} y_i'$$

$$= y_i' \left[\frac{D_1 D_2}{r} + D_1\right] \tag{7.7}$$

$$= y_i' \left[\frac{D_1 (E-D_1)}{r} + D_1\right] \tag{D.2}$$

We now find the value of r using equation (7.6), having first substituted equation (7.5) into (7.6) i.e.

$$r = \frac{(f_o - \frac{L}{6})\, D_1}{f_o - L/6 + D_1} = \frac{\{\frac{D_1\,(E-D_1)}{E} - \frac{L}{3}\}\, D_1}{\frac{D_1\,(E-D_1)}{E} - \frac{L}{3} + D_1}$$

$$= \frac{\{3\,D_1\,(E-D_1) - EL\}D_1}{3\,D_1\,(E-D_1) - EL + 3\,D_1E} \qquad (D.3)$$

Then equation (D.2) becomes

$$y_2 = y_i' \left[\frac{(E-D_1)\,\{3\,D_1\,(E-D_1) - EL + 3\,D_1E\} + D_1\{3\,D_1\,(E-D_1) - EL\}}{3\,D_1\,(E-D_1) - EL}\right]$$

$$= y_i' E\left[1 + \frac{3\,D_1(E-D_1)}{3\,D_1(E-D_1) - EL}\right] \qquad (7.8)$$

If we now differentiate equation (7.8) with respect to D_1 to find the minimum y_2 we get

$$\frac{d\,y_2}{d\,D_1} = 0 = y_i' \frac{3\,E^2L\,(E-2\,D_1)}{[3\,D_1\,(E-D_1) - EL]^2}$$

leading to $D_1 = D_2 = E/2 \qquad (7.9)$

If we substitute equation (7.9) into (7.8) we find

$$y_2 = y_i' 2\,D_1\left[1 + \frac{3\,D_1^2}{3\,D_1^2 - 2\,D_1L}\right]$$

$$= y_i'\left[\frac{4\,D_1\,(3\,D_1 - L)}{3\,D_1 - 2\,L}\right] \qquad (7.11)$$

We can find y_2 in terms of D_3 from figure 7.2 when we put $y_2 = x_3$

i.e. $y_2 = D_3\, x_i'$

and thus

$$D_3 = \frac{y_i'}{x_i'} \quad \frac{4\,D_1\,(3\,D_1 - L)}{3\,D_1 - 2\,L} \qquad (D.4)$$

From the symmetry we have $D_3 = D_4 = D_5 \qquad (7.14)$

The analogy of equations (7.9) and (D.4) for the end of the system are:

$$D_6 = D_7 \qquad (7.15)$$

$$D_5 = \frac{x_f'}{y_f'} \cdot \frac{4 D_7 (3 D_7 - L)}{3 D_7 - 2 L} \qquad (7.16)$$

which may be solved for D_7:

$$D_7 = \frac{4 L + 3 D_3 \frac{y_f'}{x_f'} \pm \left[16 L^2 - 72 L D_3 \frac{y_f'}{x_f'} + 9 D_3^2 \left(\frac{y_f'}{x_f'}\right)^2\right]^{\frac{1}{2}}}{24} \qquad \ldots (7.28)$$

(b) Waist in One Dimension Only

The focal length of Q_1 is again found from

$$\frac{1}{D_1} + \frac{1}{D_2} = \frac{1}{f_c} = \frac{1}{f_o + L/6} \qquad (7.4)$$

and (from figure 7.3)

$$\frac{1}{D_1 + P} - \frac{1}{r} = \frac{1}{f_d} = \frac{1}{L/6 - f_o} \qquad (7.21)$$

The equivalent of equation (D.1) is now

$$\frac{y_2}{D_2 + r} = \frac{y_1}{r} = \frac{y_1'(D_1 + P)}{r} \qquad (D.5)$$

and
$$y_2 = y_1' \frac{(D_2 + r)(D_1 + P)}{r}$$

$$= y_1' \left[\frac{D_1 D_2 + D_2 P}{r} + D_1 + P\right]$$

$$= y_1' \left[\frac{(D_1 + P)(E - D_1)}{r} + D_1 + P\right] \qquad (D.6)$$

Again, we substitute the value of f_o from (7.4) into (7.21) and solve for r:

$$\frac{1}{r} = \frac{1}{D_1 + P} + \frac{1}{f_o - L/6} = \frac{1}{D_1 + P} + \frac{1}{\frac{D_1 D_2}{D_1 + D_2} - \frac{L}{3}}$$

$$\therefore \quad r = \frac{(D_1 + P)\left[3 D_1 (E - D_1) - EL\right]}{3 D_1 (E - D_1) - EL + 3 E (D_1 + P)} \qquad (D.7)$$

Using (D.7) we can find y_2 in equation (D.6) as follows:

$$Y_2 = y_i' \left[\frac{(D_1 + P)(E-D_1)\{3D_1(E-D_1) - EL + 3E(D_1 + P)\}}{(D_1+P)\{3D_1(E-D_1) - EL\}} + (D_1+P) \right]$$

$$= y_i' \left[E + P + \frac{3E(E-D_1)(D_1 + P)}{3D_1(E-D_1) - EL} \right] \qquad (7.22)$$

Putting $\frac{d y_2}{d D_1} = 0$ gives us

$$\{3D_1(E-D_1) - EL\}\{E-P-2D_1\} - 3(E-D_1)(D_1 + P)(E-2D_1) = 0$$

i.e. $$D_1^2[-3P] + D_1[6EP + 2EL] - 3E^2P + ELP - E^2L = 0 \qquad (D.8)$$

and thus $$D_1 = E + \frac{EL}{3P}\left[1 - \left(1 + \frac{3P}{L} + \frac{3P^2}{EL}\right)^{\frac{1}{2}}\right] \qquad (7.23)$$

Note that we use a minus sign for the last term in (7.23), otherwise we would get $D_1 > E$.

Equation (D.8) reduces to equation (7.9) when P = 0. This is not so obvious in equation (7.23).

We now use equation (7.23) in (7.22):

$$y_2 = y_i' \left[E + P + \frac{3E\left(\frac{EL}{3P} - C\right)\left(E + P + \frac{EL}{3P} - C\right)}{3\left\{E + \frac{EL}{3P} - C\right\}\left\{\frac{EL}{3P} - C\right\} + EL} \right] \qquad (D.9)$$

where $$C = \frac{EL}{3P}\left(1 + \frac{3P}{L} + \frac{3P^2}{EL}\right)^{\frac{1}{2}} \qquad (D.10)$$

Then $$y_2 = y_i' \left[2E + P + \frac{3P^2}{3P + 2L\left\{1 - \left(1 + \frac{3P}{L} + \frac{3P^2}{EL}\right)^{\frac{1}{2}}\right\}} \right] \qquad (7.24)$$

To find D_3 we look at figure 7.3 to find that

$$\frac{y_2}{D_3} = \frac{x_3}{D_3} = \frac{x_1}{D_2} = x_i' \frac{D_1}{D_2} \qquad (D.11)$$

Thus $$D_3 = \frac{y_2}{x_i'} \frac{E-D_1}{D_1} \qquad (7.25)$$

$$\text{and } D_3 = \frac{y_i'}{x_i}\left[2E + P + \frac{3P^2}{3P + 2L\{1 - (1 + \frac{3P}{L} + \frac{3P^2}{EL})^{\frac{1}{2}}\}}\right]\left[\frac{E - D_1}{D_1}\right] \quad (7.27)$$

We still need to derive equation (7.30) from which equation (7.33) then follows with P = 0.

We find, for Q_2,

$$\frac{1}{D_2 + r} + \frac{1}{D_3} = \frac{1}{f_2 + L/6}$$

$$\text{and thus } f_2 + \frac{L}{6} = \frac{D_3 (r + D_2)}{D_3 + r + D_2}$$

$$= \frac{D_3 (E - D_1 + r)}{D_3 + E - D_1 + r} \quad (D.12)$$

We use equation (D.7) for r to find

$$f_2 + L/6 = \frac{D_3 \left[\{E-D_1\}\{3D_1 (E-D_1) - EL + 3E (D_1+P)\} + (D_1+P)\{3D_1(E-D_1) - EL\}\right]}{\left[D_3 + E - D_1\right]\{3D_1 (E-D_1) - EL + 3E (D_1+P)\} + (D_1+P) \left[3D_1 (E-D_1) - EL\right]} \quad \ldots (D.13)$$

$$\therefore \quad f_2 = \frac{D_3 \{EC_2 + PC_2 + 3P (E - D_1)^2\}}{D_3\{C_2+3D_1^2 + 3PE\} + EC_2 + PC_2 + 3P (E-D_1)^2} - \frac{L}{6} \quad (7.30)$$

$$\text{where } C_2 = 6D_1 (E-D_1) - LE \quad (7.31)$$

We have thus shown how the equations in chapter 7 were arrived at.

REFERENCES

ABD75 Abdel-Gawad A et al, Design procedures for the Julich QQDDQ high resolution spectrometer. *5th Intern. Conf. on Magnet Techn. (1975)* p 45.

ANN78 Annual Report, National Accelerator Centre, 1978.

ANN79 Annual Report, National Accelerator Centre, 1979.

BAN66 Banford A P, "The Transport of Charged Particles" Spon, London, 1966.

BEC75 Beck R, Beam transfer problems on GANIL. *7th Intern. Conf. on Cyclotrons and their Applications (1975)* p 297.

BLI64 Bliamptis E E, Reflection properties of deflecting magnet systems. *Rev. Sci. Instr.* 35 (1964) 1521.

BLO71 Blosser H G et al, Ultra-high resolution spectrometer system for charged particle studies of nuclei. *Nucl. Instr. Methods* 91 (1971) 61.

BRD64 Brown K L et al, First- and second-order magnetic optics matrix equations for the midplane of uniform-field wedge magnets. *Rev. Sci. Instr.* 35 (1964) 481.

BRO65 Brown K L, First- and second-order magnetic optics of a circular-pole uniform field magnet I. *Rev. Sci. Instr.* 36 (1965) 271.

BRO67 Brown K L, Some first- and second-order magnetic optics theorems applicable to the design of beam transport systems and charged particle spectrometers. *2nd Intern. Conf. on Magnet Techn. (1967)* p 40.

BRO69 Brown K M, A quadratically convergent Newton-like method based upon Gaussian elimination. *SIAM Journal on Numerical Analysis* 6 (1969) 560.

BRO70 Brown K L, A systematic procedure for designing high resolving-power beam transport systems or charged particle spectrometers. *3rd Intern. Conf. on Magnet Techn. (1970)* p 348.

BRO71 Brown K L, SLAC-91 Appendix, Stanford 1971, and CERN 80-04.

BRO72 Brown K L, A first- and second-order matrix theory for the design of beam transport systems and charged particle spectrometers. SLAC-75 revision 3, Stanford 1972.

BRO74 Brown K L and Iselin C, Decay Turtle, a computer program for simulating charged particle beam transport systems, including decay calculations. CERN 74-2, Geneva 1974.

BRO77 Brown K L et al, Transport: a computer program for designing charged particle beam transport systems. SLAC-91 revision 2, Stanford 1977, and CERN 80-04, Geneva 1980.

BRO79 Brown K L, A second-order magnetic optical achromat. *IEEE NS*-26 (1979) 3490.

CAR71 Carey D C, Turtle, a computer program for simulating charged particle beam transport systems. NAL-64 (1971).

CAR72a Carey D C, Second-order contributions to beam dimensions. NAL Internal Report TM-361 (1972).

CAR72b Carey D C, Computer simulation of charged particle beams. *Nucl. Instr. Methods* 104 (1972) 173.

CAR73 Carey D C, Minimization of aberrations in beam line design. *IEEE NS*-20 (1973) 493.

CHA60 Chamberlain O, Optics of high-energy beams. *Ann. Rev. Nucl. Sci.*10 (1960) 161.

CHA79a Chabert A et al, Limited energy spread in an SSC. *IEEE NS*-26 (1979) 2306.

CHA79b Chabert A et al, Chromatic correlations at injection and related ejection problems in separated-sector cyclotrons. *IEEE NS*-26 (1979) 3612.

COL70 Colonias J C and Paul A C, On-line calculation of beam transport systems to first- and second-order. *3rd Intern. Conf. on Magnet Techn. (1970)* 325.

COU71 Courant E D, Impossibility of achromatic focussing with magnetic quadrupoles and solenoids. *Part. Accel.* 2 (1971) 117.

CRO51 Cross W G, Two-directional focussing of charged particles with a sector-shaped uniform magnetic field. *Rev. Sci. Instr.* 22 (1951) 717.

DEV75 Devins D W, The IUCF transfer beamline . *IEEE NS*-22 (1975) 1601.

DRA66 Draper J E, Simple system for dispersionless deflection of beam of particles. *Rev. Sci. Instr.* 37 (1966) 969.

DRA76 Dragt A J and Finn F M, Lie series and invariant functions for analytic symplectic maps. *J. Math. Phys.* 17(1976) 2215.

DRA79 Dragt A J, A method of transfer maps for linear and non-linear beam elements. *IEEE NS*-26 (1979) 3601.

DYM64 Dymnikov A D and Yavor S Y, Four quadrupole lenses as an analogue of an axially symmetric system. *Sov. Phys. Tech. Phys.* 8 (1964) 639.

DYM65a Dymnikov A D et al, Effect of geometrical parameters on optical characteristics of a system of four quadrupole lenses similar to an axisymmetric lens. *Sov. Phys. Tech. Phys.* 10 (1965) 340.

DYM65b Dymnikov A D and Yavor S Y, System of sequentially placed electrostatic and magnetic quadrupole lenses with zero and negative chromatic aberration. *Sov. Phys. Tech. Phys.* 9 (1965) 1544.

EMM63 Emmerson J McL and Middlemas N, Symmetry properties in beam transport systems. *Nucl. Instr. Methods* 24 (1963) 93.

ENG64 Enge H A, Effect of extended fringing fields on ion-focussing properties of deflecting magnets. *Rev. Sci. Instr.* 35 (1964) 278.

ENG67 Enge H A, Deflecting Magnets. *In* "Focussing of Charged Particles" Vol. 2 (A Septier ed.) Academic Press, New York 1967 p 203.

ENG70 Enge H A and Kowalski S B, Recent spectrograph design work utilizing a fourth-order ray-tracing program. *3rd Intern. Conf. on Magnet Techn. (1970)* p 366.

ENG79 Enge H A, Magnetic spectrographs for nuclear reaction studies. *Nucl. Instr. Methods* 162 (1979) 161.

FAL76 Falk W R et al, Energy resolution improvement in scattering experiments using highly divergent accelerator beams. *Nucl. Instr. Methods* 137 (1976) 261.

FUJ77 Fujita Y et al, General method for the calculation of particle trajectories in any sector field in a third-order approximation. *Nucl. Instr. Methods* 144 (1977) 279.

FUJ78 Fujita Y, A general method for the calculation of particle trajectories in the fields having a straight mean path. *Nucl. Instr. Methods* 155 (1978) 39.

GOR68 Gordon M M, Orbit properties of the isochronous cyclotron ring with radial sectors, *Annals of Physics* 50 (1968) 571.

HAL76 Halbach K, A simple class of beam transport systems with optically axisymmetric transfer properties. *Nucl. Instr. Methods* 136 (1976) 441.

HAM62 Hamermesh M, "Group Theory and its Applications to Physical Problems". Addison-Wesley, Reading (1962).

HEN74 Hendrie D L, Magnetic detection of charged particles. *In* "Nuclear Spectroscopy and Reactions Part A" (J Cerny ed.) Academic Press, London, 1974 p 365.

HER66 Herrera H C and Bliamptis E E, Symmetry properties of beam handling magnet systems. *Rev. Sci. Instr.* 37 (1966) 183.

HIN69 Hintz R E et al, Beam analysing system for a variable energy cyclotron. *Nucl. Instr. Methods* 72 (1969) 61.

HIN73 Hinterberger F, A special class of pulsed beam preparation systems. *Nucl. Instr. Methods* 111 (1973) 189.

HIN74a Hinterberger F, Symmetrized double-monochromator systems. *Nucl. Instr. Methods* 119 (1974) 43.

HIN74b Hinterberger F et al, The VICKSI beam handling system. *Nucl. Instr. Methods* 121 (1974) 525.

HIN75a Hinderer G and Maier K H, The beam-matching system between pre- and main-accelerator for the Van de Graaff-cyclotron combination VICKSI. *IEEE NS*-22 (1975) 1722.

HIN75b Hinderer G, Das System der Strahlanpassung zwischen vor- und Hauptbeschleuniger für die Van-de-Graaff-Zyklotron-Kombination VICKSI. HMI-B165 (1975)

HIN79 Hinderer G et al, Matching of beam handling and detection system for optimum resolution in nuclear physics experiments. *Nucl. Instr. Methods* 160 (1979) 449.

JOH75 Joho W, Beam transfer between accelerators at cyclotron facilities. *7th Intern. Conf. on Cyclotrons and their Applications (1975)* p 209.

KAR76 Kartashev V P et al, Symmetric quadrupole-lens systems. *Sov. Phys. Tech. Phys.* 21 (1976) 763.

KNO63 Knowles H B, A graphical first-order treatment of dispersive magnetic particle optics problems. *Nucl. Instr. Methods* 25 (1963) 29.

KNO75 Knowles H B, An envelope equation in the dispersive plane of a bending magnet. *Part. Accel.* 6 (1975) 193.

LAR71 Larson J D, Phase space ellipse transport using two ray vectors. *IEEE NS*-18 (1971) 1088.

LAU79 Laurent H and Schapira J P, Magnetic quadrupole and solenoidal spectrometers. *Nucl. Instr. Methods* 162 (1979) 181.

LEE69 Lee-Whiting G E and Bezić N, Beam matching with quadrupole lenses. *Nucl. Instr. Methods* 71 (1969) 61.

LEH78 Lehr H et al, Untersuchungen zur Optimierung eines aus Strahl= führung und kernphysikalischen Detekoren bestehenden Experimentier-Systems HMI-B259 (1978).

LIV69 Livingood J J, "The Optics of Dipole Magnets" Academic Press, New York, 1969.

LOB70 Lobb D E, The beam envelope of an initially uncorrelated beam. *Nucl. Instr. Methods* 82 (1970) 331.

MAI79 Maier K H, Matching of beam handling and detection system for optimum resolution. *IEEE NS*-26 (1979) 1432.

MAR75 Markovits C et al, The design, assembly and performance of the SIN beam transfer line. *7th Intern. Conf. on Cyclotrons and their Applications (1975)* p 306.

MER79 Merry C M, Beam matching to targets in the experimental area, NAC Internal Report NAC/BT/79-01 (1979).

MOL66a Möller P-A et al, Optique corpusculaire - sur la possibilité de réaliser des systèmes formés de lentilles quadrupolaires et ayant une matrice de transfert unité. *C. R. Acad. Sc.* 263B (1966) 534.

MOL66b Möller P-A et al, Optique corpusculaire - sur des systèmes optiques formés de quatre lentilles quadrupolaires et possédant une matrice de transfert unité. *C. R. Acad. Sc.* 263B (1966) 955.

NOR67 Norman B A and Moore W H, Theory and design of beam transport systems, BNL Report 12138 (1967).

PAU75 Paul A C, Transport, an ion optic program, LBL version. LBL-2697 (1975).

PEN61 Penner S, Calculations of properties of magnetic deflection systems. *Rev. Sci. Instr.* 32 (1961) 150.

RAN66 Randle T C, Two graphical constructions for beam transport problems. *Nucl. Instr. Methods* 41 (1966) 319.

REE69 Reeve P A, The design of beam lines with high resolving power. *Nucl. Instr. Methods* 67 (1969) 13.

REG63 Regenstreif E, Chromatic aberrations in quadrupole multiplets. CERN 64-2, Geneva (1963).

REG67 Regenstreif E, Focussing with quadrupoles, doublets and triplets, *In* "Focussing of Charged Particles" Vol I (A Septier ed.) Academic Press, New York, 1967, p 353.

REI75 Reich J et al, Improving the energy resolution of particle detection by proper beam matching at Julic. *7th Intern. Conf. on Cyclotrons and their Applications (1975)* p 235.

RES69 Resmini F, A simple method of determining waist-to-waist transfer properties of quadrupole doublets and triplets. *Nucl. Instr. Methods* 68 (1969) 235.

SCH79 Schulte W M and Hagendoorn H L, The definition and use of the central position phase in cyclotrons. *IEEE NS*-26 (1979) 2388.

SMI79 Smith P A, Possible methods for improving the resolution of neutron time-of-flight measurements of direct reaction spectra. *Nucl. Instr. Methods* 166 (1979) 229.

SPE67 Spencer J E and Enge H A, Split-pole magnetic spectrograph for precision nuclear spectroscopy. *Nucl. Instr. Methods* 49 (1967) 181.

STE65 Steffan K G, "High Energy Beam Optics" Wiley (Interscience) New York, 1965.

TEC76 Technical Report of the Accelerator Task Group, National Accelerator Project, 1976.

WAD79 Wada T et al, The injection in IPCR separated sector cyclotron. *IEEE NS*-26(1979) 2000.